AD NUMBER

AD480309

NEW LIMITATION CHANGE

TO

Approved for public release, distribution unlimited

FROM

Distribution authorized to U.S. Gov't. agencies and their contractors; Administrative/Operational Use; MAY 1963. Other requests shall be referred to Air Force Cambridge Research Laboratory, Hanscom AFB, MA.

AUTHORITY

afcrl ltr 22 dec 1971

May 1963

# RESEARCH AND DEVELOPMENT

# OF

# ROBIN METEOROLOGICAL ROCKET BALLOON

## VOLUME II

## University of Minnesota Reports

I. Drag Coefficient of a Sphere Corresponding to a One Meter ROBIN Sphere Descending from 260,000 Feet

II. Lift and Induced Drag of a Rotating Sphere in Inviscid Flow

III. The Drag of Spheroids Related to the Drag of a Sphere with an Identical Surface Area

By

Helmut G. Heinrich
Eugene L. Haak
Ronald J. Niccum

University of Minnesota
Minneapolis, Minnesota

Contract No. AF 19(604)-8034

Prepared for:

Aerospace Instrumentation Laboratory
Air Force Cambridge Research Laboratories
Office of Aerospace Research
United States Air Force
Laurence G. Hanscom Field
Bedford, Massachusetts

TECHNICAL REPORT

# THE DRAG COEFFICIENT OF A SPHERE CORRESPONDING TO A "ONE METER ROBIN SPHERE" DESCENDING FROM 260,000 FT ALTITUDE (REYNOLDS NOS 789 TO 23,448, MACH NOS 0.056 TO 0.90)

Helmut G. Heinrich
Ronald J. Niccum
Eugene L. Haak

G. T. Schjeldahl Company
Northfield, Minnesota

## ABSTRACT

The drag coefficient of a sphere was established experimentally over a range of Reynolds numbers with Mach number as a parameter.

The conditions of Reynolds and Mach number were related to a falling one meter "ROBIN" reconnaisance sphere used for determining upper air density.

An error analysis was performed on the data to determine the reliability.

TABLE OF CONTENTS

LIST OF TABLES

## LIST OF FIGURES

## LIST OF SYMBOLS

| | |
|---|---|
| $a$ | = speed of sound |
| $C_D$ | = drag coefficient of the sphere |
| $d$ | = diameter of the sphere |
| $D$ | = drag of the sphere |
| $D_w$ | = drag of the 0.003" diameter suspension wires |
| $L$ | = Perpendicular distance from the wire suspension point to the point of attachment to the sphere |
| $M$ | = $V/a$ = Mach number |
| $n$ | = number of experimental points |
| $P$ | = static pressure |
| $P_T$ | = total pressure |
| $\Delta P$ | = $P_T - P$ = differential pressure measured in wind tunnel |
| $q$ | = $\frac{1}{2}\rho V^2$ = dynamic pressure |
| $R$ | = gas constant |
| $Re$ | = $\frac{\rho V d}{\mu}$ = Reynolds number |
| $S$ | = $\frac{\pi d^2}{4}$ = projected area of the sphere |
| $T$ | = absolute temperature ($^\circ$F) |
| $V$ | = air velocity |
| $w$ | = weight of sphere |
| $w'$ | = suspended weight used to determine the wire drag correction |
| $x$ | = displacement of the sphere due to aerodynamic drag on the system |
| $x'$ | = displacement of the small weight $w$ used to determine the wire drag correction |
| $\rho$ | = air density |
| $\mu$ | = air viscosity |

# I. INTRODUCTION

In order to determine reliably the air density from the descent velocity of a sphere, the drag coefficient of the sphere in regard to the related Mach and Reynolds numbers must be known with a high degree of accuracy. Drag data, which encompasses the descent of a ROBIN sphere from 260,000 ft altitude, was obtained at the University of Minnesota by means of wind tunnel experiments.

The required Reynolds and Mach number range was established from exploratory descent tests, and is shown in Fig 1 (Atmospheric data was taken from Ref 1). Parameters which can be varied in a wind tunnel are velocity, static pressure, and model size. In general, the velocity is fixed by the required Mach number of the descent, while the related Reynolds number can be obtained by varying static pressure and/or model size. Since variation in model size is neither desirable nor easily attained, as will be pointed out later, it was decided to vary the static pressure over a sufficient range in order to obtain the desired Reynolds numbers.

In this manner a considerable number of experiments were made; the summary results are shown in Fig 19.

The experiments were carried out by graduate and undergraduate students of the University of Minnesota. Messrs. Richard Strom and Joseph Bushard contributed significantly in the performance of the experiments and reduction of data. Mr. Lawrence W. Rust, Research Fellow, was instrumental in the chapter of error analysis.

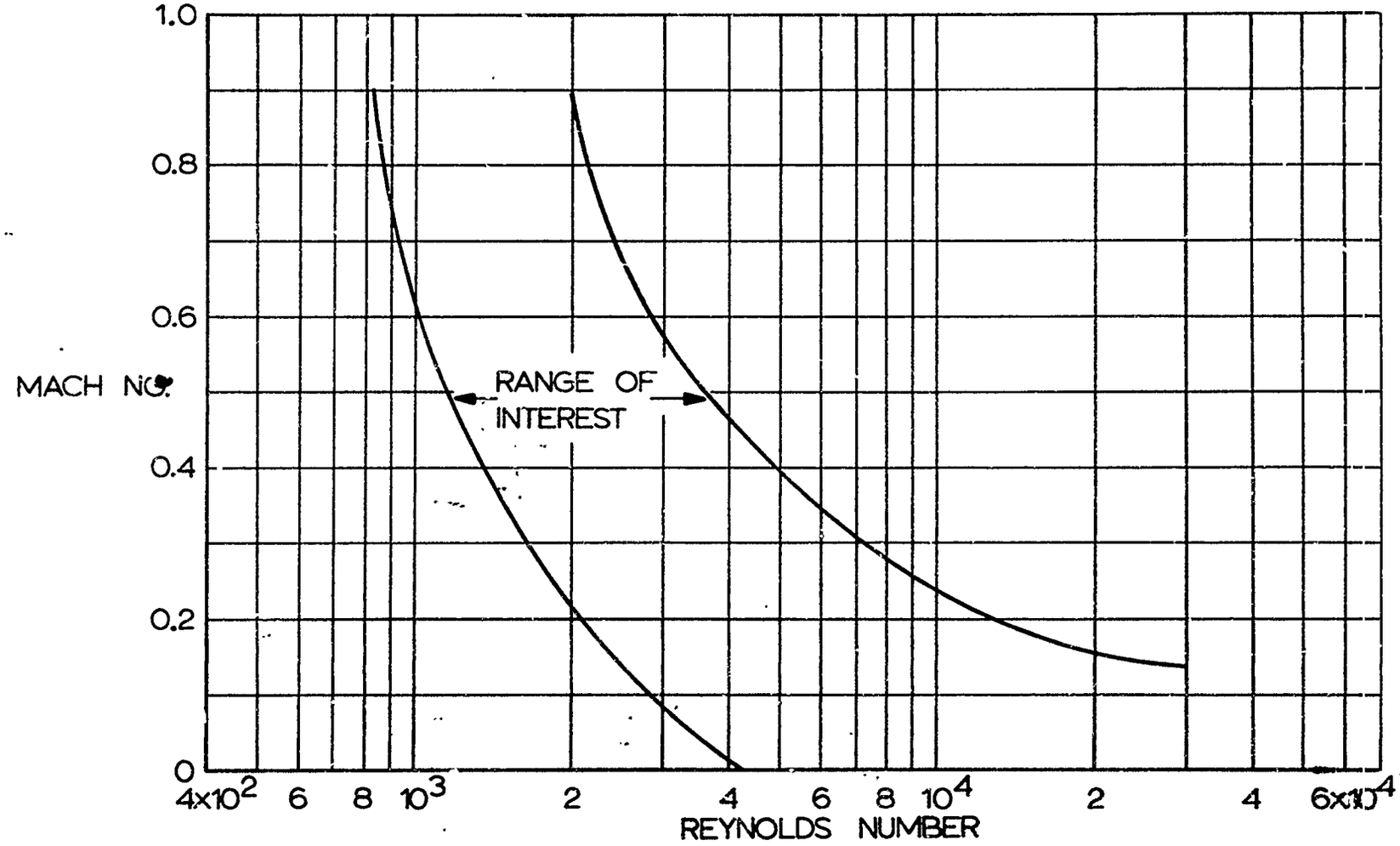


FIG 1. MACH AND REYNOLDS NO REGION OF INTEREST FOR A ROBIN SPHERE

## II. EXPERIMENTAL EQUIPMENT AND TECHNIQUE

### A. Wind Tunnel

The drag studies were conducted in the University of Minnesota continuous flow, variable density, subsonic wind tunnel shown schematically in Fig 2.

A centrifugal compressor capable of producing continuous flow at near critical pressure ratios is used to create test section speeds in the subsonic and transonic range, up to approximately M = 0.93. The velocity in the test section is regulated by means of a control valve located on the outlet side of the compressor.

Velocity surging initially arose in tunnel operations at very low Mach numbers ( $M < 0.1$) because the volumetric flow rate was less than the minimum rated flow of the compressor. To overcome this difficulty, a by-pass was installed to increase the mass flow through the compressor and yet allow the small mass flow required through the test section. This procedure allowed wind tunnel operations at Mach numbers as low as 0.05.

As shown in Fig 2, the wind tunnel incorporates several methods to provide uniform test section flow with minimum turbulence, including a large stilling chamber, long diffuser, and a honeycomb section. In addition, the test section has a return flow channel as shown in Fig 3. Figures 4 and 5 present the dynamic pressure variation of the flow downstream of the 4 inch and 8 inch nozzles, respectively (Fig 6). It is seen that there is less than a two per cent variation of dynamic pressure in the core of flow.

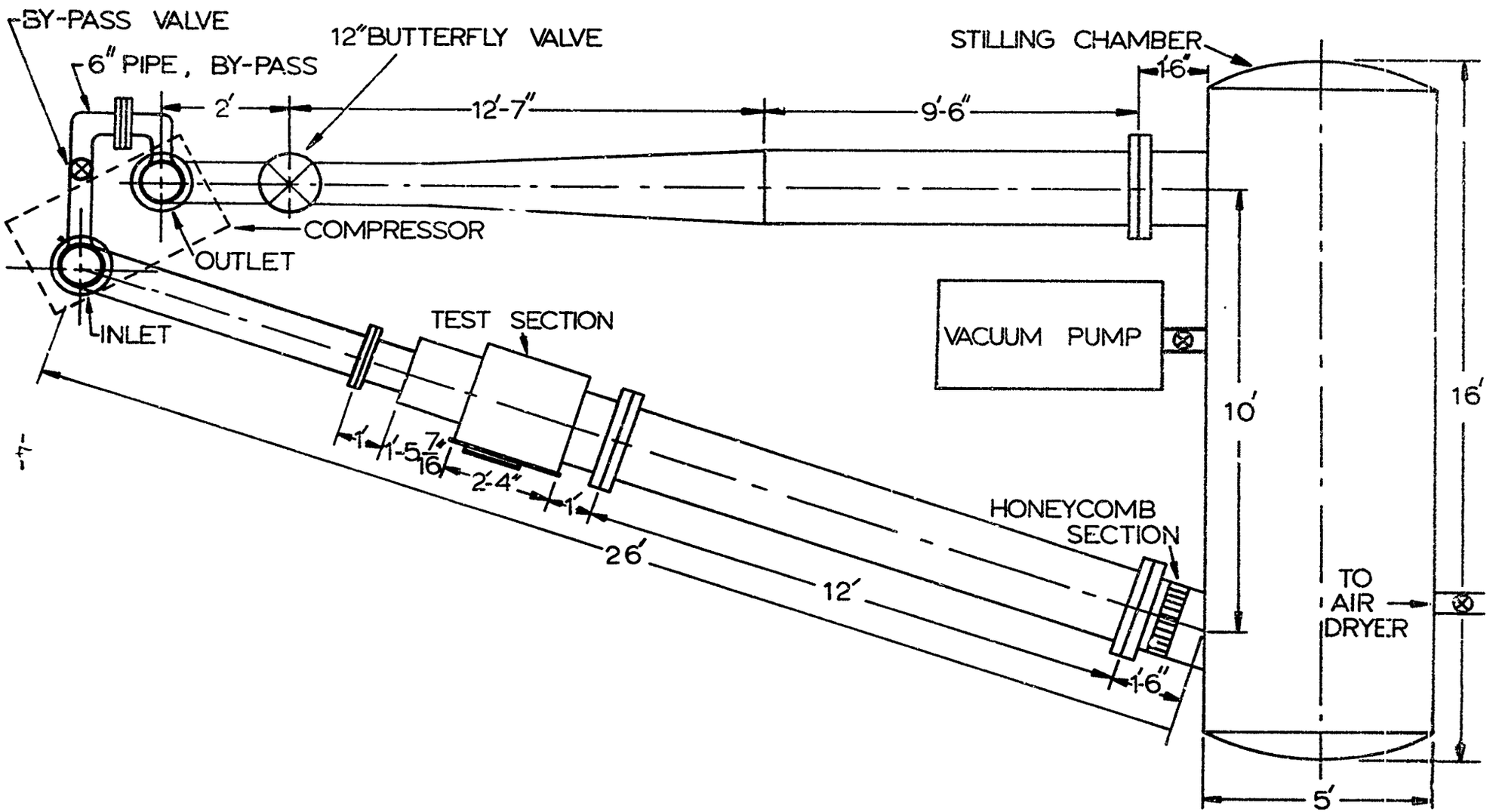


FIG 2A. LOW DENSITY WIND TUNNEL LAYOUT

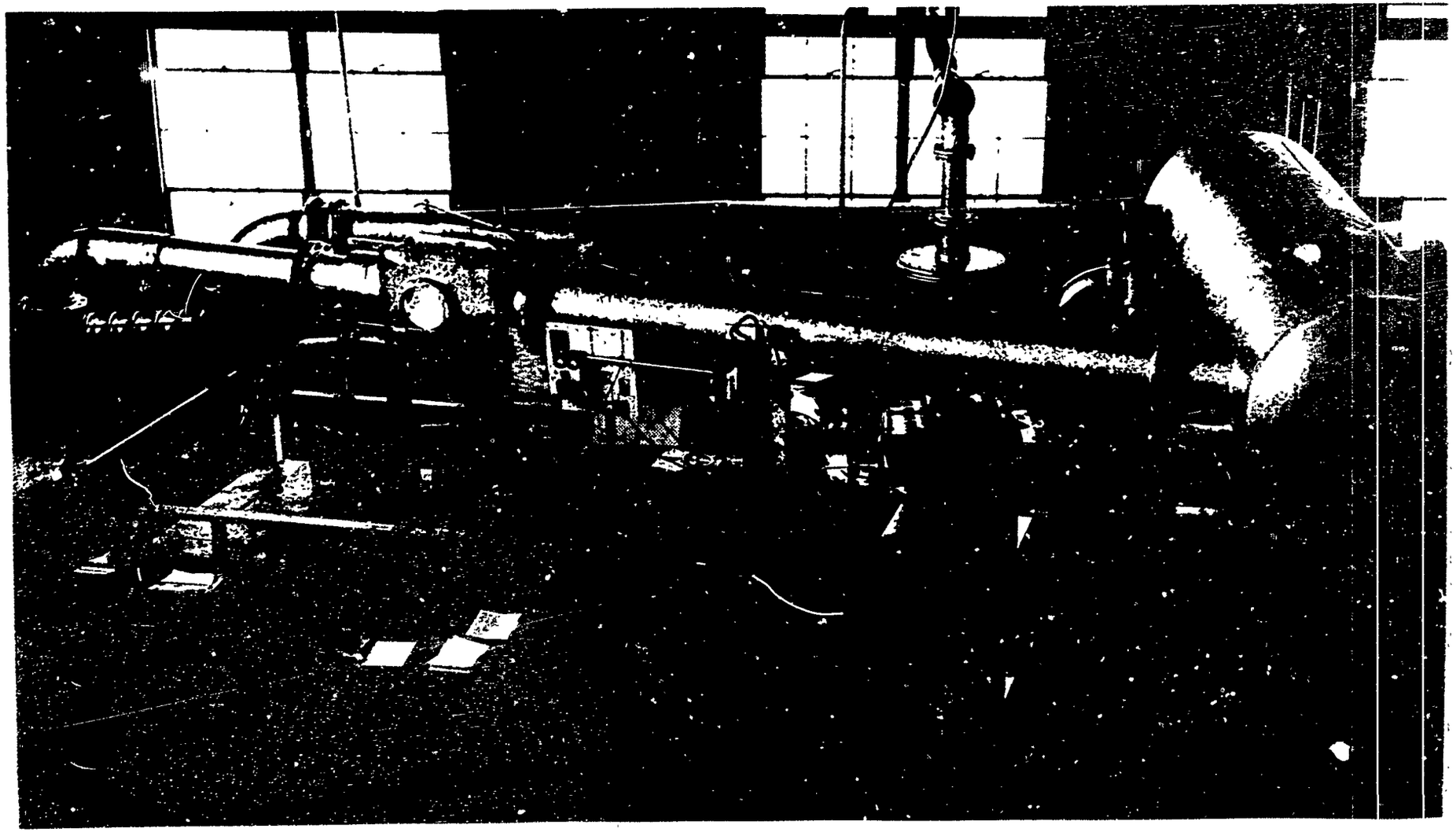

FIG 2b. LOW DENSITY WIND TUNNEL

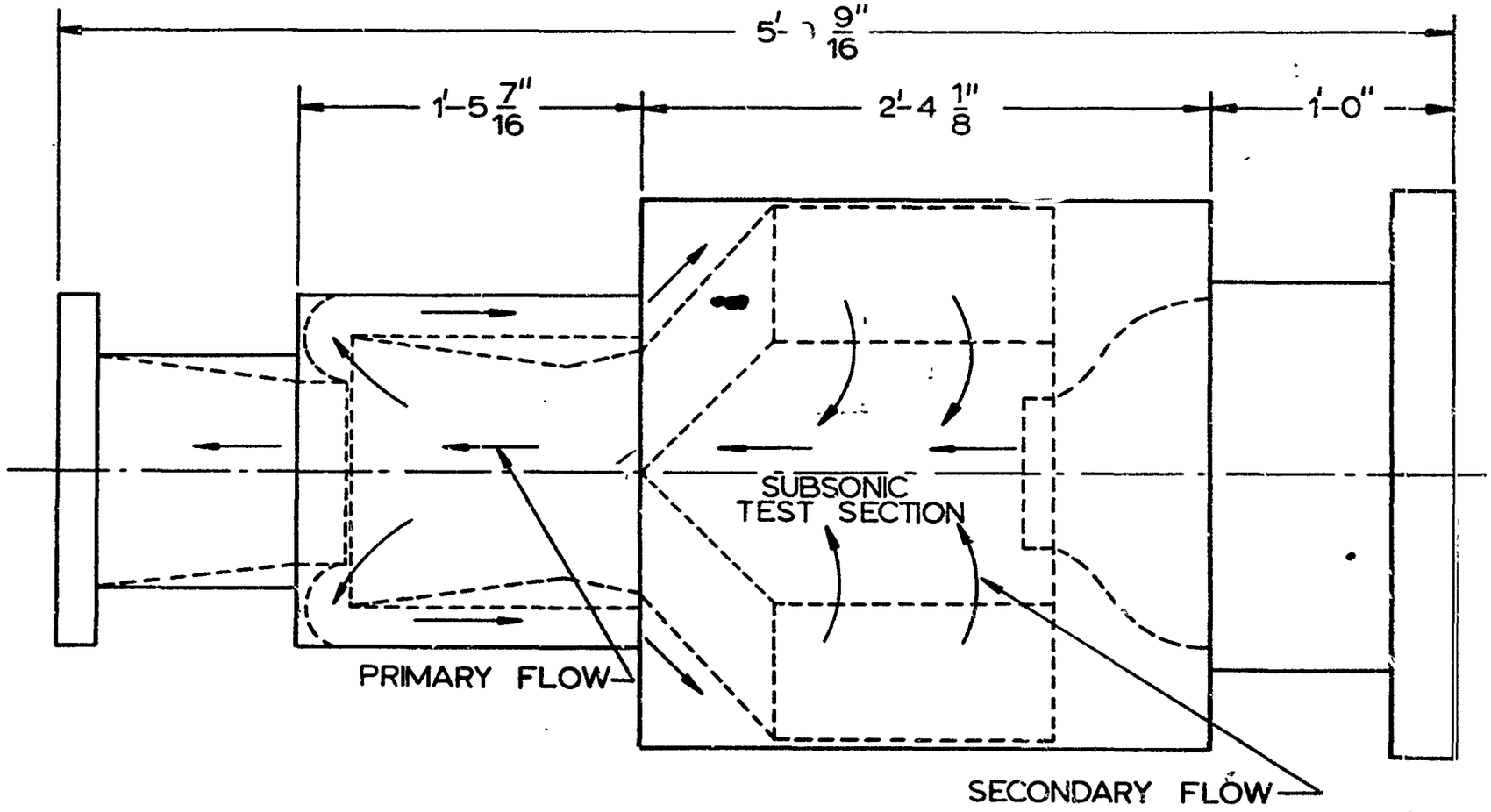


FIG 3. LOW DENSITY WIND TUNNEL TEST SECTION LAYOUT

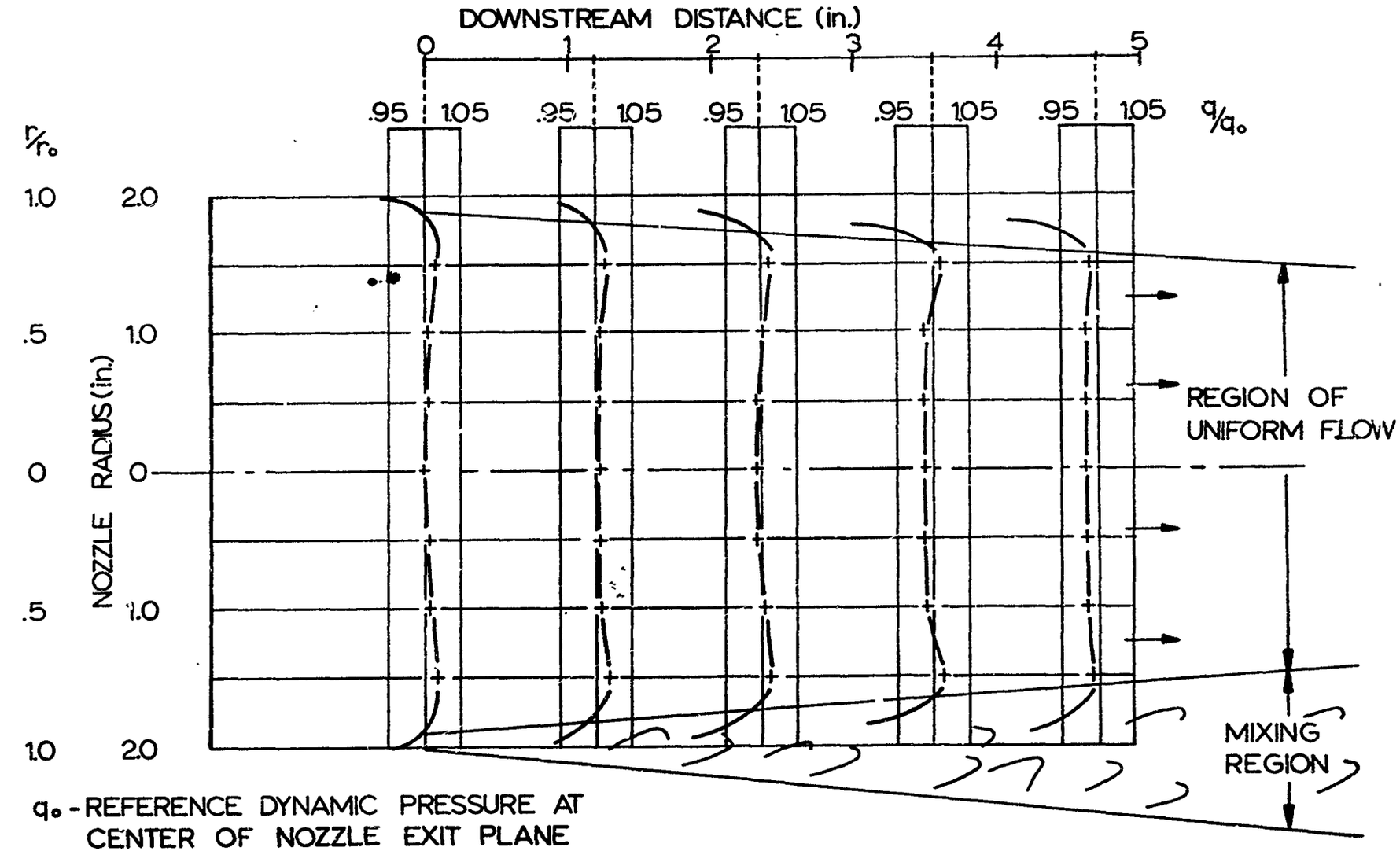


FIG 4. DYNAMIC PRESSURE PROFILE FOR 4" NOZZLE

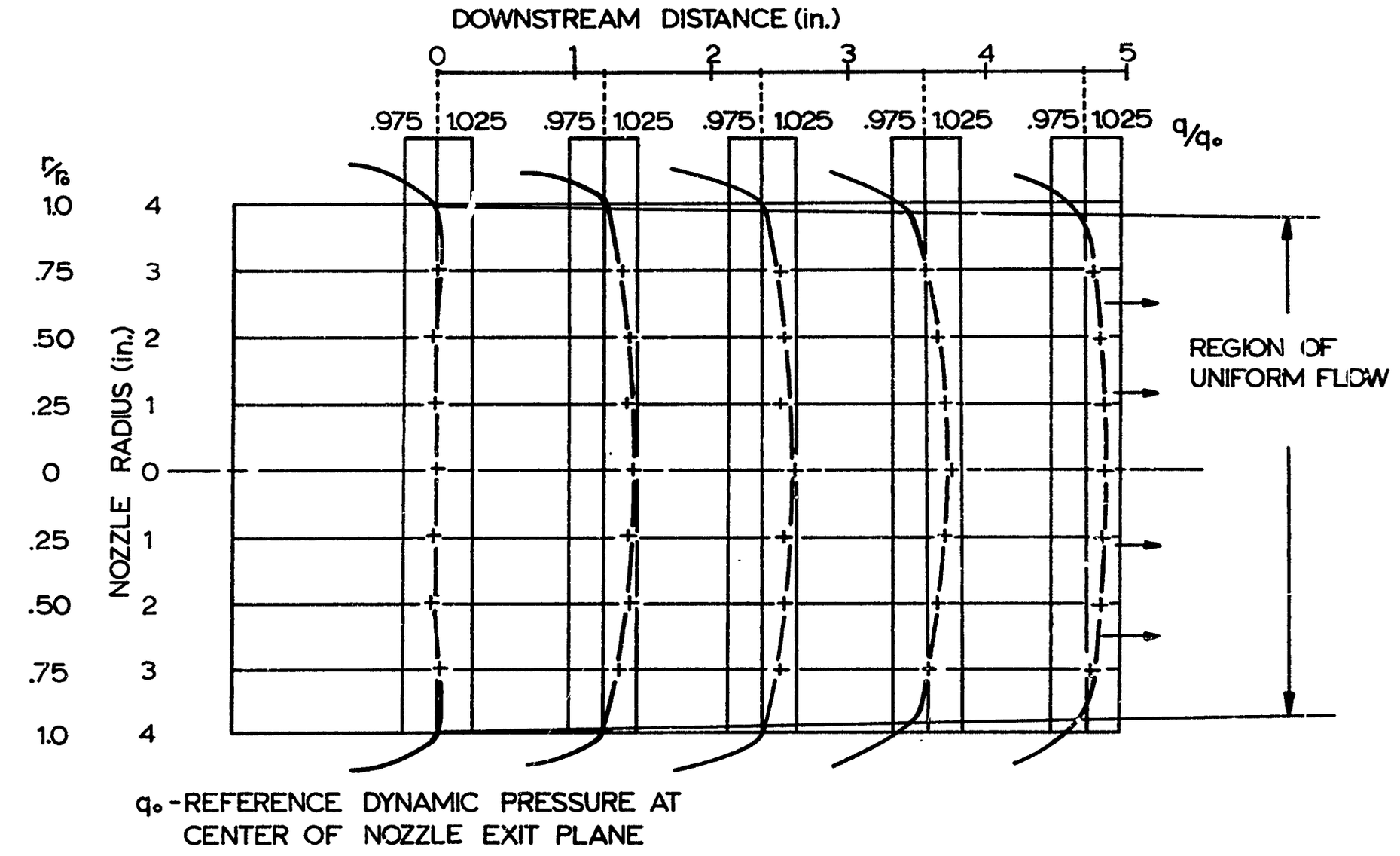


FIG 5. DYNAMIC PRESSURE PROFILE FOR 8" NOZZLE

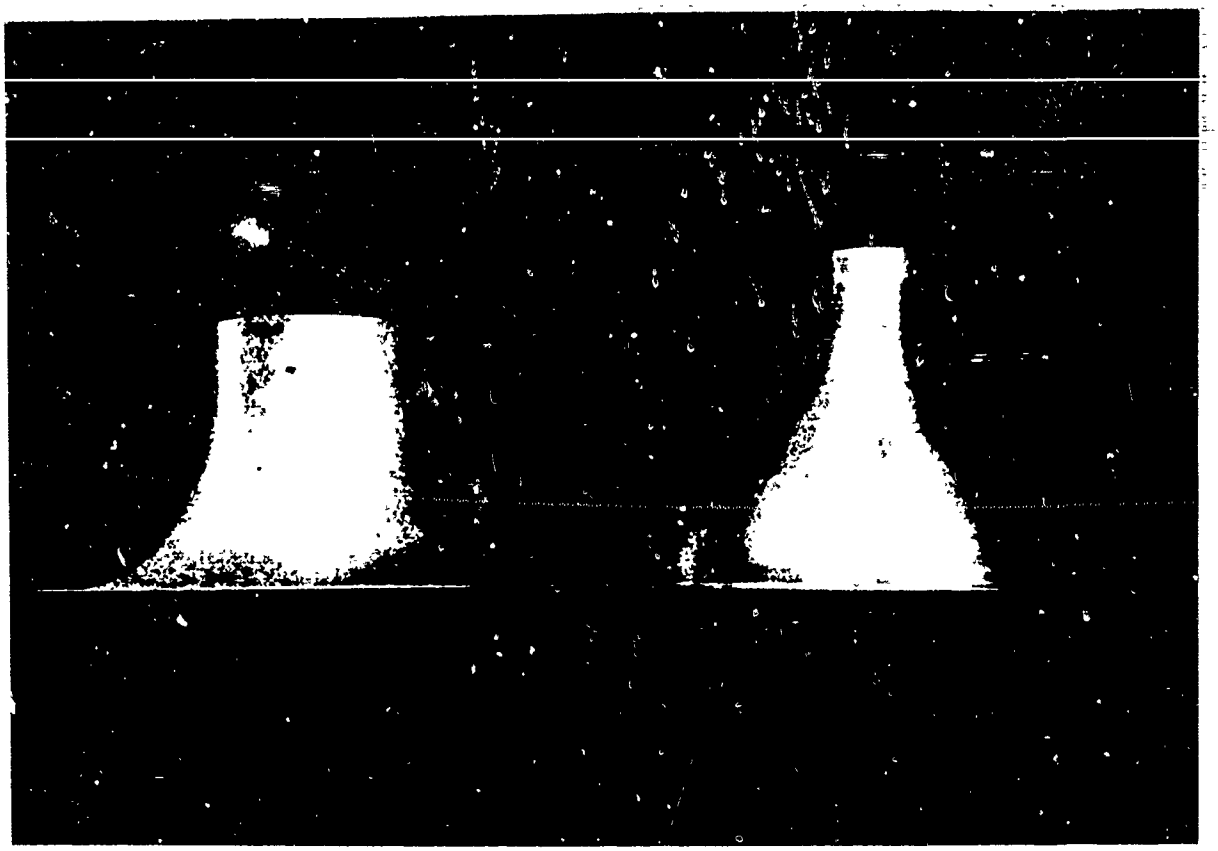

FIG 6. 4 in. AND 8 in. SUBSONIC NOZZLES

FIG 7. LOW DENSITY WIND TUNNEL AIR DRYER

The wind tunnel is equipped with a rotary piston type vacuum pump capable of evacuating at a rate of 850 cfm. With this pump, tunnel static pressure of less than 1 mm Hg are obtained in a few minutes. The duration of test runs at the low pressures was limited by the tunnel leak rate of approximately 1.0 mm Hg/min.

For moisture control an air dryer is used which consists of a 9ft$^3$ bed of Sova Bead dessicant which has a drying capacity of 7040 ft$^3$ of 60% relative humidity air (Fig 7).

The dessicant can be regenerated by an automatically controlled forced hot air unit.

B. Models

The spheres tested were made from nylon, aluminum, and steel. In order to avoid flow blockage and other interference effects the projected area of the model sphere was in all cases held to less than four per cent of the nozzle area. On the other hand the models could not be made too small since, in general, the drag of the support system cannot be measured as accurately as the drag of the entire system. Therefore, the spheres were made large enough that the drag of the support amounted to approximately 10 per cent of the total drag.

With these restraints on model size, it was decided to test spheres ranging from 0.750 in. to 1.500 in. Model tolerances were $\pm$ 0.001 in. on diameter and $\pm$ 0.001 in. on sphericity. Model spheres of 0.75 in. and 1.50 in. are shown in Fig 8 while Fig 9 shows a model suspended in the test section.

ROBIN MODELS

PROJECTED AREA
$12.27 \times 10^{-3} ft^2$

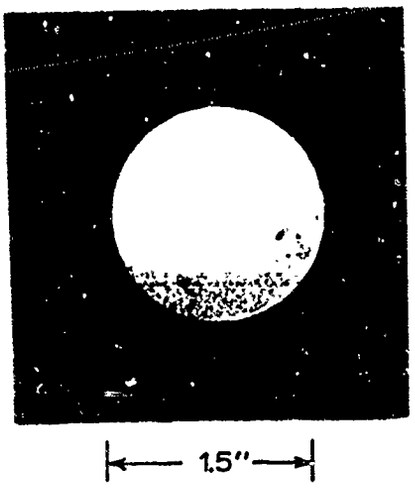


1.5" SPHERE

PROJECTED AREA
$3.068 \times 10^{-3} ft^2$

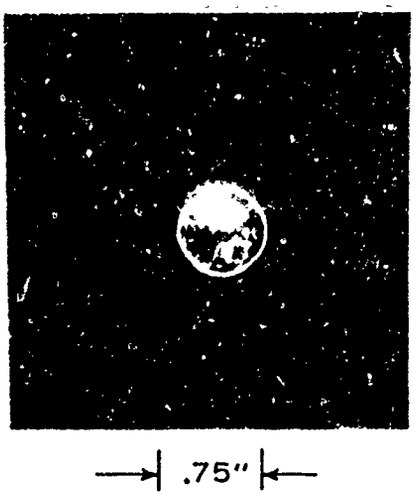


.75" SPHERE

FIG 8. TYPICAL ROBIN SPHERE MODELS

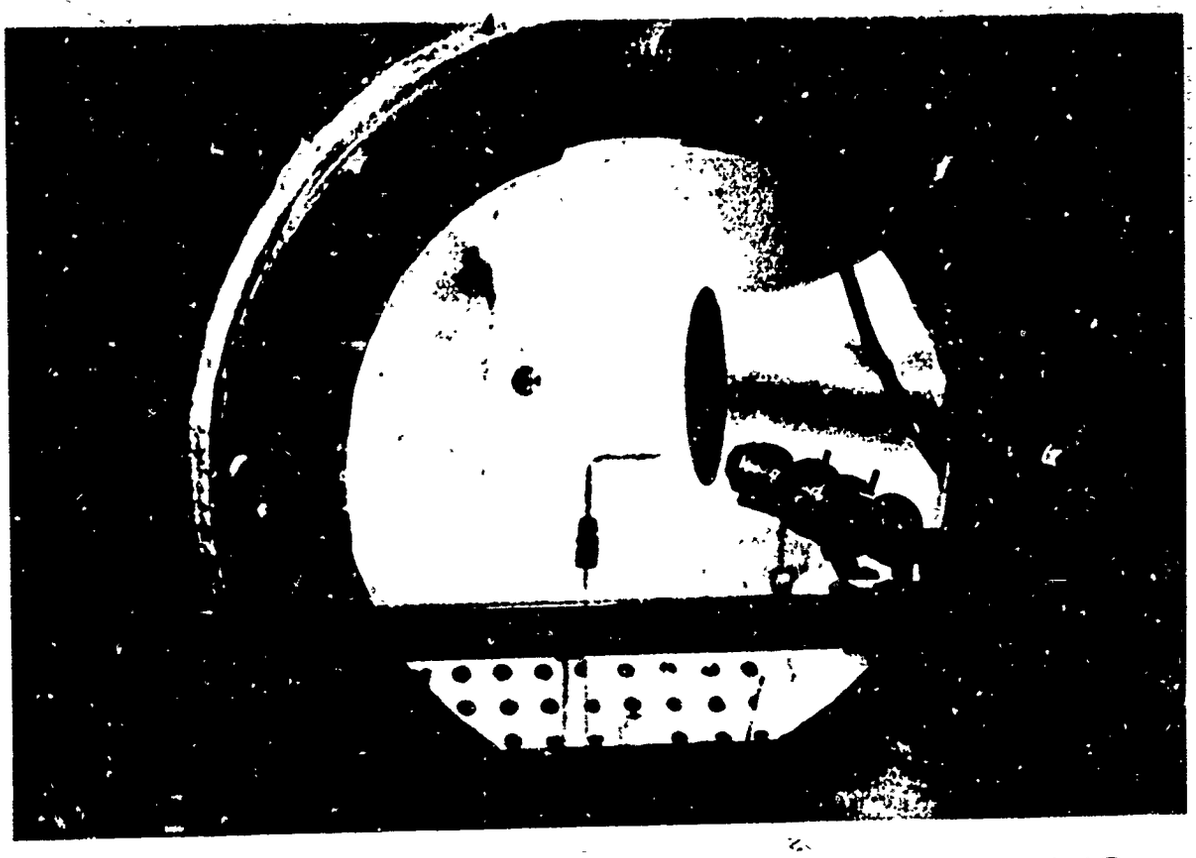

FIG 9. VIEW OF TEST SECTION SHOWING EXPERIMENTAL SET-UP

C. Instrumentation

The determination of drag coefficient, Mach and Raynolds numbers required measurement of total drag, support system drag, dynamic pressure, static pressure, and temperature, all of which, possibly with the exception of the temperature, had to be measured as accurately as possible.

1) Drag Measurements

The drag of the sphere with the suspension wire was determined by the pendulum method as illustrated in Fig 10. The model was freely suspended from two 0.0031 in. diameter wires which were attached to the support systems in the upper part of the test section. Because of this suspension, the sphere was displaced by the aerodynamic force. However, it became apparent that the model must be held in the same position in the flow throughout the tests in order to avoid deviations caused by the slight velocity variation in the downstream direction. This was accomplished by changing the origin of the model support wires and their length with two variable speed reversing motors as seen in Fig 10. The exact model position was maintained through the use of a cathetometer mounted outside the test section window.

After oscillations of the model had damped out, the model support system was moved in order to restore the model to its original position and this displacement was measured directly by an Ames dial gage micrometer. The displacements were used to calculate the aerodynamic drag. The sensitivity

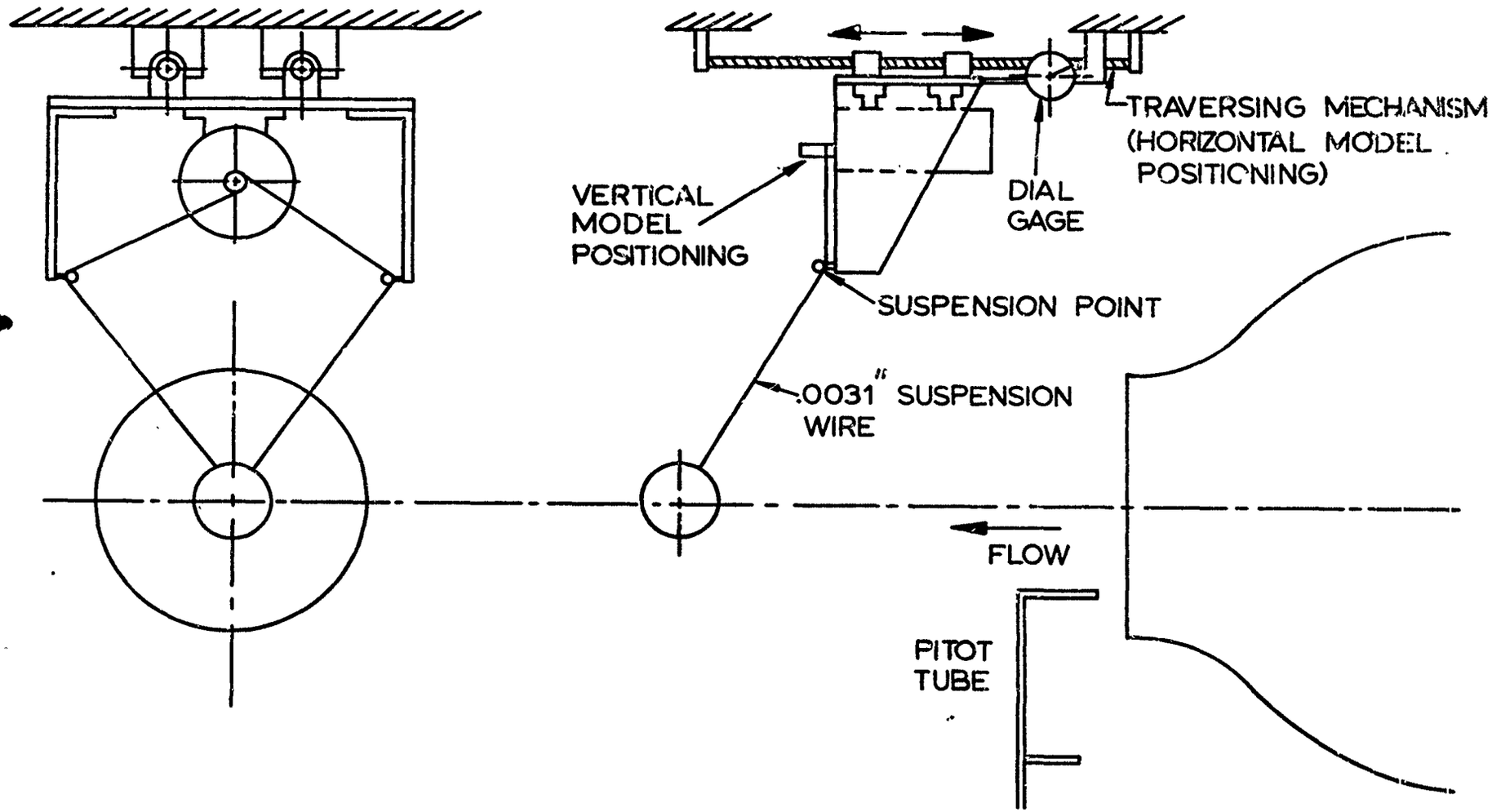


FIG 10. SCHEMATIC LAYOUT OF DRAG BALANCE AND MODEL SUSPENSION SYSTEM

of the system was varied by changing the weights of the spheres used.

A similar method shown in Fig 11 was used to determine the wire drag (model support drag). Again the wire was suspended from a movable support. However, rather than being attached to a sphere, the wire was attached to a small weight enclosed in a hollow sphere filled with a damping fluid. This rigidly mounted hollow sphere merely served to recreate the same flow field as present during the total drag measurements. The enclosed damping fluid reduced wire vibration. The wire and hollow sphere were electrically charged so that contact between the two was detectable. The movement of the support system necessary to eliminate this contact was measured as in the total drag tests.

The sphere drag could now be determined from the condition of the moment equilibrium (see Fig 12). With respect to point 0, equilibrium requires:

$$D(L + r) + D_w(L_w) = W(\Delta X + \delta). \quad (1)$$

About the point P one gets

$$W \cdot \delta = D \cdot r. \quad (2)$$

Combining Eqns 1 and 2,

$$D \cdot L + D_w L_w = W\ (\Delta X). \quad (3)$$

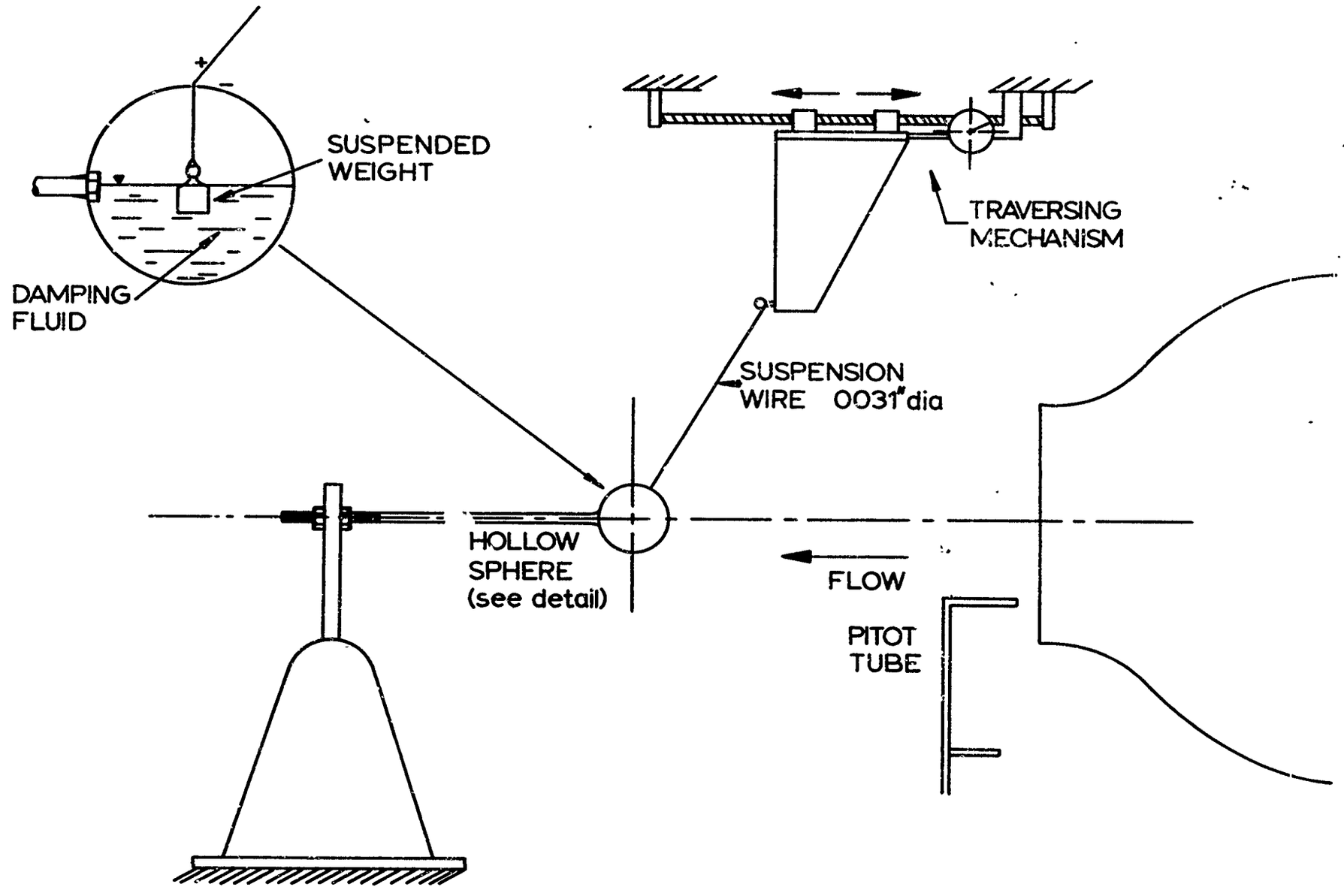


FIG 11. SCHEMATIC LAYOUT OF SUSPENSION WIRE DRAG MEASURING SYSTEM

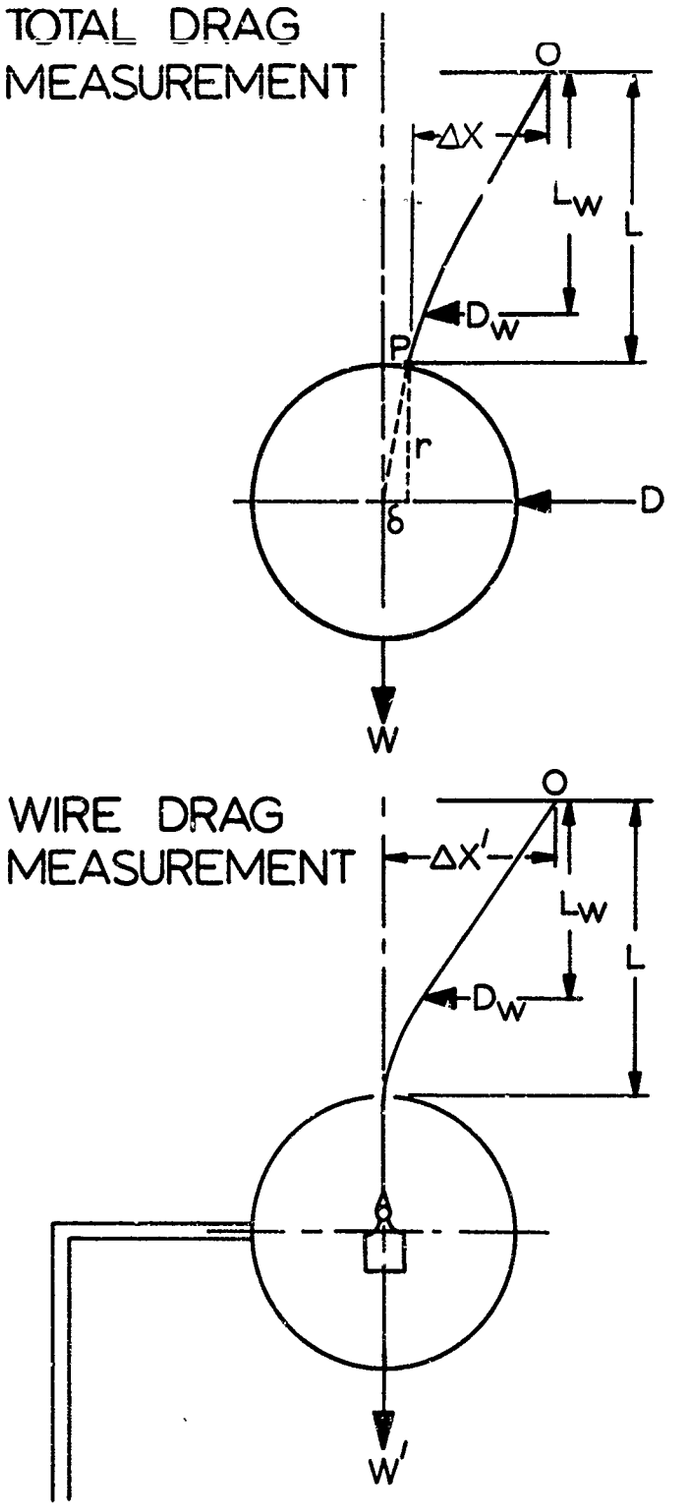


FIG 12. DIAGRAM FOR DEVELOPMENT OF SPHERE DRAG EXPRESSION

The measurement of wire drag provides

$$D_w \cdot L_w = W' \cdot \Delta X' . \qquad (4)$$

Therefore

$$D = \frac{W \cdot \Delta X}{L} - \frac{W' \Delta X'}{L} . \qquad (5)$$

One observes that only the horizontal displacement of the model support is needed to determine the sphere drag.

2) Dynamic Pressure Measurement

The extremely low dynamic pressures of these tests were measured with a pitot-static probe placed near the edge of the core flow just downstream from the nozzle in combination with a Statham differential diaphragm transducer gage using a galvanometer readout system shown schematically in Fig 13. Ordinary liquid manometers were not suitable due to their low sensitivity and the relatively high vaporization pressure of most manometer fluids. The Statham gage provided sufficient accuracy, and was found to have very little calibration drift. Calibration curves for the gage at different bridge sensitivities are shown in Fig 14. As can be seen the curves are linear throughout the entire range.

As mentioned earlier, measurements were made of the

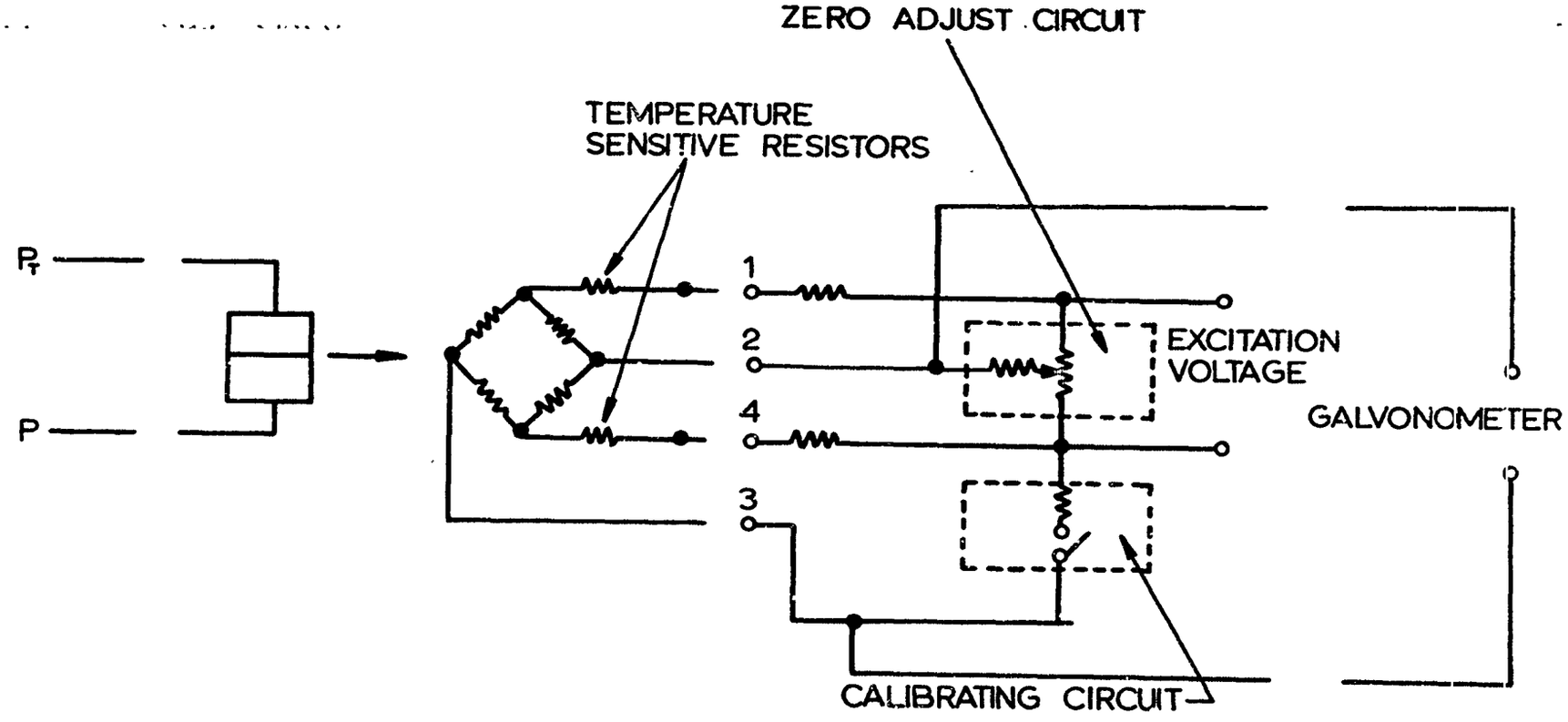


FIG 13A SCHEMATIC AND CIRCUIT DIAGRAM FOR MEASUREMENT OF DYNAMIC PRESSURE

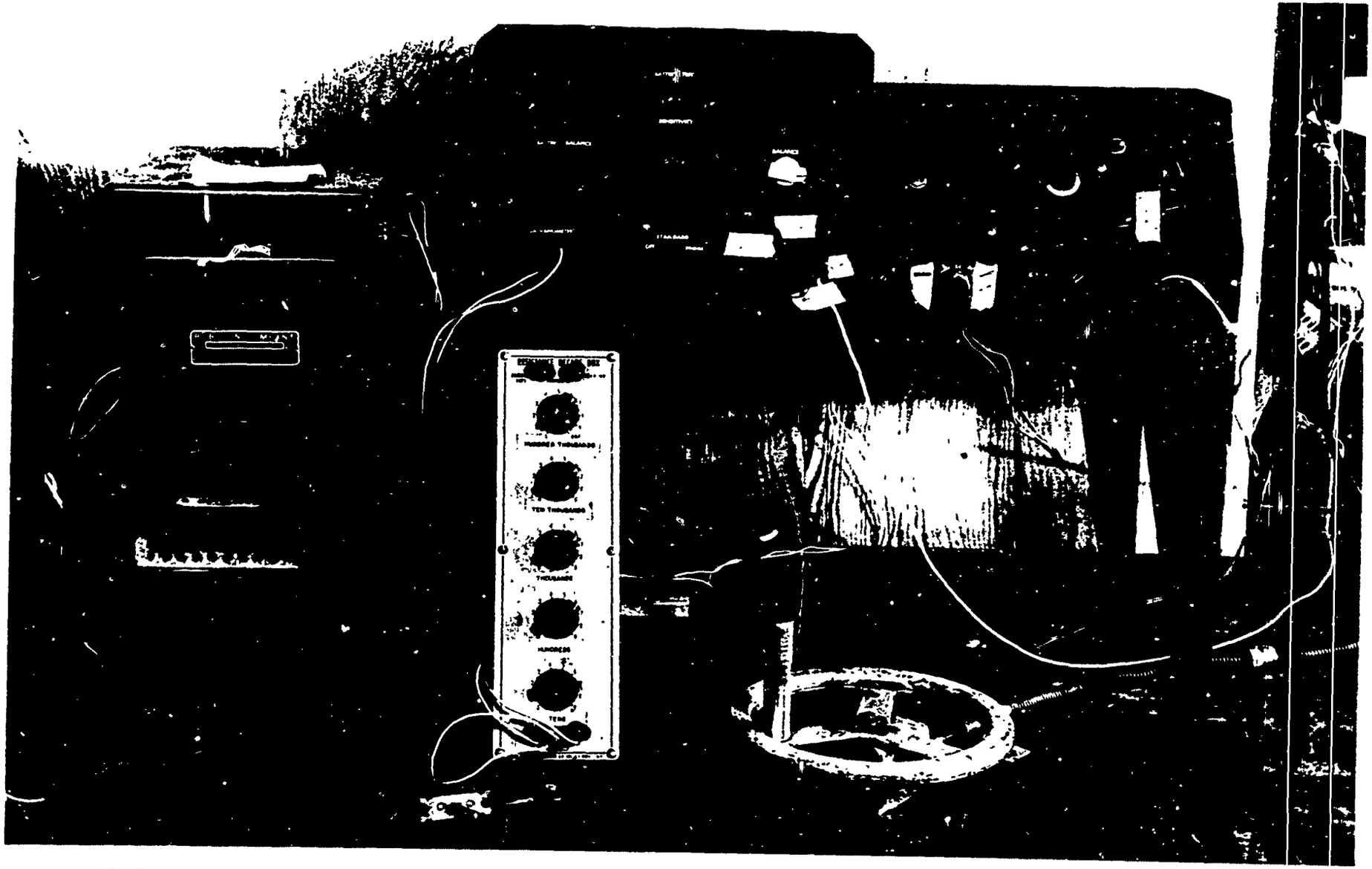

FIG 13b. GALVANOMETERS AND BRIDGE CIRCUITS USED IN THE MEASUREMENT OF DYNAMIC PRESSURE

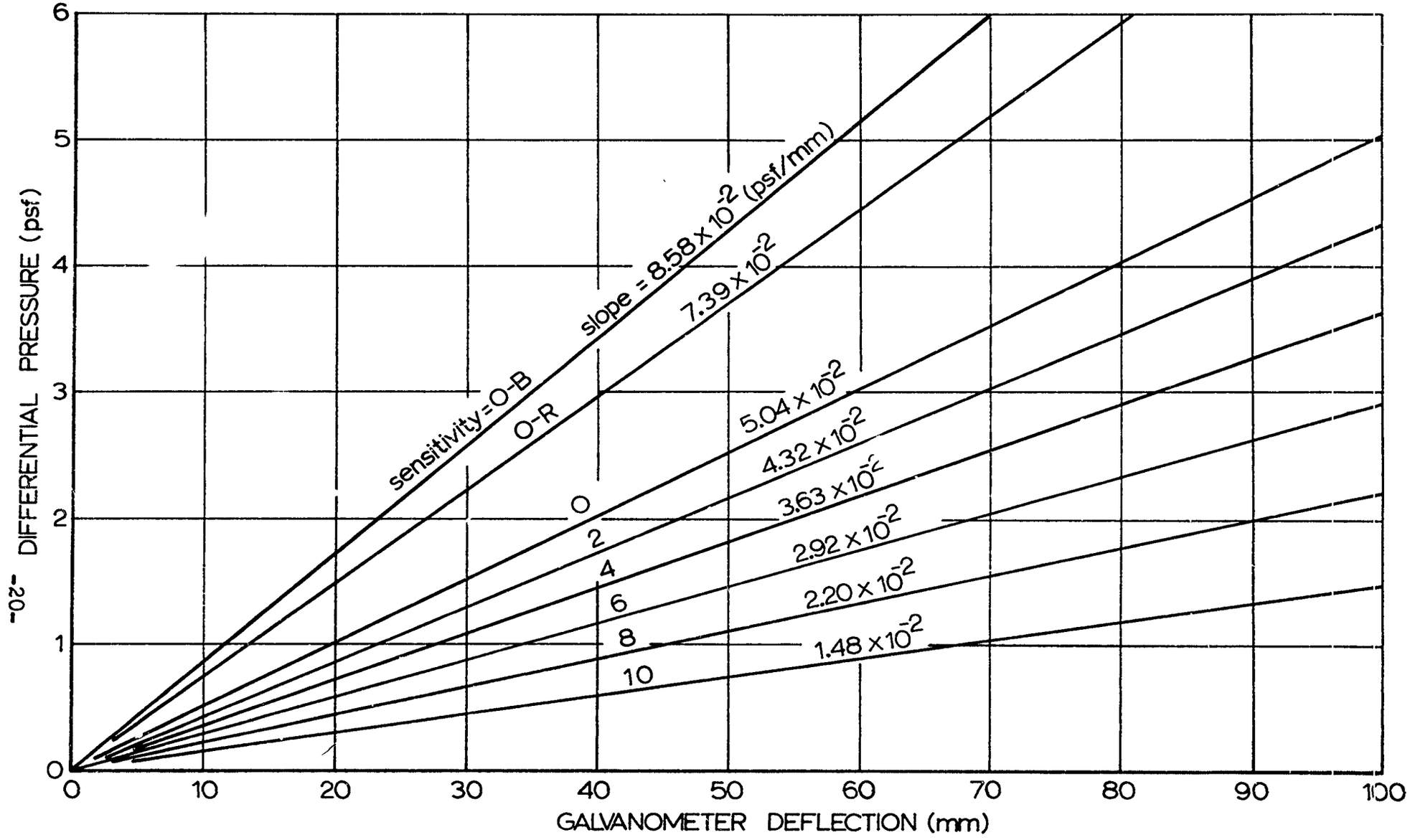


FIG 14. CALIBRATION CURVES FOR .05 psid STATHAM GAGE

dynamic pressure variations across the core flow as presented in Figs 4 and 5. In addition, simultaneous measurements of the dynamic pressures at the probe position and at the stagnation point of the model were made. A small variation was found, and a correction factor was established for each Mach number condition to be used in the calculations. It was found that the correction factor is not constant with pressure at the higher Mach numbers thus a variable correction factor was applied to the calculation of dynamic pressure.

3) Static Pressure Measurement

To cover the full range of static pressures necessary in the tests, two static pressure gages were used. For static pressures above 20 mm Hg, an ordinary differential mercury manometer was used. The evacuated side provided a zero pressure reference level, with the scale adjusted according to changes in atmospheric pressure. Static pressures below 20 mm Hg were measured with a more sensitive Dubrovin gage (Fig 15).

The static pressure probe was located at the top of the test section. No measurable variation in static pressure was found between this position and the static pressure measured in free stream flow.

4) Temperature Measurement.

The static temperature of the flow was measured with a radiation shielded themocouple located in the test section, with direct readout obtained using a Brown Recorder (Fig 16).

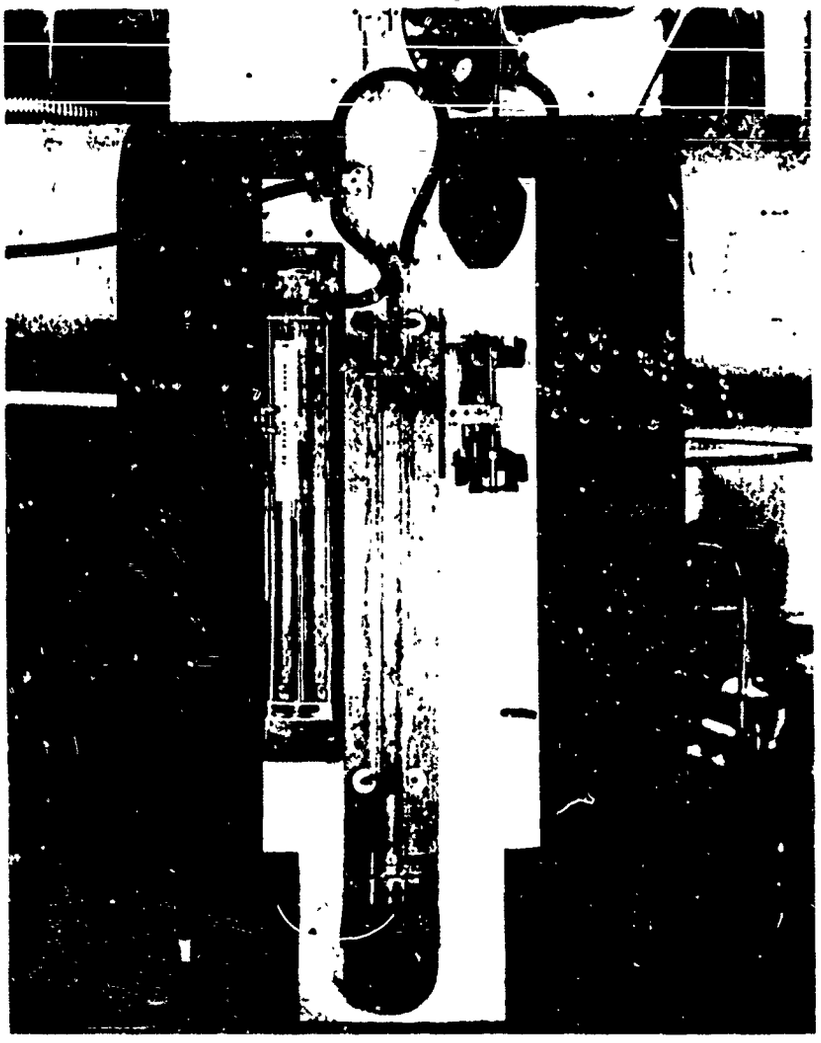

FIG 15. DUBROVIN GAGE AND MERCURY MANOMETER USED FOR STATIC TEMPERATURE MEASUREMENT

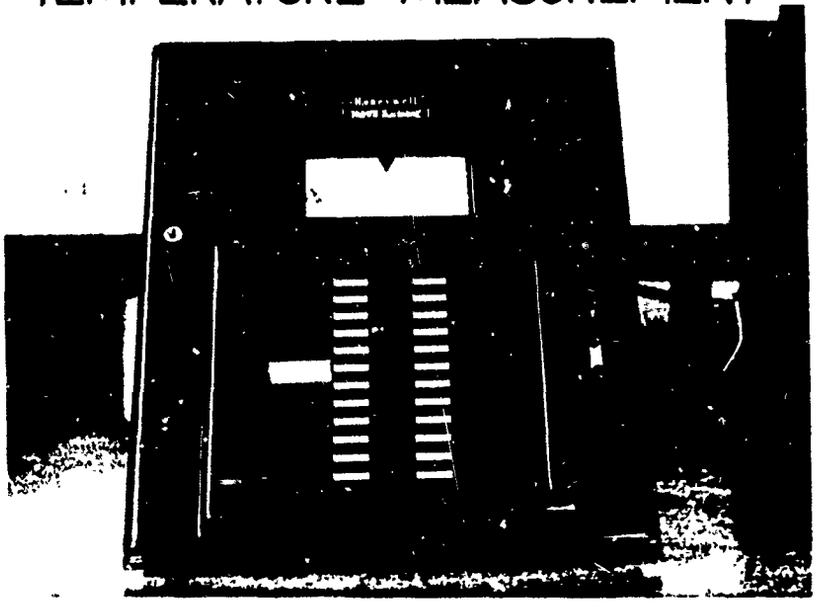

FIG 16. BROWN RECORDER USED FOR TEMPERATURE MEASUREMENT

At the low operating densities involved there is only little frictional heating in the flow resulting in a small temperature variation from room temperature throughout the wind tunnel, thus eliminating the need for an obstructing probe in the core flow. Furthermore, temperature is not one of the critical measurements, entering only in the calculation of Reynolds numbers.

D. Experimental Procedure

The test procedure necessary to obtain the required data was to keep the Mach number constant during a test sequence while varying the Reynolds number through the required range. With the tunnel evacuated to the lowest required static pressure, the compressor control valve was adjusted to give the desired Mach number. When steady state conditions were reached, readings of model deflection, dynamic pressure, static pressure, and temperature were taken simultaneously by two observers. For each data point, this procedure was repeated up to 15 times in order to obtain very reliable average values.

Air was then bled into the system until the next higher static pressure (Reynolds number) was obtained. Since the Mach number varies slightly with static pressure, a slight readjustment of the control valve was necessary. When steady static conditions were reached, readings were taken. This process was repeated over the entire static pressure range. A sample run sheet is shown in Fig 17.

ROBIN SPHERE  4" NOZZLE  DATE: DEC. 15, 1961

M= .750

3/4" STEEL SPHERE

WT.= 28.073 gm.  L = 1398 cm.

| P mm Hg | ΔP mm defl. | SENS. | X (inches) | T(°F) | REMARKS |
|---|---|---|---|---|---|
| | | | $X_o$ = 1.913 | | |
| 2.20 | 96.5 | 6 | 1.525 | 84 | |
| 2.80 | 95.7 | 4 | 1.439 | 84 | |
| 3.30 | 95.2 | 2 | 1.340 | 84 | |
| 3.90 | 97.0 | 0 | 1.232 | 85 | |
| 4.40 | 64.5 | 0-B | 1.164 | 85 | |
| 5.00 | 72.5 | 0-B | 1.069 | 84 | |
| | | | | | |
| | | | $X_o$= 1.913 | | |

FIG 17. SAMPLE RUN SHEET

## III. RESULTS

### A. Method of Calculation

A sample calculation sheet is shown in Fig 18. The methods of calculation used to obtain the drag coefficient, $C_D$, Mach number, and Reynolds number are given in the following paragraphs.

The drag coefficient is defined in the usual manner as

$$C_D = \frac{D}{qS} \tag{6}$$

where D = model drag

q = dynamic pressure

S = model projected area.

The drag of the sphere was given in Equation 5 in terms of measured quantities. In subsonic and transonic flow the dynamic pressure is

$$q = \frac{1}{2}\rho V^2 = \frac{P_T - P}{1 + \frac{M^2}{4} + \frac{M^4}{40} + \frac{M^6}{1600} + \cdots} \tag{7}$$

where $P_T - P = \Delta P$= measured differential pressure, and the denominator represents the Mach factor. In this study, the NACA 1135 tables were used to find $q/P_T$ from the pressure ratio $P/P_T$.

The Mach number was read from the NACA 1135 tables

$C_D = \frac{D}{QS}$ $\quad Q = \frac{Q}{P_T} P_T$ $\quad D = \frac{W}{}$

| 1 RUN NO | 2 P (mm galvo defl.) | 3 SENS | 4 P (PSF) 2 x Slope | 5 P (mm Hg) | 6 P (PSF) 5 x 2.783 | 7 $P_T$ (PSF) 4 + 6 | 8 $P/P_T$ 6/7 | 9 M | 10 $Q/P_T$ NACA REPORT 1135 | 11 Q (PSF) 7 x 1( |
|---|---|---|---|---|---|---|---|---|---|---|
| 6 | 96.5 | 6 | 2.817 | 2.20 | 6.123 | 8.940 | .6849 | .7557 | .2738 | 2.448 |
| 6 | 95.7 | 4 | 3.474 | 2.80 | 7.792 | 11.27 | .6910 | .7463 | .2694 | 3.035 |
| 6 | 95.2 | 2 | 4.117 | 3.30 | 9.184 | 13.30 | .6905 | .7471 | .2697 | 3.587 |
| 6 | 97.0 | 0 | 4.891 | 3.90 | 10.85 | 15.75 | .6894 | .7488 | .2705 | 4.259 |
| 6 | 64.5 | 0-B | 5.532 | 4.40 | 12.25 | 17.78 | .6888 | .7497 | .2710 | 4.818 |
| 6 | 72.5 | 0-B | 6.218 | 5.00 | 13.92 | 20.13 | .6912 | .7460 | .2692 | 5.420 |

STATHAM GAGE CALIBRATION SLOPES

| Sensitivity | Slope ($10^{-2}$ psf/mmhg) |
|---|---|
| 0-B | 8.577 |
| 0-R | 3.390 |
| 0 | 5.043 |
| 2 | 4.325 |
| 4 | 3.630 |
| 6 | 2.920 |
| 8 | 2.190 |
| 10 | 1.476 |

(FIG 18) FIG 18

(FIG 1

$D = \frac{W}{L}\frac{X}{\quad} - \frac{W'}{L}\frac{X'}{\quad}$ Re =

| 11 Q (PSF) 7 x 10 | 12 $QS_3$ ($10^{-3}$ lbs) | 13 $X_o$ (IN) | 14 X (IN) | 15 $\Delta X$ (IN) 13 − 14 | 16 L (IN) | 17 W/L ($10^{-3}$ lb/in) | 18 $\frac{W\Delta X}{I}$ ($10^{-3}$ lb) 15 − 17 | 19 $\frac{W'X'}{L}$ ($10^{-3}$ lb) Wire Drag |
|---|---|---|---|---|---|---|---|---|
| 2.448 | 7.510 | 1.913 | 1.525 | 0.388 | 5.504 | 11.244 | 4.363 | .483 |
| 3.035 | 9.311 | 1.913 | 1.439 | 0.474 | 5.504 | 11.244 | 5.370 | .56 |
| 3.587 | 11.01 | 1.913 | 1.340 | 0.573 | 5.504 | 11.244 | 6.443 | .562 |
| 4.259 | 13.07 | 1.913 | 1.232 | 0.681 | 5.504 | 11.244 | 7.660 | .642 |
| 4.818 | 14.78 | 1.913 | 1.164 | 0.749 | 5.504 | 11.244 | 8.422 | .732 |
| 5.420 | 16.63 | 1.913 | 1.069 | 0.844 | 5.504 | 11.244 | 9.490 | .805 |
| | | | | | | | | .869 |

CONVERSION FACTORS

1 in = 2.34 cm

1 mmHg = 2.783 psf

1 in Hg = 70.66 psf

1 gm = $2.2046 \times 10^{-3}$ lb

* from $\mu = 2.27 \frac{T^{3/2}}{T + 198.6} \times 10^{-8} \frac{\text{lb-sec}}{\text{ft}^2}$

(FIG 18)

SAMPLE CALCULATION SHEET

-26-a(Continued)

(FIG 18)

$$Re = \frac{MPK}{\mu\sqrt{T}}$$

$$K = \sqrt{\frac{\gamma}{R}}\, d$$

| 19 $\frac{W' X'}{i}$ ($10^{-3}$ lb) Wire Drag | 20 D ($10^{-3}$ lb) 18 - 19 | 21 $C_D$ 20/12 | 22 | 23 T ($^oF$) | 24 T ($^oR$) 460 +23 | 25 $\mu\sqrt{T}$ x $10^8$ * | 26 M.P $6 x_9$ | 27 MPK $x_3$ $10^3$ k x 26 | 28 Re 27/25 |
|---|---|---|---|---|---|---|---|---|---|
| .483 .56 | 3.880 | .5167 | | 84 | 544 | 904.3 | 4.627 | 8.259 | 913 |
| .562 | 4.868 | .5228 | | 84 | 544 | 904.3 | 5.817 | 10.38 | 1148 |
| .642 | 5.801 | .5271 | | 84 | 544 | 904.3 | 6.861 | 12.25 | 1354 |
| .732 | 6.926 | .5300 | | 85 | 545 | 906.7 | 8.127 | 14.51 | 1600 |
| .805 | 7.617 | .5153 | | 85 | 545 | 906.7 | 9.180 | 16.38 | 1807 |
| .869 | 8.521 | .5124 | | 84 | 544 | 904.3 | 10.38 | 18.53 | 2049 |

CONSTANTS

$\gamma = 1.4$

$R = 1716\ ft^2/sec^2\ ^oR$

$\sqrt{\gamma/R} = 0.02856$

$d = 0.75\ in = 0.0625\ ft$

$S = \frac{\pi d^2}{4} = 3.068 \times 10^{-3}\ ft^2$

$W = 28.073\ gm = 0.06189\ lb$

$k = \sqrt{\gamma/R}(d) = 1.785 \times 10^{-3}$

(FIG 18)

-26-b (Completed)

for each value of $P/P_T$ obtained above.

The Reynolds number is $$R_e = \frac{\rho V d}{\mu} , \tag{8}$$

where d= model diameter

V= velocity

$\rho$= density

$\mu$= viscosity.

Inserting the perfect gas law,

$$\rho = \frac{P}{RT} , \tag{9}$$

and the Mach number relationship,

$$V = M \cdot a , \tag{10}$$

the Reynolds number is then given as

$$R_e = \left(\frac{P}{RT}\right)(M \cdot a)\frac{d}{\mu} . \tag{11}$$

With

$$a = \sqrt{\gamma RT} , \tag{12}$$

the Reynolds number is

$$R_e = \frac{P \cdot M \cdot d}{\mu\sqrt{T}}\sqrt{\frac{\gamma}{R}} . \tag{13}$$

In this equation, the factor $d\sqrt{\frac{\delta}{R}}$ is a constant, P has been measured, $\mu\sqrt{T}$ is a function of temperature which was tabulated for the required range, and M can be calculated as above.

B. Discussion of Results

Figure 19 presents the drag coefficient of the sphere as a function of Reynolds number with Mach number as a parameter. A larger size of the same plot with an extension to connecting data is contained in Appendix A of this report as Fig A-1. It can be seen that all curves have a common trend. There is only a small variation of $C_D$ with Reynolds number while the effect of Mach number becomes increasingly important as the Mach number itself increases.

For the Reynolds number range presented in this report, only data in the incompressible flow regime was found in literature. For example, the drag coefficients related to velocities of $M \leq 0.39$ which were established in this study, can be compared with those of Ref 7. Both sets of data seem to agree perfectly with each other. No source was found that would give comparable data for higher Mach numbers in this Reynolds number range. Reference 6 shows drag coefficients of spheres in the same Mach number range but for higher Reynolds numbers. This data is shown in Fig A-1, Appendix A and seems to be in agreement with those obtained in this study.

A possible effect of importance, which may influence

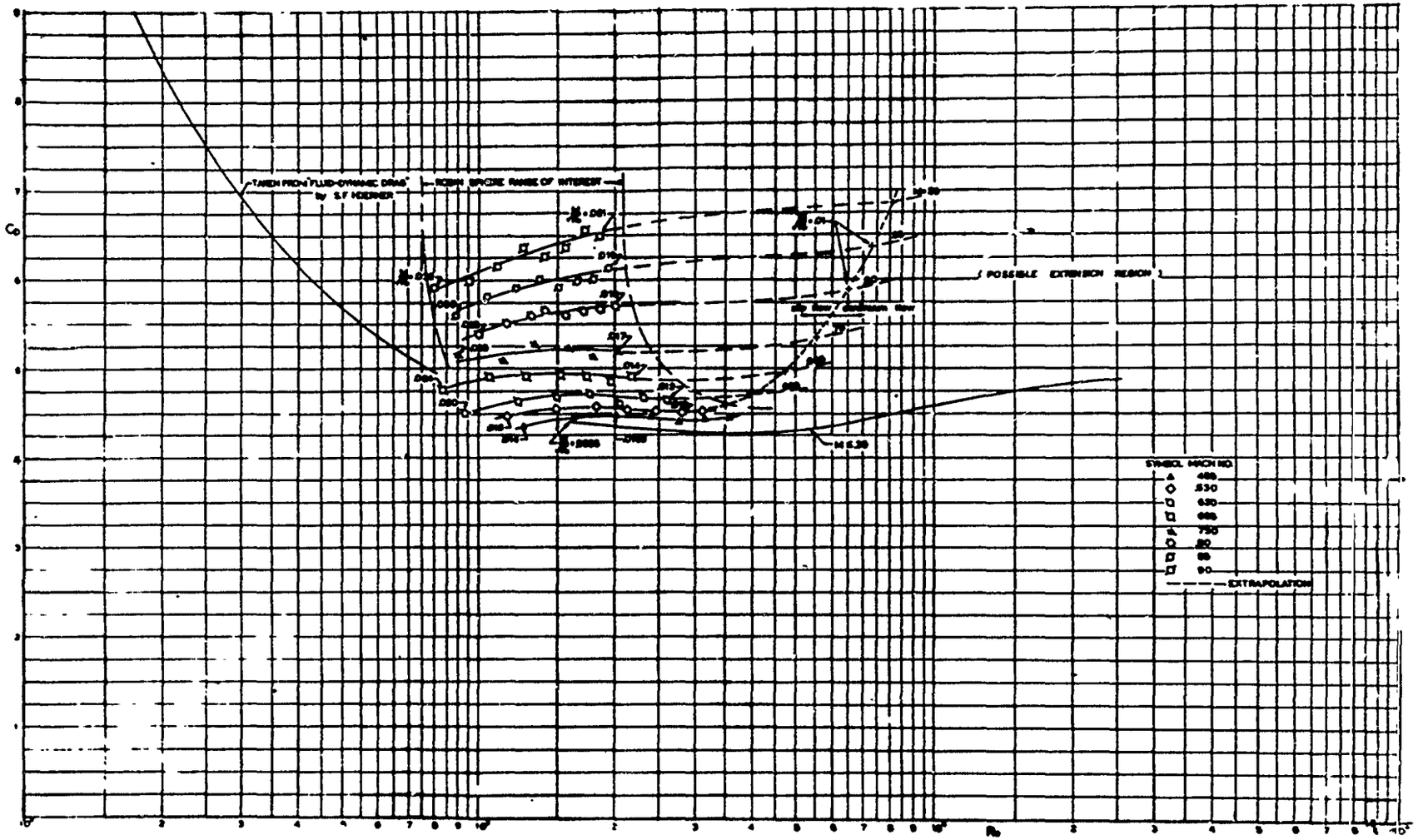


FIG 19. DRAG COEFFICIENT OF A SPHERE AT VARIOUS Re

the higher Mach number range is that of rarified gas phenomena. The transition point from continuum to slip flow is usually given at $M/\sqrt{Re} = 0.01$, and from Fig 19, it can be seen that many of the drag coefficients are located between the characteristic numbers of $0.01 \leq M/\sqrt{Re} \leq 0.032$. The slip flow effect will certainly become more noticeable when the region of interest of the ROBIN sphere should be extended into higher speed and lower density regions.

# IV. ERROR ANALYSIS*

## A. Analytical Method

The results of physical measurements incorporate errors which may be broadly classified as Random and Instrument errors.

Random errors arise from the faulty reading of instruments. These are also referred to as "round off" errors since it is assumed to be impossible to read this instrument to an accuracy greater than one-half of the minimum division of its scale, and the operator usually rounds off the instrument reading to one-half of the smallest division (e.g., if the smallest division is one millimeter, the operator can read the instrument to only one-half of a millimeter accurately).

The instrument errors are inherent in the instrument, and are usually established by the manufacturer.

The purpose of this analysis will be to obtain an upper estimate of the possible errors characteristic for established drag coefficient of a sphere as shown in Fig 19.

The derivation of the error equations is presented in Appendix B.

In this section, the results are only repeated for a discussion of the important terms.

---

* Mr. Lawrence W. Rust, Research Fellow, University of Minnesota, was instrumental in the establishment of this chapter.

From Appendix B, the error equations for the drag coefficient, and the Reynolds and Mach number are respectively:

$$\left[\frac{\delta C_D}{C_D}\right]_{MAX.} = \frac{\delta W}{W} + \frac{\delta \Delta X}{\Delta X} + \frac{2\delta d}{d} + \frac{\delta \Delta P}{\Delta P} + \frac{\delta L}{L} + \frac{\Delta X' \delta W'}{\Delta X W} + \frac{W' \delta \Delta X'}{W \Delta X}$$

$$\left[\frac{\delta Re}{Re}\right]_{MAX.} = \frac{1}{2}\left[\frac{\delta P}{P} + \frac{\delta \Delta P}{\Delta P}\right] + \frac{\delta d}{d} + \left[2 - \frac{T}{T+198.6}\right]\frac{\delta T}{T}$$

$$\left[\frac{\delta M}{M}\right]_{Max.} = \frac{1}{2}\left[\frac{\delta P}{P} + \frac{\delta \Delta P}{\Delta P}\right] .$$

The error in W and W' is less than 0.05%. Therefore, these terms have been neglected in the following efforts.

In order to find the total drag coefficient error one must also consider the error in $C_D$ induced by Mach and Reynolds number error. For this analysis we use:

$$\left.\frac{\delta C_D}{C_D}\right|_M = \left(\frac{\delta M}{M}\right)\left(\frac{M}{C_D}\right)\left(\frac{\delta C_D}{\delta M}\right)$$

and

$$\left.\frac{\delta C_D}{C_D}\right|_{Re} = \left(\frac{\delta Re}{Re}\right)\left(\frac{Re}{C_D}\right)\left(\frac{\delta C_D}{\delta Re}\right) ,$$

where $\frac{\partial C_D}{\partial M}$ is the slope of the $C_D$ versus M curve,

$\frac{\partial C_D}{\partial Re}$ is the slope of the $C_D$ versus Re curve,

$\frac{\delta C_D}{C_D}\Big|_M$ is the maximum possible error in $C_D$ due to Mach number error,

and $\frac{\delta C_D}{C_D}\Big|_{Re}$ is the maximum possible error in $C_D$ due to Reynolds number error.

Combining the errors in these three parameters we find that the maximum total error in drag coefficient is:

$$\frac{\delta C_D}{C_D}\Big|_{tot} = \frac{\delta C_D}{C_D} + \frac{\delta C_D}{C_D}\Big|_M + \frac{\delta C_D}{C_D}\Big|_{Re} .$$

Since the drag coefficient does not vary sharply with Reynolds number, errors in Reynolds number are negligible in the determination of total drag coefficient error (see Table II). Whereas, above M = 0.55, the Mach number error (Table II) does become important due to the increasing effect of compressibility on the drag coefficient.

1. The random errors

The various random errors of the measurements are presented in Table I. These errors were taken as one-half

| Instrument | Physical Quantity Measured | Random Error |
|---|---|---|
| Differential Statham gage | Dynamic pressure (q) | ± 0.5 mm deflection |
| Dubrovin gage | Static pressure<br>0 P 20 mm Hg | ± 0.1 mm Hg |
| Differential Mercury Manometer | Static pressure<br>0 P 5 in. Hg | ± 0.005 in. Hg |
| Differential Mercury Manometer | Static pressure<br>5 in. Hg P 1 atm. | ± 0.025 in. Hg |
| Dial gage | Sphere deflection | ± 0.004 in. |
| Scientific Balance | Sphere weight (W)<br>Sphere diameter (d)<br>Support wire length<br>± 0.02 cm | All possible errors included in instrument |
| Brown Temperature Indicator and Thermocouple | Temperature (T) | ± 0.5° F. |

TABLE I. RANDOM ERRORS

| Instrument | Physical Quantity Measured | Instrument Error |
|---|---|---|
| Differential Statham gage | Dynamic pressure (q) | Manufacturer's specification, non-linear and hysterisis not to exceed ± 0.5% of full scale deflection. In actual calibration no significant deviation was observed; therefore, this instrument error has been neglected. |
| Dubrovin vacuum gage | Static pressure<br>0 P 20 mm Hg | Manufacturer's error specification not available. For the measurements a "zero point" was established at a pressure of 0.1 micron, by means of a vacuum pump for which the manufacturer guarantees this pressure level (Welch Duo-Seal pump). The actual minimum working pressure is 100 microns. Any error which may exist in the zero point becomes insignificant for the working pressure. Therefore, the possible instrument error has been neglected. |
| Differential Mercury Manometer | Static pressure<br>20 mm Hg P 1 atm. | Barometric type manometer. Zero point established as with Dubrovin gage. Minimum working pressure is 2000 microns. Instrument error is insignificant. |
| Dial Gage | Sphere pressure<br>x | In view of the measuring technique, all possible errors are included in the random error. |
| Scientific Balance | Sphere weight (W)<br>Sphere diameter (d)<br>Support wire length (l) | ± 0.0005 gm<br>± 0.001 in.<br>All possible errors included in random error. |
| Brown Temperature Indicator and Thermocouple | Temperature (T) | ± 2° F (manufacturer's specification) |

TABLE II. INSTRUMENT ERRORS

the smallest division of the scale.

2. Instrument errors

The instrument errors are presented and described in the following Table II.

3. Results

The preceding analysis leads to the maximum possible error in drag coefficient, and Mach and Reynolds number due to the random and instrument errors. These errors have been calculated and are shown in Table III. It can be seen that the maximum possible error of the drag coefficients presented in Figs 17 and 18 ranges from $\pm$ 1.16 to $\pm$ 5.48. The lowest error occurs for a high Reynolds and low Mach number, while the highest error is connected with a low Reynolds and high Mach number.

In the process of error calculation it became evident that the errors in the establishment of the sphere deflection and the recording of the dynamic and static pressure contributed the largest part to the total error.

In the development of the error equations for $C_D$, M, and Re, all negative signs were changed to positive signs to obtain a maximum possible error. In doing this a certain amount of natural cancellation between the various sources of error was omitted. Furthermore, in all cases, a considerable number of tests were conducted at each condition of M and Re, and the errors in the results of the measurements are decreased due to the averaging process and the random

| M | Re | $\frac{\delta C_D}{C_D}$ (± %) | $\frac{\delta Re}{Re}$ (± %) | $\frac{\delta C_D}{C_D}\Big\|_{Re}$ (± %) | $\frac{\delta M}{M}$ (± %) | $\frac{\delta C_D}{C_D}\Big\|_{M}$ (± %) | $\frac{\delta C_D}{C_D}\Big\|_{TOT}$ (± %) |
|---|---|---|---|---|---|---|---|
| 0.10 | 3,043 | 2.97 | 1.52 | 0 | 0.92 | 0 | 2.97 |
| | 4,913 | 1.94 | 1.1[illegible] | 0 | 0.5[illegible] | 0 | 1.94 |
| | 7,821 | 1.34 | 0.9[illegible] | 0 | 0.35 | 0 | 1.34 |
| | 9,816 | 1.36 | 0.9[illegible] | 0 | 0.38 | 0 | 1.36 |
| | 16,712 | 1.22 | 1.10 | 0 | 0.51 | 0 | 1.22 |
| | 23,448 | 1.16 | 1.04 | 0 | 0.44 | 0 | 1.16 |
| 0.2[illegible] | 1,724 | 2.12 | 1.48 | 0 | 0.87 | 0 | 2.12 |
| | 2,006 | 1.89 | 1.3[illegible] | 0 | 0.75 | 0 | 1.89 |
| | 2,455 | 2.11 | 1.4[illegible] | 0 | 0.8[illegible] | 0 | 2.11 |
| | 3,163 | 1.73 | 1.31 | 0 | 0.71 | 0 | 1.73 |
| | 4,277 | 1.38 | 1.13 | 0 | 0.52 | 0 | 1.38 |
| | 5,931 | 1.44 | 1.13 | 0 | 0.53 | 0 | 1.44 |
| 0.[illegible]3 | 1,164 | 1.69 | 2.15 | 0 | 1.55 | 0.16 | 1.86 |
| | 1,487 | 1.78 | 1.9[illegible] | 0 | 1.39 | 0.15 | 1.93 |
| | 1,830 | 1.52 | 1.74 | 0 | 1.14 | 0.12 | 1.64 |
| | 2,158 | 1.37 | 1.56 | 0 | 0.96 | 0.10 | 1.47 |
| | 2,476 | 1.24 | 1.42 | 0 | 0.[illegible]3 | 0.09 | 1.33 |
| | 2,807 | 1.47 | 1.48 | 0 | 0.89 | 0.09 | 1.56 |
| | 3,136 | 1.37 | 1.39 | 0 | 0.80 | 0.08 | 1.45 |
| 0.80 | 1,000 | 1.64 | 3.20 | 0.05 | 2.60 | 2.34 | 4.03 |
| | 1,141 | 1.49 | 2.85 | 0.03 | 2.25 | 2.03 | 3.55 |
| | 1,285 | 1.3[illegible] | 2.60 | 0.02 | 2.00 | 1.80 | 3.19 |
| | 1,453 | 1.2[illegible] | 2.38 | 0.01 | 1.78 | 1.60 | 2.87 |
| | 1,591 | 1.5[illegible] | 2.40 | 0 | 1.80 | 1.62 | 3.16 |
| | 1,759 | 1.4[illegible] | 2.22 | 0 | 1.62 | 1.45 | 2.89 |
| | 1,904 | 1.36 | 2.10 | 0 | 1.50 | 1.35 | 2.71 |
| | 2,031 | 1.30 | 2.01 | 0 | 1.41 | 1.27 | 2.57 |
| 0.90 | 789 | 1.70 | 4.14 | 0.08 | 3.54 | 3.70 | 5.48 |
| | 953 | 1.48 | 3.53 | 0.05 | 2.93 | 3.06 | 4.59 |
| | 1,086 | [illegible].34 | 3.16 | 0.05 | 2.56 | 2.68 | 4.07 |
| | 1,244 | 1.24 | 2.81 | 0.03 | 2.21 | 2.30 | 3.57 |
| | 1,330 | 1.92 | 2.29 | 0.02 | 2.19 | 2.29 | 3.83 |
| | 1,536 | 1.39 | 2.55 | 0.02 | 1.95 | 2.04 | 3.45 |
| | 1,680 | 1.32 | 2.38 | 0.02 | 1.78 | 1.88 | 3.22 |
| | 1,826 | 1.24 | 2.24 | 0.02 | 1.64 | 1.71 | 2.97 |

TABLE III. MAXIMUM POSSIBLE ERRORS IN DRAG COEFFICIENT, REYNOLDS NUMBER AND MACH NUMBER AND THE TOTAL MAXIMUM POSSIBLE ERROR IN $C_D$

nature of the readings. The analysis, however, considers merely one measurement with maximum deviations.

One other factor tending to confirm that actual errors are smaller than the calculated maximum errors is the fact that all of the resultant curves do become quite dissimilar, particularly at the low values of Re, where the largest errors could occur.

From the above discussion, it appears that the errors predicted by this analysis are generous and one would expect the actual maximum errors of the presented drag coefficients to be smaller than the predicted values (Table III).

As illustration to Table III, Figure B-1 shows the trends of the maximum possible error based on analytical considerations as well as from statistical analysis. The latter method shall be discussed in the next chapter.

b. Statistical Methods

In order to arrive at an error from an examination of the quality of the data by statistical means, a standard deviation defined by $\sigma = \sqrt{\frac{\Sigma(C_{D_{avg.}} - \overline{C_D})^2}{n}}$ was evaluated for all experimental points tested. This distribution in the form of $\frac{\sigma}{C_D}$ is presented in Figure B-1. It can be seen that only in six cases $\frac{\sigma}{C_D}$ is greater than 4%.

Three of these points are insignificant since they are at low Mach numbers where there is sufficient data to determine a reliable drag coefficient. The other points are at M = 0.90 and low Reynolds numbers, where accuracy is inhibited by variations induced by transonic phenomena and the measurement of low pressures. Measurements in this region are always difficult.

The statistical deviations as shown in Figure B-2 are correlated to the drag coefficients which are suggested in Figure 19. The result is shown in Figures B-3 through B-7.

The statistical approach shows, as does the analytical one, a decreasing error with increasing Reynolds numbers and minimum error in the region of M = 0.48. An average standard deviation for each Mach number is shown to be, in general, lower than the maximum error predicted by the analytical method, as a comparison with Table III and Figure B-2 will show.

In view of the preceding discussion, it appears that the statistical results do indicate the actual error better than the analytical error analysis. The analytical treatment merely indicates the possible upper limit of errors included in the drag coefficients shown in Figures 19 and A-1.

## REFERENCES


1. Minzner, R. A., Champion, K. S. W., and Pond, H.L.: The ARDC Model Atmosphere, 1959, August.

2. Goldstein, S.: Modern Developments in Fluid Dynamics, Vol. 1, Oxford, 1938.

3. Kane, E. D.: Sphere Drag at Supersonic Speeds and Low Reynolds Numbers, Journal of the Aeronautical Sciences, Vol. 18, No.4, pp.259-270, April, 1951.

4. Sphere Drag in Rarefied Supersonic Gas Flows, Research Summary No. 36-5, Vol. II, pp. 10-11, Jet Propulsion Laboratory, Pasadena, California, November 1, 1960.

5. Ashkenas, H. I.: Sphere Drag at Low Reynolds Numbers and Supersonic Speeds, Research Summary No. 36-12, Vol. I, pp. 93-96, Jet Propulsion Laboratory, Pasadena, California, January 2, 1962.

6. Naumann. Alexander: Aerodynamische Gesichtspunkte Der Windkanalentwicklung, Jahrbuch, 1954, Der Wissenschaftlichen Gesellschaft fuer Luftfahrt, E.V.(WGL)

7. Hoerner, S. F.: Fluid Dynamic Drag, published by author, Midland Park, New Jersey, 1958.

8. Taylor, Angus E.: Advanced Calculus, Ginn and Co., Boston, Massachusetts, 1955.

# APPENDIX A

## DRAG COEFFICIENT OF A SPHERE AT VARIOUS MACH NUMBERS VERSUS REYNOLDS NUMBER

See fold-out graph in pocket of back cover.

## APPENDIX B

Derivation of Error Equations.

1. Error included in the Drag Coefficient $C_D$

In order to obtain the error expression the drag coefficient has to be presented in terms of the measured variables. Figure 19 shows the test arrangement and forces acting. From moment equilibrium about the wire suspension point "0" one obtains,

$$D(L+r) + D_w(L_w) = W(\Delta X + \delta) \quad . \qquad (1)$$

While the same condition about the point P located at the sphere provides

$$W \cdot \delta = D \cdot r \quad . \qquad (2)$$

Substituting this into Equation 1, we obtain:

$$D \cdot L + D_w \cdot L_w = W \cdot \Delta X \quad . \qquad (3)$$

The wire drag was determined by using a similar test arrangement with the following modifications. A small weight was attached to the support wire, but this weight was enclosed in a hollow sphere of the same dimension of the sphere

under investigation. The hollow sphere was supported by a sting to the floor of the test section. Under these circumstances the wire drag gives the following relation (see Figure 1):

$$D_w L_w = W' \Delta X' \quad . \tag{4}$$

Combining Equations 3 and 4 gives the sphere drag

$$D = \frac{W \Delta X}{L} - \frac{W' \cdot \Delta X'}{L} \quad . \tag{5}$$

where $\frac{W' \Delta X'}{L}$ is the wire drag correction term.

From Equation 5 the drag coefficient of the sphere follows:

$$C_D = \frac{D}{qS} = \frac{D}{q\frac{\pi}{4}d^2} = \frac{4}{\pi}\left\{\frac{W \Delta X}{q d^2 L} - \frac{W' \Delta X'}{q d^2 L}\right\} , \tag{6}$$

in terms of all the measured variables subject to quantitative errors.

To evaluate the error in $C_D$ the assumption is made that the error in the measured quantity of the differential pressure $\Delta P$ is not magnified in making the compressibility corrections in order to get the dynamic pressure q.

Replacing $q$ by $\Delta P$ one can write:

$$C_D = C_D\,(W, \Delta X, \Delta P, d, W', \Delta X', L). \quad (7)$$

The small change in $C_D$ due to changes in the independent variables follows from (Ref 8):

$$\delta C_D = \frac{\partial C_D}{\partial W} \cdot \delta W + \frac{\partial C_D}{\partial \Delta X} \cdot \delta \Delta X + \frac{\partial C_D}{\partial \Delta P} \cdot \delta \Delta P \quad (8)$$

$$+ \frac{\partial C_D}{\partial d} \cdot \delta d + \frac{\partial C_D}{\partial L} \cdot \delta L + \frac{\partial C_D}{\partial W'} \cdot \delta W' + \frac{\partial C_D}{\partial \Delta X'} \cdot \delta \Delta X' \,.$$

This equation can also be interpreted as the error in $C_D$ due to small errors in the measured variables.

The fractional error in $C_D$ is $\frac{\delta C_D}{C_D}$, where $C_D$ is taken from Equation 6. For simplification one can neglect the wire drag correction term in $C_D$, which is small compared to the remainder of the expression. Hence dividing Equation 8 by $C_D \simeq \frac{4W\Delta X}{\pi \Delta P d^2 L}$ and performing the necessary differentiation one gets:

$$\frac{\delta C_D}{C_D} = \frac{\delta W}{W} + \frac{\delta \Delta X}{\Delta X} \quad \frac{\delta \Delta P}{\Delta P} + \frac{2\,\delta d}{d} \quad (9)$$

$$- \frac{\delta L}{L} - \frac{\Delta X'}{\Delta X} \frac{\delta W'}{W} - \frac{W'}{W} \frac{\delta \Delta X'}{\Delta X} \,.$$

The maximum error occurs where all the individual errors have the same sign, therefore

$$\frac{\delta C_D}{C_D} = \frac{\delta W}{W} + \frac{\delta \Delta X}{\Delta X} - \frac{\delta \Delta P}{\Delta P} + \frac{2\delta d}{d} + \frac{\delta L}{L} + \frac{\Delta X'}{\Delta X}\frac{\delta W'}{W} + \frac{W'}{W}\frac{\delta \Delta X'}{\Delta X} \quad . \tag{10}$$

2) Errors in Reynolds Number

The Reynolds number is given by:

$$R_e = \frac{\rho V d}{\mu} \tag{11}$$

V is given by:

$$V = \sqrt{\frac{2}{\rho} q} \quad . \tag{12}$$

Using the perfect gas law, one may write:

$$\rho = \frac{P}{RT} \quad . \tag{13}$$

Sutherland's formula for air viscosity is:

$$\mu = 2.27 \frac{T^{3/2}}{T+198.6} \times 10^{-8} \quad \frac{lb.-sec.}{ft.^2} \quad . \qquad (14)$$

Substituting Equations 12 and 13 into 11 gives:

$$R_e = \sqrt{\frac{2P}{RT} \cdot g} \quad \frac{d}{\mu} \quad . \qquad (15)$$

Using the same differentiation formula as before, one obtains:

$$\frac{\delta R_e}{R_e} = \frac{1}{2}\left[\frac{\delta P}{P} + \frac{\delta \Delta P}{\Delta P}\right] + \frac{\delta d}{d} + \frac{\delta \mu\sqrt{T}}{\mu\sqrt{T}} \quad . \qquad (16)$$

Introducing the relationship shown in Equation 14, provides:

$$\frac{\delta \mu\sqrt{T}}{\mu\sqrt{T}} = \left[2 - \frac{T}{T+198.6}\right] \quad \frac{\delta T}{T} \quad . \qquad (17)$$

Substituting Equation 17 into 16 yields the maximum possible error

$$\left[\frac{\delta R_e}{R_e}\right]_{MAX.} = \frac{1}{2}\left[\frac{\delta P}{P} + \frac{\delta \Delta P}{\Delta P}\right] + \frac{\delta d}{d} + \left[2 - \frac{T}{T+198.6}\right]\frac{\delta T}{T} \qquad (18)$$

3) Errors in Mach Numbers

The Mach number is given by:

$$M = \frac{V}{a} \tag{19}$$

where a = speed of sound = $\sqrt{\gamma RT}$ . (20)

Substituting Equations 20 and 12 into Equation 19 gives:

$$M = \sqrt{\frac{2}{\gamma P}}\, q \cdot \tag{21}$$

Differentiation leads to the maximum error:

$$\left[\frac{\delta M}{M}\right]_{MAX.} = \frac{1}{2}\left[\frac{\delta P}{P} + \frac{\delta \Delta P}{\Delta P}\right] \cdot \tag{22}$$

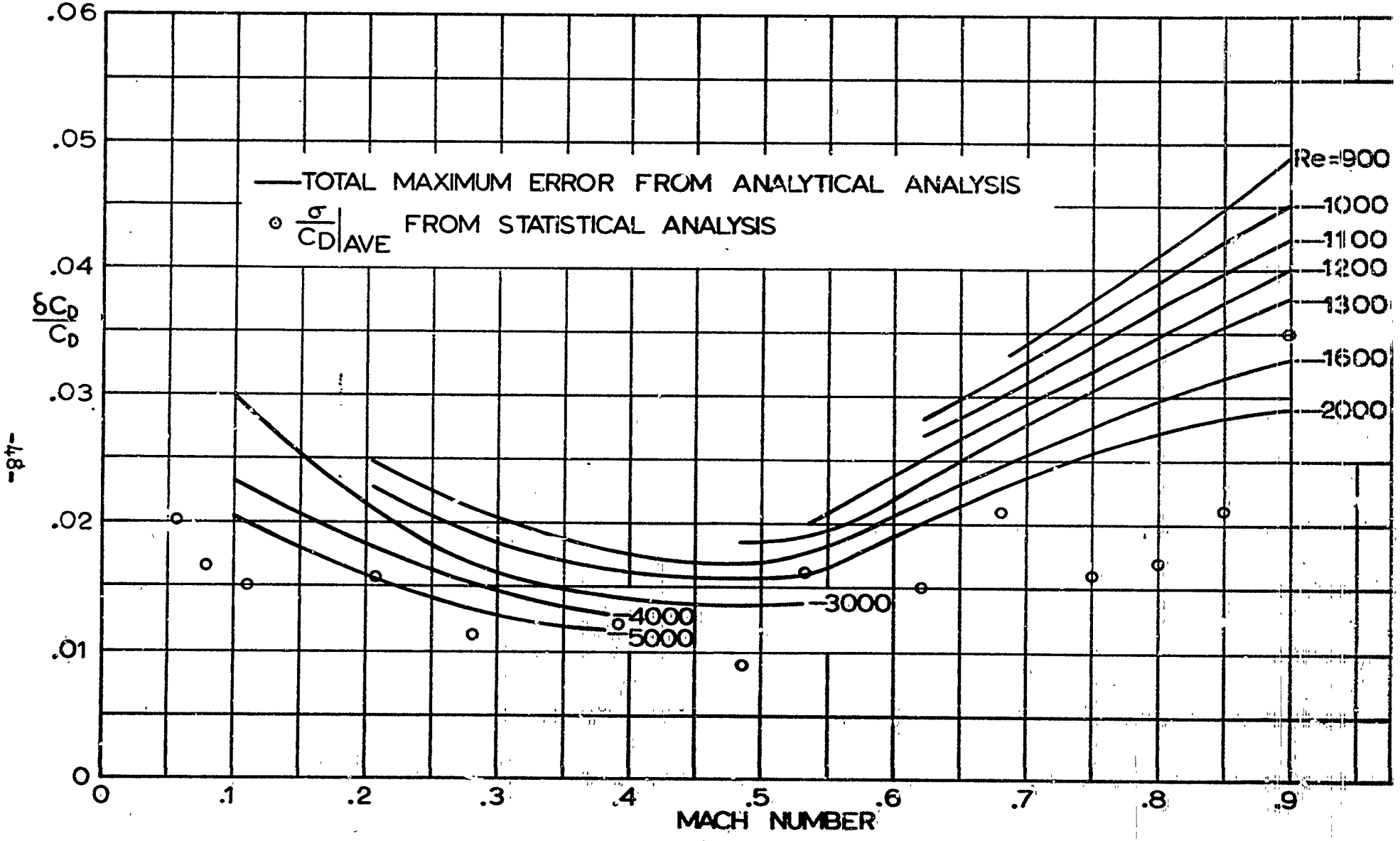


FIG B-1. MAXIMUM TOTAL ERROR IN $C_D$ CALCULATED FROM ERRORS OF MEASUREMENT COMPARED TO STATISTICAL RESULTS

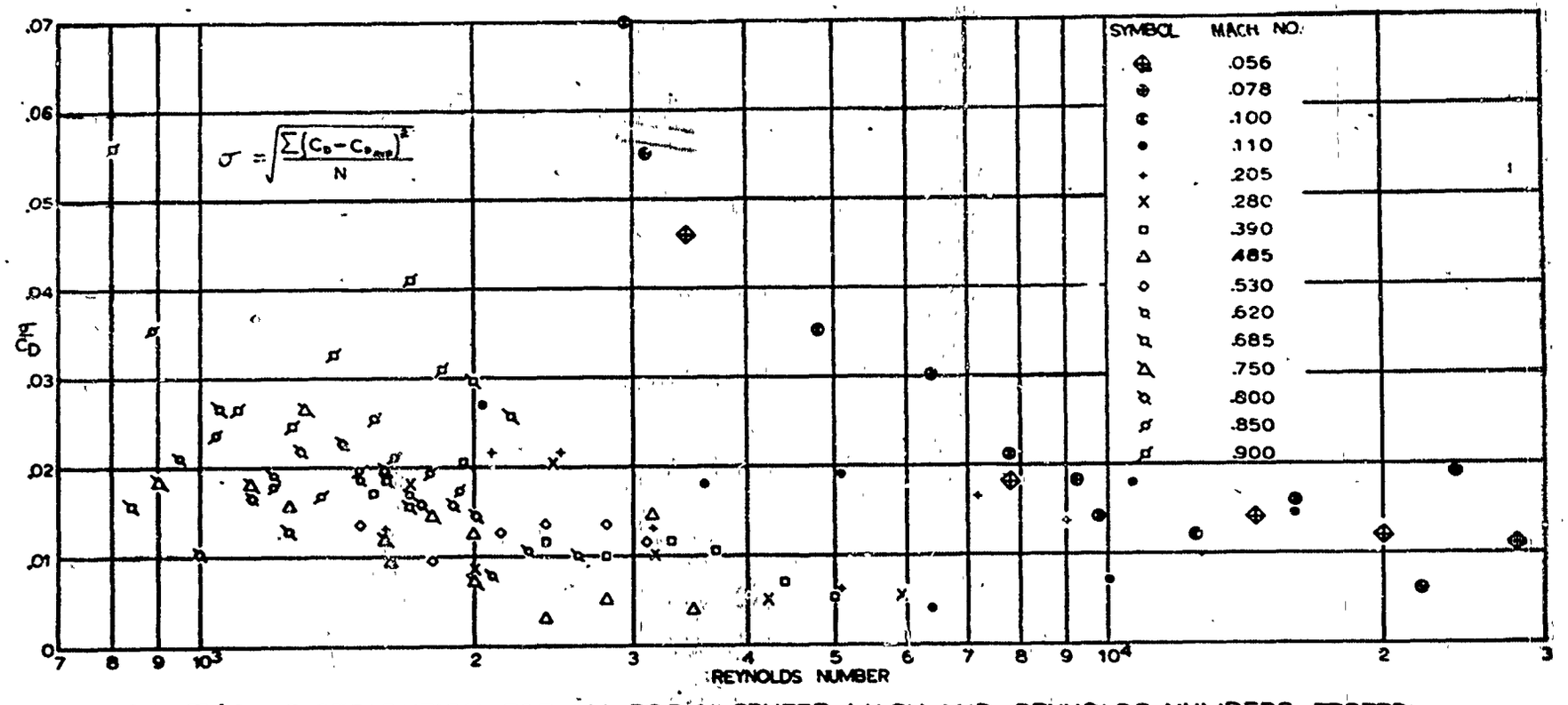


FIG 3-2. $\sigma/C_D$ DISTRIBUTION FOR ALL ROBIN SPHERE MACH AND REYNOLDS NUMBERS TESTED

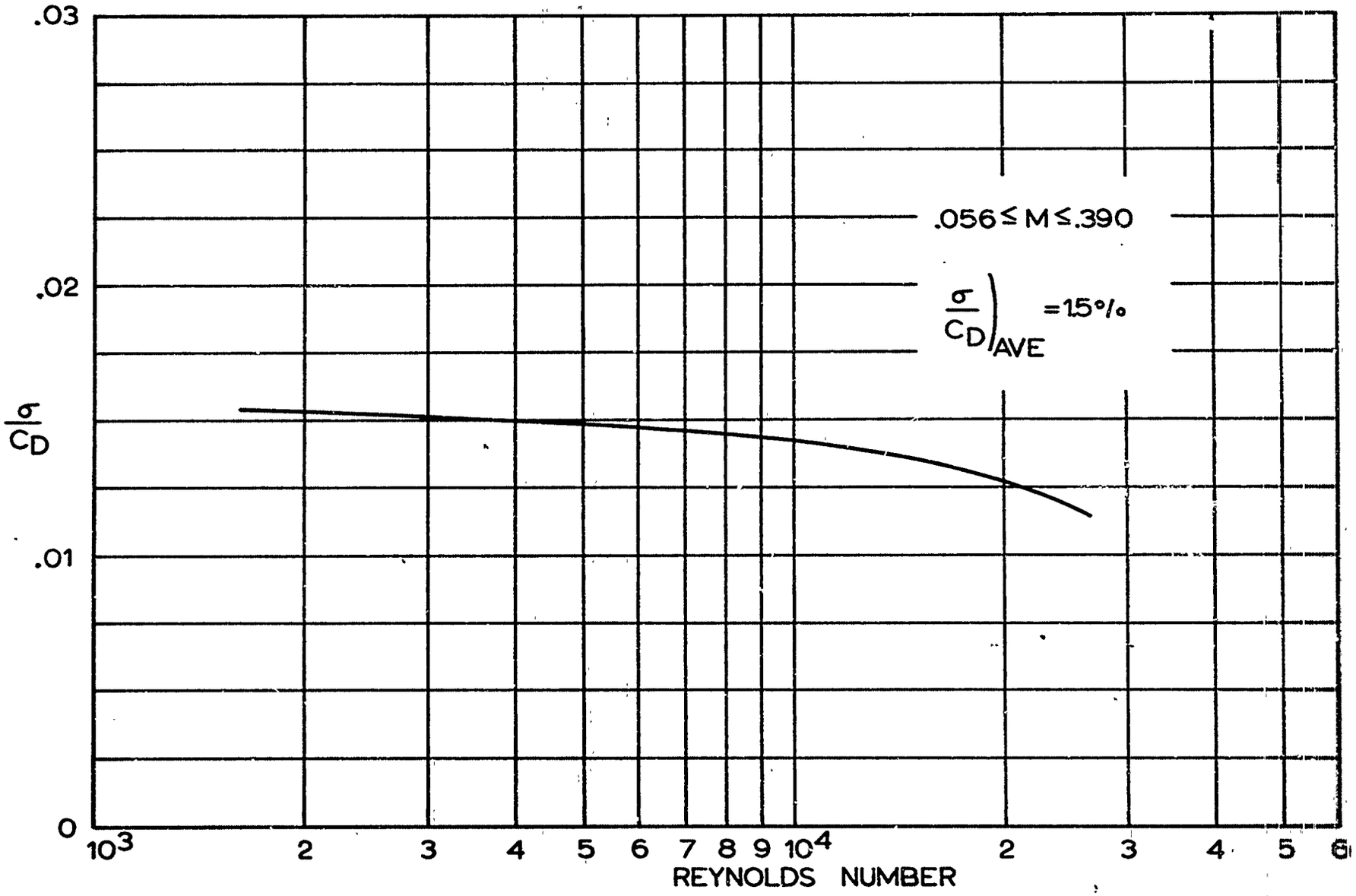


FIG B-3. VARIATION OF NORMALIZED STANDARD DEVIATION FOR .056≤M≤.390

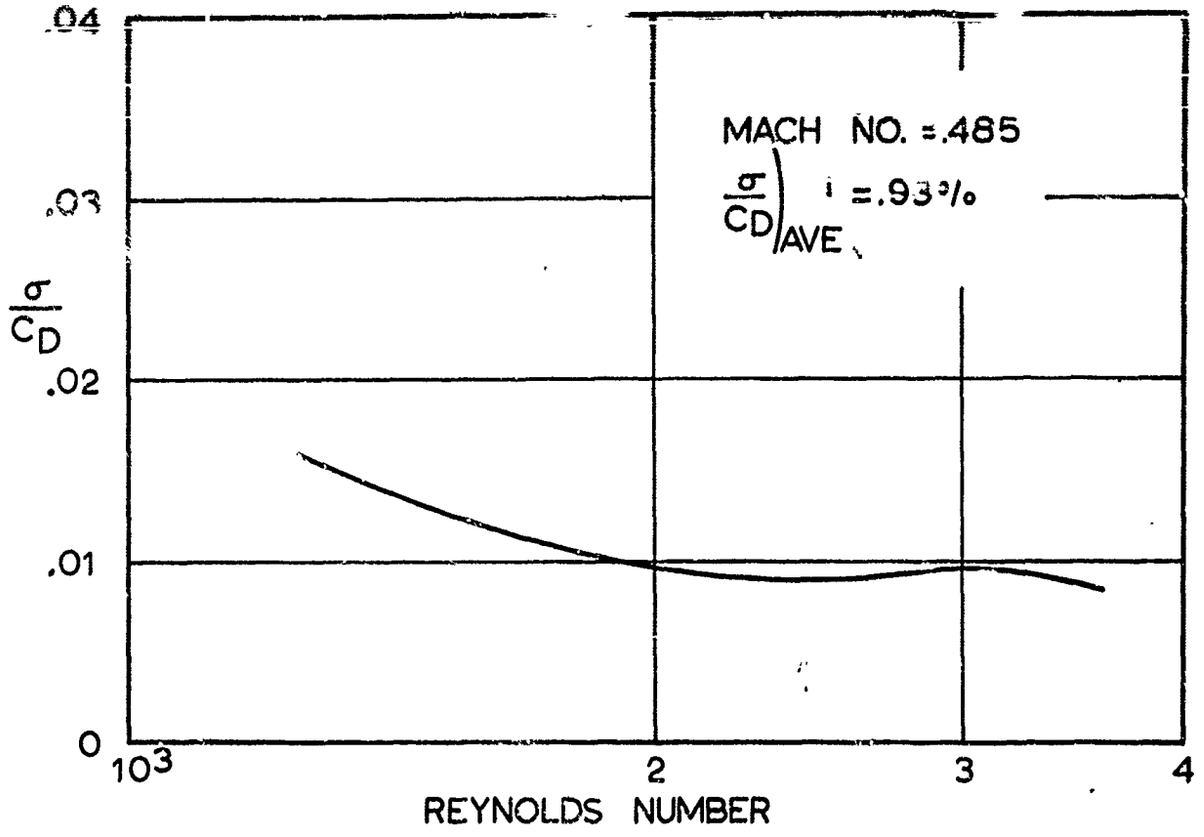


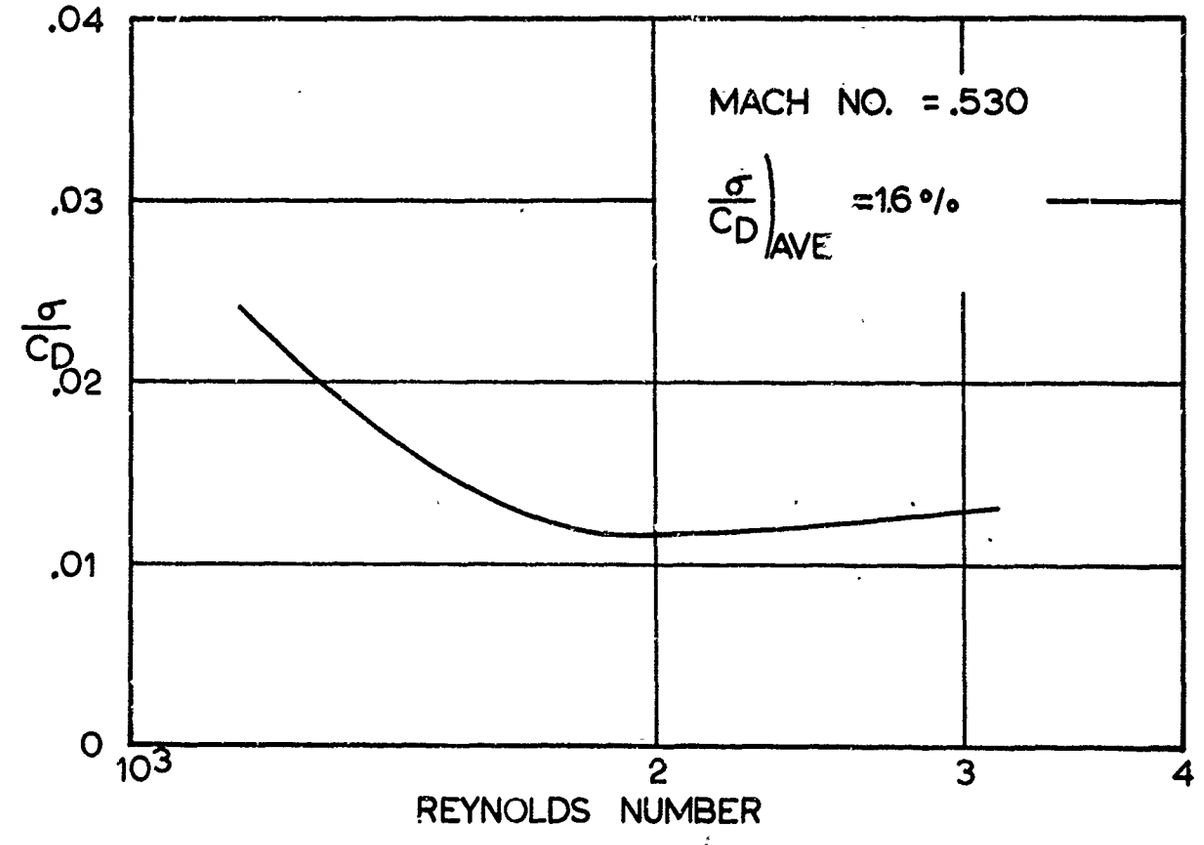


FIG B-4. VARIATION OF NORMALIZED STANDARD DEVIATION FOR M = .485 AND .530

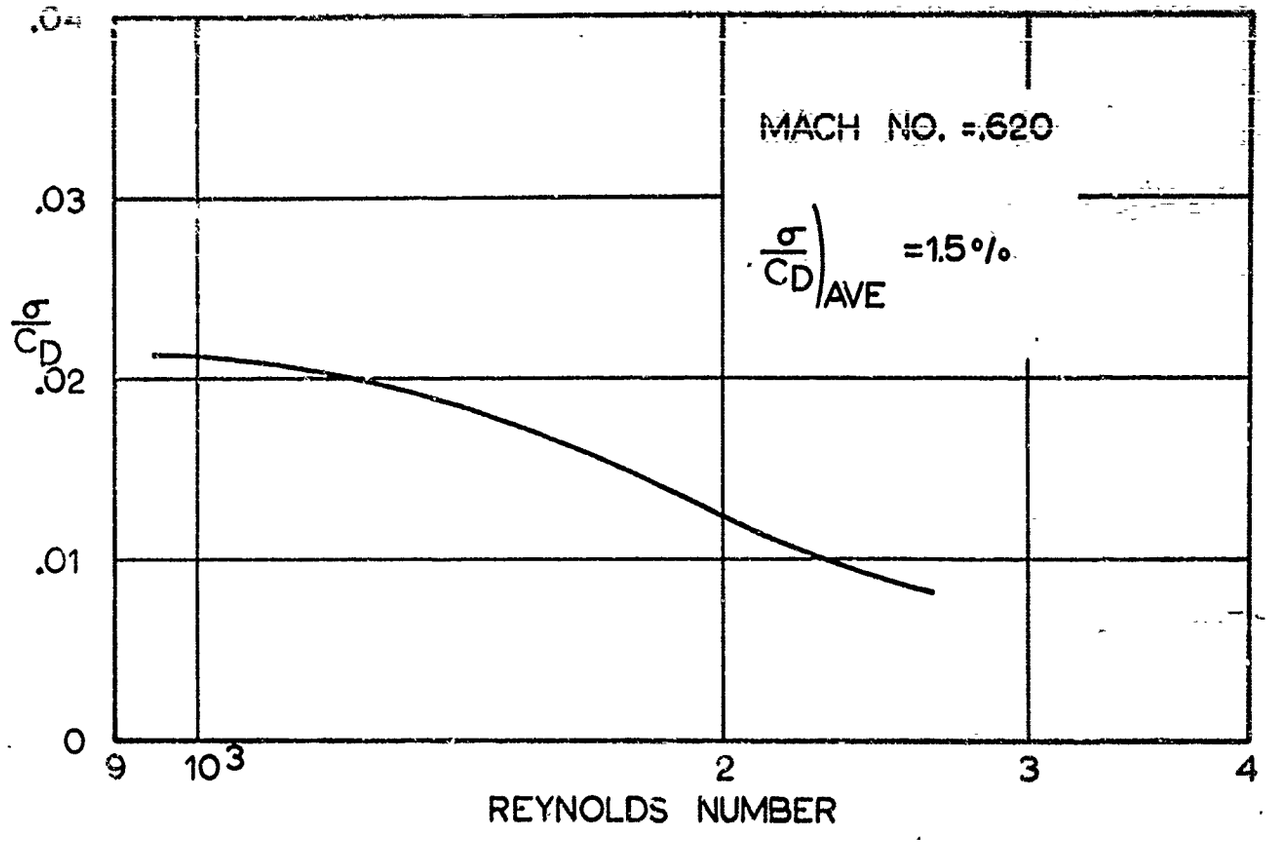


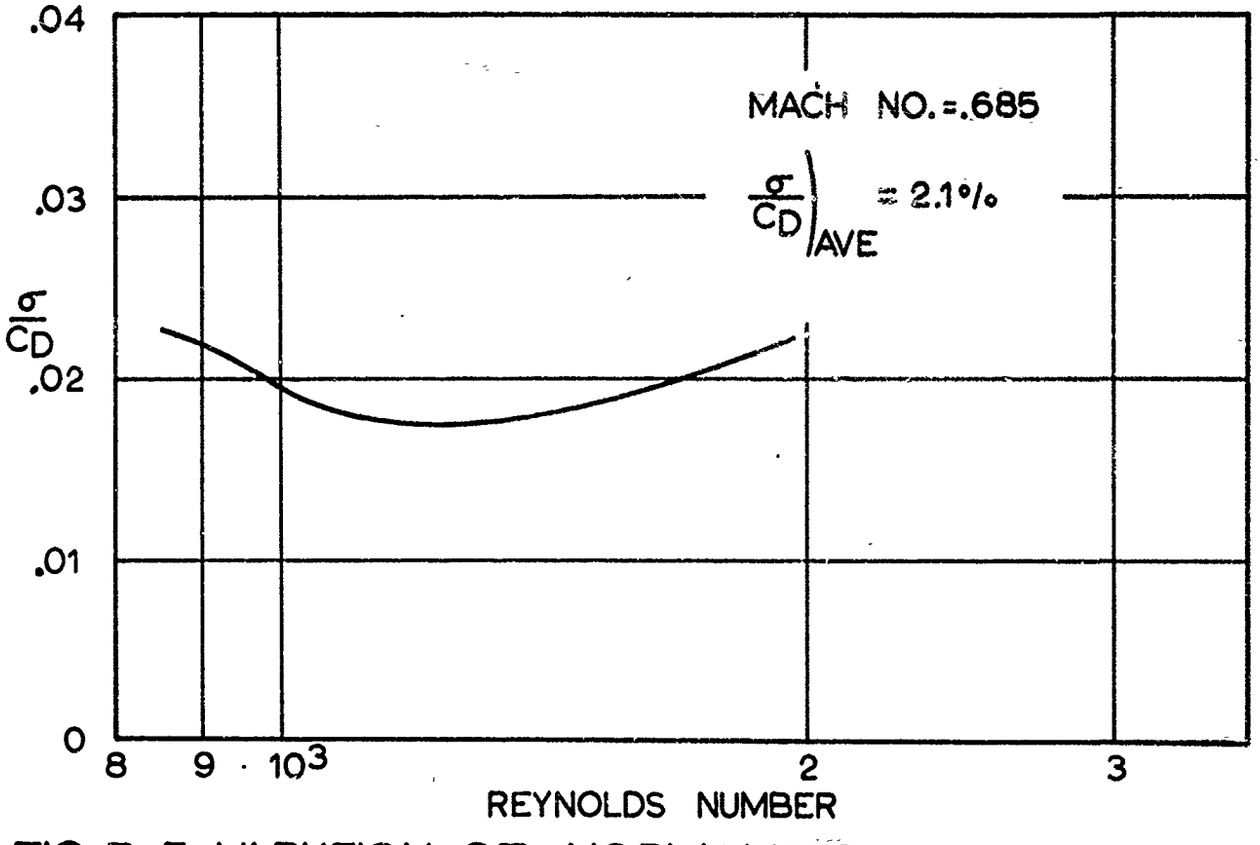


FIG B-5. VARIATION OF NORMALIZED STANDARD DEVIATION FOR M=.620 AND .685

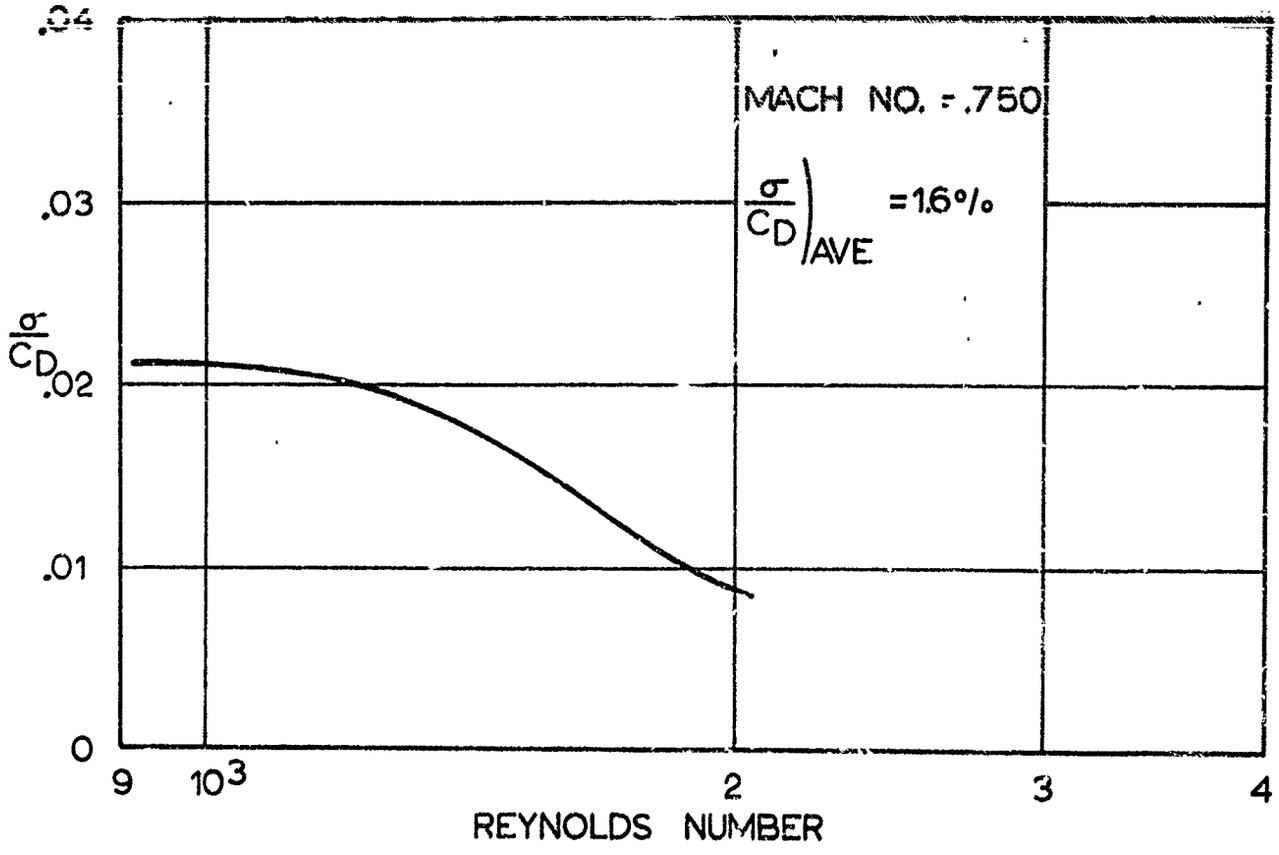


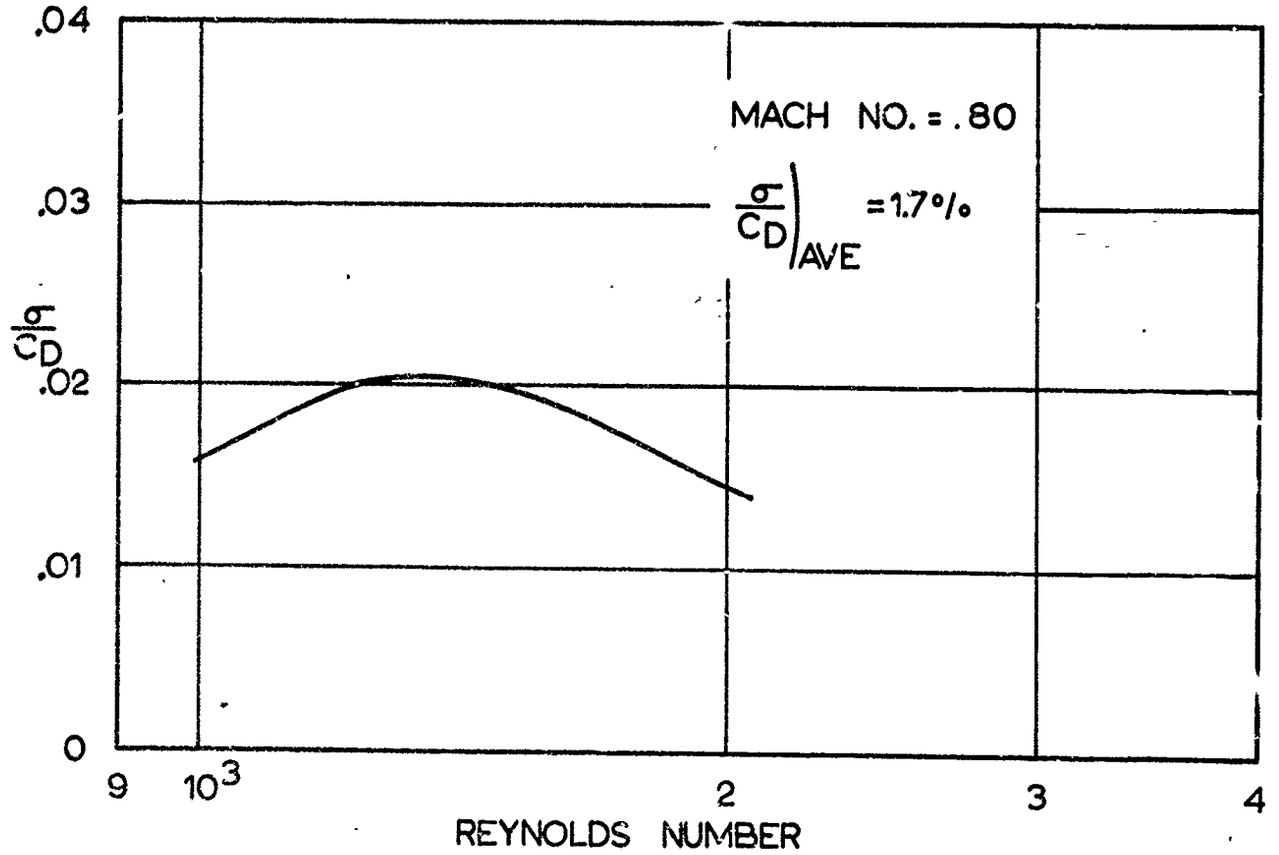


FIG B-6. VARIATION OF NORMALIZED STANDARD DEVIATION FOR M= .750 AND .80

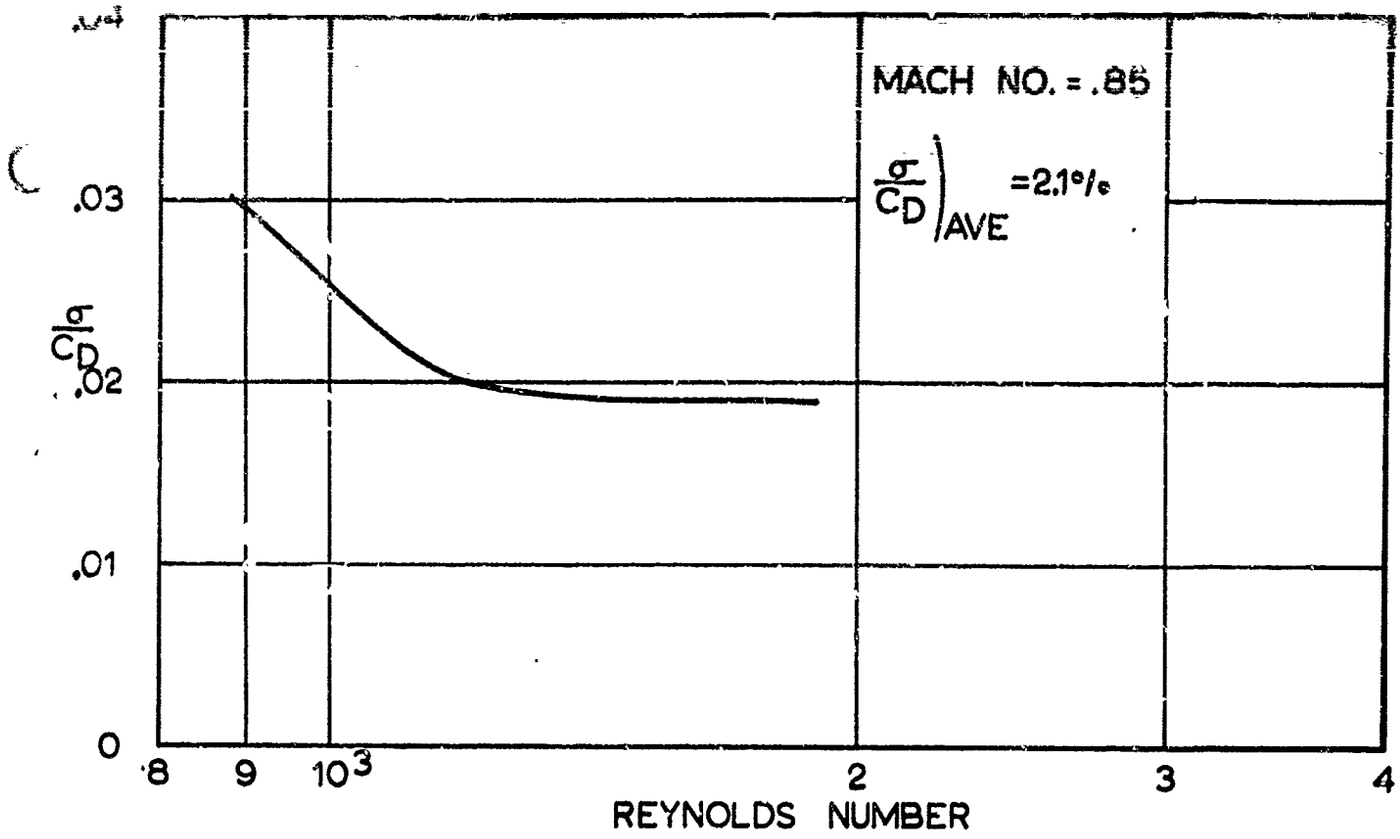


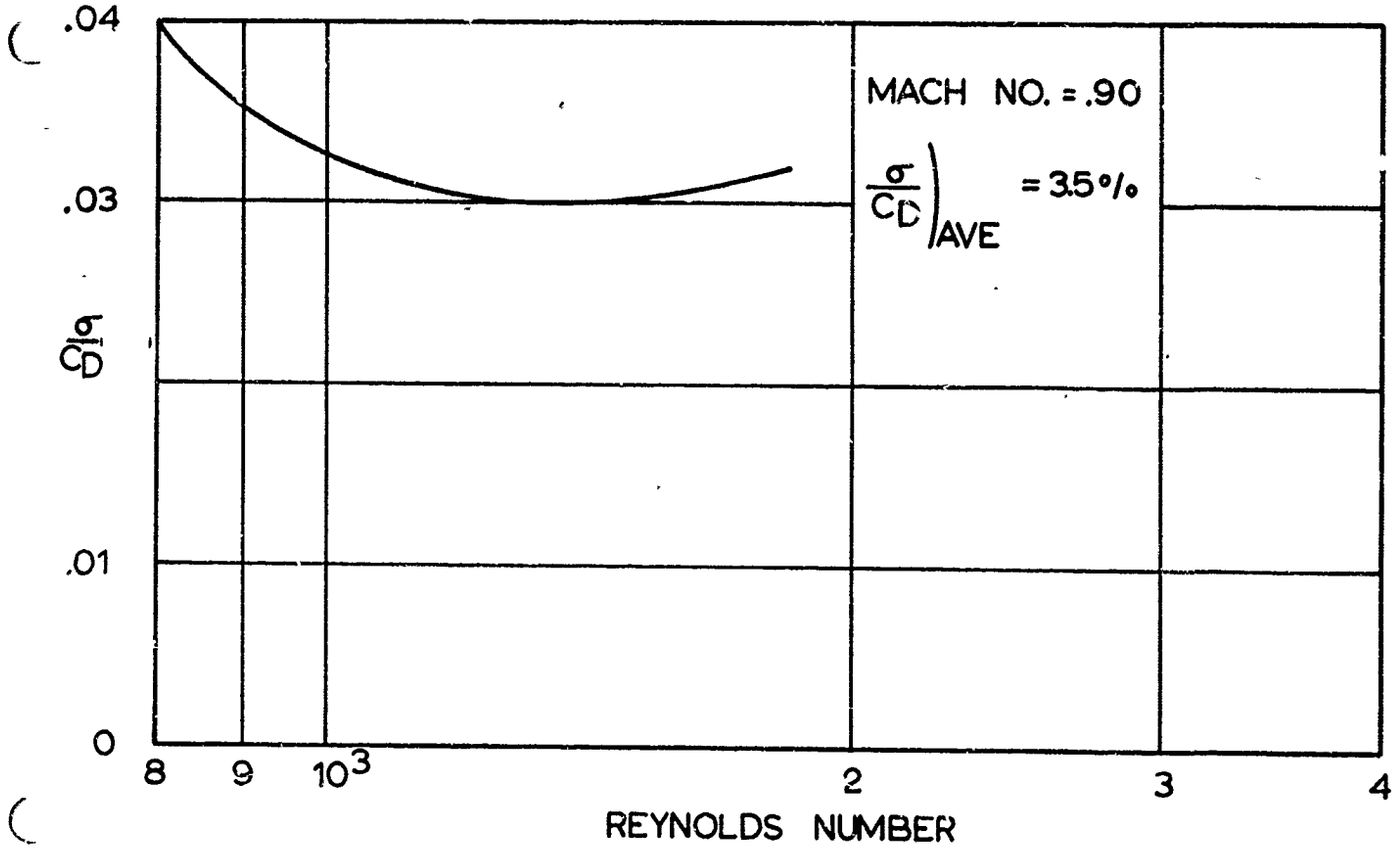


FIG B-7. VARIATION OF NORMALIZED STANDARD DEVIATION FOR M = .85 AND .90

# LIFT AND INDUCED DRAG OF A ROTATING SPHERE IN INVISCID FLOW

by

Helmut G. Heinrich
and
Lawrence W. Rust, Jr.

University of Minnesota
Minneapolis, Minnesota

The
Project was sponsored by
G. T. Schjeldahl Company, Northfield, Minnesota

ABSTRACT

A solution is presented which predicts the lift and induced drag acting on a rotating sphere immersed in a uniform, rectilinear flow. The theory neglects the viscous effect and is thus primarily applicable for small Reynolds number conditions.

The coefficients of lift and induced drag depend on the dimensionless parameter $\omega R/U$ where $\omega$ represents the angular velocity of the sphere, R signifies its radius, and U the free stream velocity.

TABLE OF CONTENTS

## LIST OF ILLUSTRATIONS

## LIST OF SYMBOLS

| | | |
|---|---|---|
| $V_\theta$ | = | Velocity on surface of sphere due to potential flow |
| | = | Velocity on surface of sphere due to rotation of sphere |
| $U$ | = | Free stream velocity |
| $\omega$ | = | Angular velocity |
| $\vec{V}$ | = | $\vec{V}_\theta + \vec{V}_\beta$ = Resultant velocity |
| $\alpha$ | = | Angle between axis of rotation and x-axis |
| $L$ | = | Lift |
| $D_i$ | = | Induced drag |
| $P$ | = | Surface pressure |
| $R$ | = | Radius of sphere |
| $C_L$ | = | Coefficient of lift |
| $C_{D_i}$ | = | Coefficient of induced drag |
| $L'$ | = | Lift per unit span |
| $w$ | = | Downwash velocity due to trailing vortex sheet |
| $D_i'$ | = | Induced drag per unit span |

# I. INTRODUCTION

The effects on the motion of a sphere due to rotation may become significant in many practical problems. For example, in the ROBIN Project, which attempts to determine the air density at high altitudes through measurements of a sphere's motion, a knowledge of the lift and induced drag of the sphere due to rotation is necessary to accurately interpret the experimental results. Similarly, this effect could conceivably influence the results of experiments, where attempts are made to determine the wind at various altitudes through the use of an inflated, rising sphere.

## II. DETERMINATION OF THE LIFT DISTRIBUTION ON A ROTATING SPHERE

### A. Coordinate System

The coordinate system used for this analysis is presented in Fig 1. The free stream rectilinear flow is assumed to be in the negative y direction. Three separate coordinate systems are seen in Fig 1. The x'-y'-z' system is obtained by rotation of the x-y-z system about the y-axis through an angle $\phi$ . The x"-y"-z" system is obtained by rotation of the x-y-z system about the z-axis through the angle $\alpha$ . $\theta$ represents the angle between the y-axis and a ray from the origin to a point of interest on the sphere. To determine $\beta$ , we pass a plane, perpendicular to x", through the point of interest (P) on the sphere. The x"-axis represents the axis of rotation of the sphere.

### B. Analysis of the Velocity Distribution

The fluid velocity at the surface of the sphere is composed of two components:

1) Velocity due to the potential flow

2) Velocity due to the rotation of the sphere .

The surface velocity due to the potential flow is given by (Ref 1, p 67):

$$\vec{V}_\theta = \frac{3}{2} U \sin\theta \, \hat{i}_\theta \quad . \qquad (1)$$

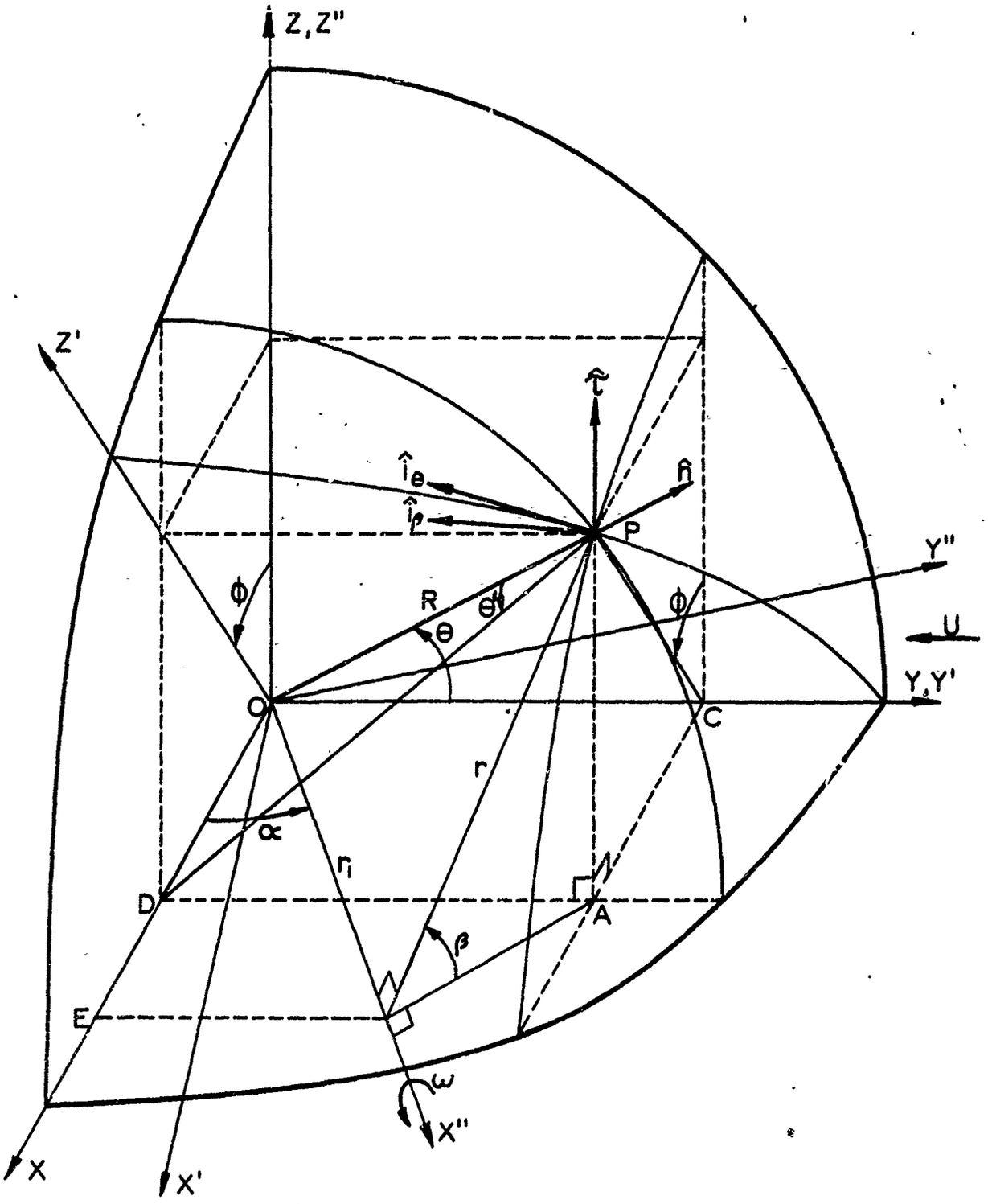


FIG 1. GEOMETRIC RELATIONSHIPS OF A SURFACE ELEMENT.

The rotational component is given by:

$$\vec{V}_\beta = \omega r \hat{i}_\beta \ , \qquad (2)$$

where:

$\omega$ = angular velocity of sphere about x" axis

$r$ = distance from x" axis to the point in question.

The vector sum of the two components is:

$$\vec{V} = \vec{V}_\theta + \vec{V}_\beta \ . \qquad (3)$$

We will shortly have need of the square of the total velocity. This is given by:

$$V^2 = \vec{V}\cdot\vec{V} = (\vec{V}_\theta + \vec{V}_\beta)\cdot(\vec{V}_\theta + \vec{V}_\beta)$$

$$= |\vec{V}_\theta|^2 + |\vec{V}_\beta|^2 + 2|\vec{V}_\theta||\vec{V}_\beta|\hat{i}_\theta\cdot\hat{i}_\beta \ .$$

If we let $V_\theta = |\vec{V}_\theta|$ , $V_\beta = |\vec{V}_\beta|$ , we obtain:

$$V^2 = V_\theta^2 + V_\beta^2 + 2 V_\theta V_\beta \hat{i}_\theta\cdot\hat{i}_\beta \ , \qquad (4)$$

where

$$V_\theta = \tfrac{3}{2} U \sin\theta$$

$$V_\beta = \omega r \ .$$

From Eqn (4) we see that we must determine the quantity $\hat{i}_\theta\cdot\hat{i}_\beta$ . To do this, we first express $\hat{i}_\theta$ and $\hat{i}_\beta$ in terms of $\hat{i}$, $\hat{j}$, $\hat{k}$; the unit vectors in the x, y, and z directions, respectively.

Let us first consider $\hat{i}_\beta$ . From Fig 1, we see that it may be expressed in terms of the x"-y"-z" coordinate

system as:

$$\hat{i}_\beta = -\sin\beta\,\hat{j}'' + \cos\beta\,\hat{k}'',$$

or, since $\hat{k}'' = \hat{k}$, we have:

$$\hat{i}_\beta = -\sin\beta\,\hat{j}'' + \cos\beta\,\hat{k} \quad ; \tag{5}$$

also, from geometry, we see that:

$$\hat{j}'' = -\sin\alpha\,\hat{i} + \cos\alpha\,\hat{j} \,.$$

Using this relation, we find:

$$\hat{i}_\beta = \sin\alpha\,\sin\beta\,\hat{i} - \cos\alpha\,\sin\beta\,\hat{j} + \cos\beta\,\hat{k} \,. \tag{6}$$

We next consider $\hat{i}_\theta$ . From Fig 1 we note that:

$$\hat{i}_\theta = -\sin\theta\,\hat{j}' + \cos\theta\,\hat{k}' \,.$$

or, since $\hat{j}' = \hat{j}$:

$$\hat{i}_\theta = -\sin\theta\,\hat{j} + \cos\theta\,\hat{k}' \,. \tag{7}$$

Again, from Fig 1, we note that $\hat{k}'$ may be expressed as:

$$\hat{k}' = \sin\phi\,\hat{i} + \cos\phi\,\hat{k} \,.$$

Substituting this relation into (7), we obtain:

$$\hat{i}_\theta = \cos\theta\,\sin\phi\,\hat{i} - \sin\theta\,\hat{j} + \cos\theta\cos\phi\,\hat{k} \,. \tag{8}$$

Taking the dot product of (5) and (8) yields:

$$\hat{i}_\theta \cdot \hat{i}_\beta = \sin\alpha\,\sin\beta\,\cos\theta\sin\phi + \cos\alpha\,\sin\beta\,\sin\theta + \cos\beta\cos\theta\cos\phi. \tag{9}$$

Thus, Eqn (4) becomes:

$$V^2 = V_\theta^2 + V_\beta^2 + 2V_\theta V_\beta [\sin\alpha \sin\beta \cos\theta \sin\phi + \cos\alpha \sin\beta \sin\theta + \cos\beta \cos\theta \cos\phi] . \quad (10)$$

Since $\vec{V}$ is the velocity on the surface of the sphere, it depends on only two space variables. We shall eliminate $\beta$ from Eqn (10) through the use of geometric properties.

We note that the vertical distance AP can be written as:

$$AP = r \sin\beta = PC \cos\phi . \quad (11)$$

We also see that:

$$PC = R \sin\theta , \quad (12)$$

where R = radius of sphere.

Substituting Eqn (12) into (11) yields:

$$r \sin\beta = R \sin\theta \cos\phi . \quad (13)$$

We next observe that the distance AD can be written as:

$$AD = r_1 \sin\alpha + r \cos\beta \cos\alpha = R \cos\theta ,$$

or

$$r \cos\beta \cos\alpha + r_1 \sin\alpha = R \cos\theta . \quad (14)$$

Finally, we note that:

$$OE = OD + DE ,$$

But:

$$OD = AC = R \sin\theta \sin\phi ,$$

and:

$$DE = r \cos\beta \sin\alpha ;$$

therefore:

$$OE = R \sin\theta \sin\phi + r \cos\beta \sin\alpha \quad . \tag{15}$$

But, we also have from Fig 1:

$$OE = r_1 \cos\alpha \quad .$$

Thus:

$$R \sin\theta \sin\phi + r \cos\beta \sin\alpha = r_1 \cos\alpha \quad . \tag{16}$$

Equations (13), (14), and (16) present three relations between the variables r, $r_1$, $\theta$, $\phi$, $\beta$ (Note: $\alpha$ is not a variable **but remains** fixed for any given problem). Thus, any three of these variables can be written in terms of the remaining two. We choose to solve these equations for $\beta$ in terms of $\theta$ and $\phi$.

Re-writing Eqns (14) and (16), we obtain:

$$r_1 = \frac{R \cos\theta - r \cos\beta \cos\alpha}{\sin\alpha} \quad ,$$

and

$$r_1 = \frac{R \sin\theta \sin\phi + r \cos\beta \sin\alpha}{\cos\alpha} \quad .$$

This yields:

$$R \cos\theta - r \cos\beta \cos\alpha = \tan\alpha (R \sin\theta \sin\phi + r \cos\beta \sin\alpha) \, ,$$

or:

$$R[\cos\theta - \tan\alpha \sin\theta \sin\phi] = r[\tan\alpha \cos\beta \sin\alpha + \cos\beta \cos\alpha] \tag{17}$$

Dividing Eqn (17) by (13) we obtain:

$$\frac{\cos\theta - \tan\alpha \sin\theta \sin\phi}{\sin\theta \cos\phi} = \frac{\tan\alpha \cos\beta \sin\alpha + \cos\beta \cos\alpha}{\sin\beta} ,$$

which may be solved for $\tan\beta$ to give:

$$\tan\beta = \frac{\cos\phi \sin\theta}{\cos\alpha[\cos\theta - \tan\alpha \sin\theta \sin\phi]} . \qquad (18)$$

Since

$$\sin\beta = (1 + \cot^2\beta)^{-1/2}$$

$$\cos\beta = (1 + \tan^2\beta)^{-1/2} ,$$

we obtain:

$$\sin\beta = \left[1 + \frac{\cos^2\alpha (\cos\theta - \tan\alpha \sin\theta \sin\phi)^2}{\cos^2\phi \sin^2\theta}\right]^{-1/2} \qquad (19)$$

$$\cos\beta = \left[1 + \frac{\cos^2\phi \sin^2\theta}{\cos^2\alpha(\cos\theta - \tan\alpha \sin\theta \sin\phi)^2}\right]^{-1/2} . \qquad (20)$$

Let us now turn to each term in Eqn (10). For $V_\theta^2$ we obtain:

$$V_\theta^2 = \frac{9}{4} U^2 \sin^2\theta . \qquad (21)$$

Let us next examine $V_\beta$. Solving Eqn (13) for r, we find:

$$r = \frac{R \sin\theta \cos\phi}{\sin\beta} \quad . \tag{22}$$

Thus, we find:

$$V_\beta = \omega r = \frac{\omega R \sin\theta \cos\phi}{\sin\beta} \quad , \tag{23}$$

and

$$V_\beta^2 = \omega^2 R^2 \frac{\sin^2\theta \cos^2\phi}{\sin^2\beta} \quad . \tag{24}$$

Substituting Eqns (21), (23), and (24) into Eqn (10) we find:

$$V^2 = \frac{9}{4} U^2 \sin^2\theta + \frac{\omega^2 R^2 \sin^2\theta \cos^2\phi}{\sin^2\beta} +$$

$$+ 3U \sin\theta \frac{\omega R \sin\theta \cos\phi}{\sin\beta} \left[ \sin\alpha \sin\beta \cos\theta \sin\phi + \right.$$

$$\left. + \cos\alpha \sin\beta \sin\theta + \cos\beta \cos\theta \cos\phi \right] .$$

Utilizing relations (18) through (20), this equation becomes:

$$V^2 = \frac{9}{4}U^2\sin^2\theta + \omega^2R^2\sin^2\theta\cos^2\phi\left[1 + \frac{\cos^2\alpha\left[\cos\theta - \tan\alpha\sin\theta\sin\phi\right]^2}{\cos^2\phi\sin^2\theta}\right] +$$

$$+ 3U\omega R\sin^2\theta\cos\phi\left[\sin\alpha\cos\theta\sin\phi + \cos\alpha\sin\theta + \cot\beta\cos\theta\cos\phi\right]$$

$$= \frac{9}{4}U^2\sin^2\theta + \omega^2R^2\left[\sin^2\theta\cos^2\phi + \cos^2\alpha\left(\cos\theta - \tan\alpha\sin\theta\sin\phi\right)^2\right] +$$

$$+ 3U\omega R\sin^2\theta\cos\phi\left[\sin\alpha\cos\theta\sin\phi + \cos\alpha\sin\theta + \frac{\cos\alpha\cos\theta\cos\phi}{\cos\phi\sin\theta}\left(\cos\theta - \tan\alpha\sin\theta\sin\phi\right)\right],$$

which may be simplified to:

$$V^2 = \frac{9}{4}U^2\sin^2\theta + 3U\omega R\cos\alpha\sin\theta\cos\phi +$$

$$+\omega^2R^2\left[\cos^2\phi\sin^2\theta + \cos^2\alpha\cos^2\theta + \sin^2\alpha\sin^2\theta\sin^2\phi - \right.$$

$$\left. - 2\cos\alpha\sin\alpha\cos\theta\sin\theta\sin\phi\right],$$

or, finally:

$$V^2 = \frac{9}{4}U^2\sin^2\theta + 3\omega RU\cos\alpha\sin\theta\cos\phi +$$

$$+\omega^2R^2\left[1 - \sin^2\phi\sin^2\theta + \sin^2\alpha\left(\sin^2\theta\sin^2\phi - \cos^2\theta\right) - \right. \qquad (25)$$

$$\left. - 2\sin\alpha\cos\alpha\sin\theta\cos\theta\sin\phi\right].$$

Thus, we have expressed $V^2$ as a function of the two variables $\theta$ and $\phi$.

C. Determination of Lift Force

The net force acting on a small area dA of the sphere (neglecting the viscous forces) is given by:

$$d\vec{F} = -P\hat{n}\,dA \quad , \tag{26}$$

where:

P = pressure

$\hat{n}$ = outward normal unit vector

dA = increment of area.

The components of dF in the x, y, and z directions are then given by:

$$\begin{aligned} dF_x &= d\vec{F}\cdot\hat{i} = -P\,dA\,\hat{n}\cdot\hat{i} \\ dF_Y &= d\vec{F}\cdot\hat{j} = -P\,dA\,\hat{n}\cdot\hat{j} \\ dF_z &= d\vec{F}\cdot\hat{k} = -P\,dA\,\hat{n}\cdot\hat{k} \quad . \end{aligned} \tag{27}$$

The unit normal vector can be expressed in terms of the x'-y'-z' system as

$$\hat{n} = \cos\theta\,\hat{j}' + \sin\theta\,\hat{k}' .$$

But $\hat{j}' = \hat{j}$ and $\hat{k}' = \sin\phi\,\hat{i} + \cos\phi\,\hat{k}$.

Therefore:

$$\hat{n} = \sin\theta\sin\phi\,\hat{i} + \cos\theta\,\hat{j} + \sin\theta\cos\phi\,\hat{k} \quad . \tag{28}$$

Thus we find:

$$\begin{aligned} dF_X &= -P\,dA\sin\theta\sin\phi \\ dF_Y &= -P\,dA\cos\theta \\ dF_Z &= -P\,dA\sin\theta\cos\phi \quad . \end{aligned} \tag{29}$$

In terms of $\theta$ and $\phi$, we may write dA as:

$$dA = (R\sin\theta\,d\phi)(R\,d\theta) = R^2\sin\theta\,d\theta\,d\phi \quad .$$

Thus, Eqn (29) becomes:

$$dF_x = - PR^2 \sin^2\theta \sin\phi \, d\theta \, d\phi$$

$$dF_y = - PR^2 \sin\theta \cos\theta \, d\theta \, d\phi \qquad (30)$$

$$dF_z = - PR^2 \sin^2\theta \cos\phi \, d\theta \, d\phi \, .$$

In general, real flow is viscid and not irrotational, and strictly speaking Bernoulli's equation is not applicable. If we restrict the analysis to small Reynolds number conditions, the flow will be almost irrotational and consequently, we may use Bernoulli's equation as an approximation. Therefore, one may write:

$$P + \tfrac{1}{2}\rho V^2 = P_\infty + \tfrac{1}{2}\rho U^2, \qquad (31)$$

or:

$$-P = -P_\infty + \tfrac{1}{2}(V^2 - U^2) \, .$$

And thus Eqn (30) becomes:

$$dF_x = \left[\tfrac{1}{2}\rho(V^2 - U^2) - P_\infty\right] R^2 \sin^2\theta \sin\phi \, d\theta \, d\phi$$

$$dF_y = \left[\tfrac{1}{2}\rho(V^2 - U^2) - P_\infty\right] R^2 \sin\theta \cos\theta \, d\theta \, d\phi \qquad (32)$$

$$dF_z = \left[\tfrac{1}{2}\rho(V^2 - U^2) - P_\infty\right] R^2 \sin^2\theta \cos\phi \, d\theta \, d\phi \, .$$

To obtain the total force acting on the sphere in each direction, we must integrate Eqn (32). Examination of Fig 1 gives the limits of integration as:

$$0 \le \theta \le \pi$$

$$0 \le \phi \le 2\pi \, .$$

and therefore

$$F_X = \int_{\phi=0}^{2\pi} \int_{\theta=0}^{\pi} \left[\tfrac{1}{2}\rho(V^2 - U^2) - P_\infty\right] R^2 \sin^2\theta \sin\phi \, d\theta \, d\phi$$

$$F_Y = \int_{\phi=0}^{2\pi} \int_{\theta=0}^{\pi} \left[\tfrac{1}{2}\rho(V^2 - U^2) - P_\infty\right] R^2 \sin\theta \cos\theta \, d\theta \, d\phi \qquad (33)$$

$$F_Z = \int_{\phi=0}^{2\pi} \int_{\theta=0}^{\pi} \left[\tfrac{1}{2}\rho(V^2 - U^2) - P_\infty\right] R^2 \sin^2\theta \cos\phi \, d\theta \, d\phi \; .$$

Since

$$\int_0^{2\pi} \sin\phi \, d\phi = \int_0^{\pi} \sin\theta \cos\theta \, d\theta = \int_0^{2\pi} \cos\phi \, d\phi = 0 ,$$

all integrations with constant multiplying factors become zero and thus:

$$F_X = \int_{\phi=0}^{2\pi} \int_{\theta=0}^{\pi} \tfrac{1}{2}\rho V^2 R^2 \sin^2\theta \sin\phi \, d\theta \, d\phi$$

$$F_Y = \int_{\phi=0}^{2\pi} \int_{\theta=0}^{\pi} \tfrac{1}{2}\rho V^2 R^2 \sin\theta \cos\theta \, d\theta \, d\phi \qquad (34)$$

$$F_Z = \int_{\phi=0}^{2\pi} \int_{\theta=0}^{\pi} \tfrac{1}{2}\rho V^2 R^2 \sin^2\theta \cos\phi \, d\theta \, d\phi \; .$$

If one substitutes relation (25) for $V^2$ into these equations, all integrals vanish except one in the $F_z$ equation. Equation (34) then becomes:

$$F_x = F_y = 0 . \tag{35}$$

$$\begin{aligned} F_z &= \int_{\phi=0}^{2\pi}\int_{\theta=0}^{\pi} \frac{1}{2}\rho R^2 3\omega R U \cos\alpha \sin^3\theta \cos^2\phi \, d\theta \, d\phi \\ &= \frac{3}{2}\rho R^3 \omega U \cos\alpha \int_{\phi=0}^{2\pi}\int_{\theta=0}^{\pi} \sin^3\theta \cos^2\phi \, d\theta \, d\phi \\ &= \frac{3}{2}\rho R^3 \omega U \cos\alpha \int_{\phi=0}^{2\pi} \cos^2\phi \, d\phi \int_{\theta=0}^{\pi} \sin^3\theta \, d\theta . \end{aligned} \tag{36}$$

These integrals may be evaluated to give:

$$\int_{\phi=0}^{2\pi} \cos^2\phi \, d\phi \int_{\theta=0}^{\pi} \sin^3\theta \, d\theta = \frac{4\pi}{3} ,$$

and thus:

$$F_z = 2\pi\rho R^3 \omega U \cos\alpha .$$

We designate $F_z$ as the lift due to rotation and write:

$$L = 2\pi\rho R^3 U \cos\alpha . \tag{37}$$

Making use of the conventional definition of lift coefficient:

$$C_L = \frac{L}{\frac{1}{2}\rho U^2 S} = \frac{L}{\frac{1}{2}\rho U^2 \pi R^2} , \tag{38}$$

where S = projected area $= \pi R^2$,

we obtain:

$$C_L = \frac{2\pi\rho R^3 \omega U \cos\alpha}{\frac{1}{2}\rho U^2 \pi R^2}$$

or

$$C_L = 4\frac{\omega R}{U}\cos\alpha \quad . \tag{39}$$

## III. INDUCED DRAG

### A. Introduction

The classical theory of lift (Kutta-Joukowski theory) states that lift cannot occur unless circulation exists about the body. Thus, since we have found that lift does exist when the sphere rotates, the rotating sphere has a vortex distribution around it. Since a vortex filament cannot end in a free fluid, the vortex filaments forming the circulation are shed and carried downstream by the free stream. Thus, we have what is referred to as a vortex sheet extending to infinity behind the rotating sphere. This infinite number of infinitesimal vortex filaments is depicted graphically in Fig 2.

The object of this section is to determine analytically the induced angle of attack due to this vortex sheet so that we may eventually calculate the induced drag and drag coefficient in a manner similar to the classical finite wing theory.

As can be seen from Fig 3, the vortex sheet induces a downward velocity which in turn changes the direction of the relative velocity of the air near the sphere. Since the resultant force acts perpendicular to this new resultant velocity, we, so to speak, tilt the resultant force vector backwards through an angle $\alpha_i$ and consequently obtain a component of force in the free stream direction (which represents the induced drag).

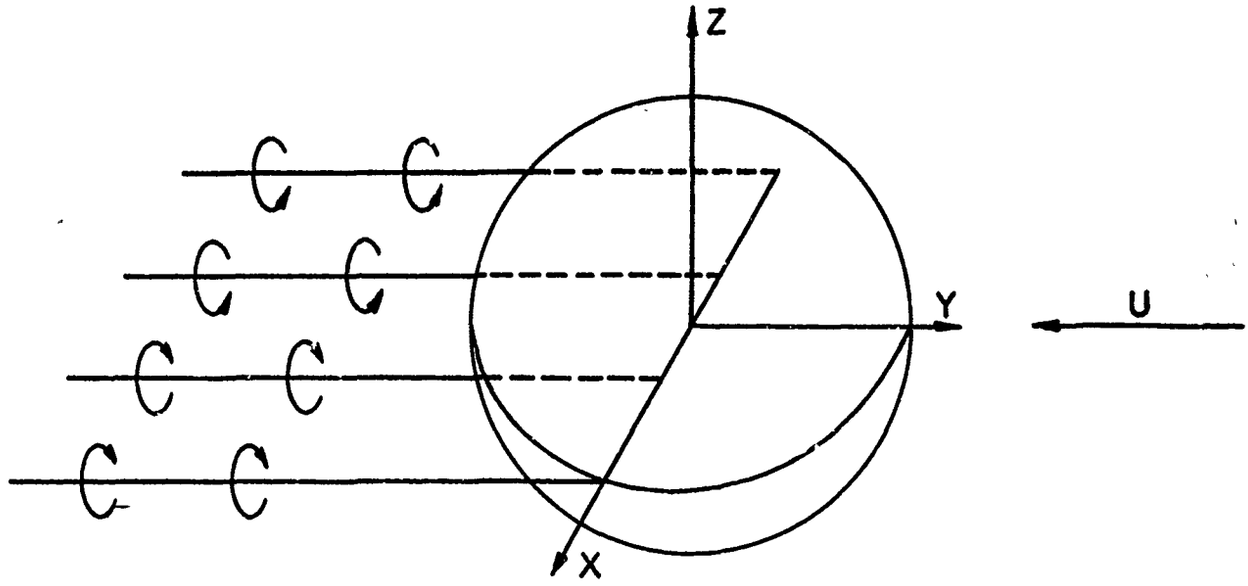


A. THREE-DIMENSIONAL VIEW

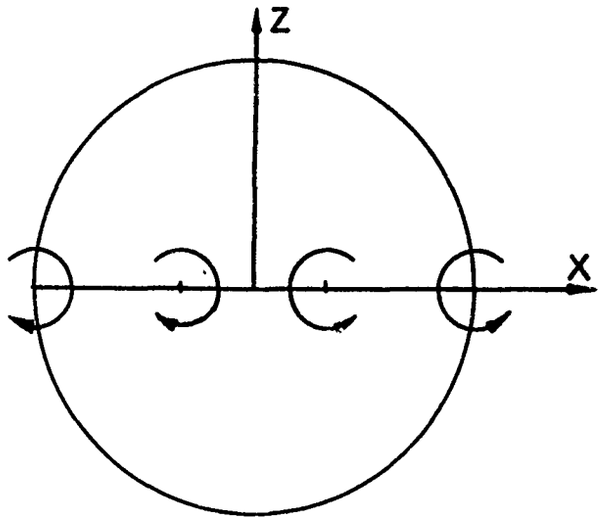


B. REAR VIEW

FIG. 2. DISTRIBUTION OF VORTEX FILAMENTS BEHIND A ROTATING SPHERE.

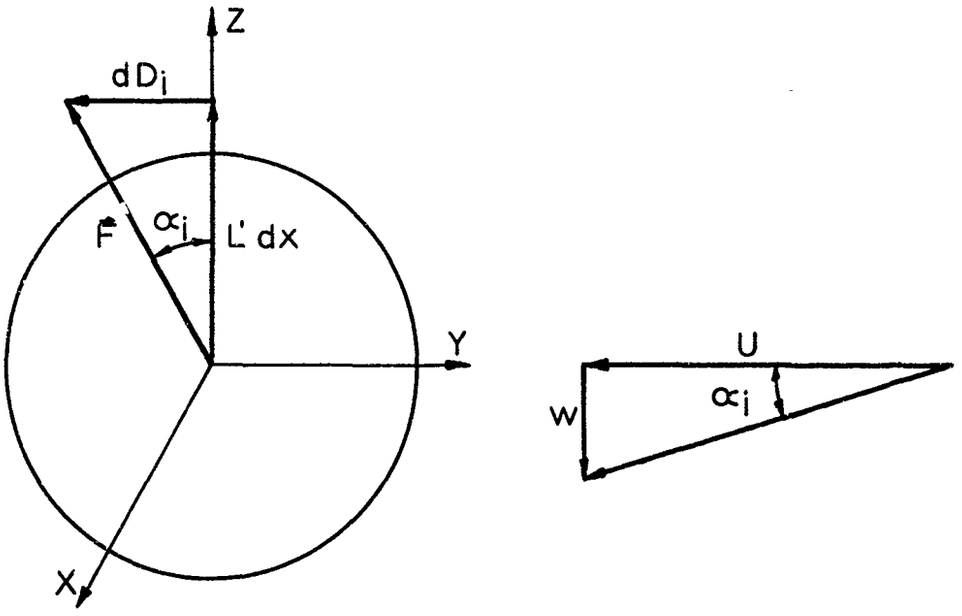


FIG 3. THE INDUCED ANGLE OF ATTACK FOR A ROTATING SPHERE.

From the geometry of Fig 3, we see that

$$\tan \alpha_i = \frac{dD_i}{L'dX} \quad , \tag{40}$$

and

$$\tan \alpha_i = \frac{w}{U} \quad , \tag{41}$$

and thus:

$$dD_i = \frac{w}{U} L'dX \quad . \tag{42}$$

where:

$w$ = local downward velocity

$U$ = free stream velocity

$dD_i$ = induced drag for the segment of the sphere from x to x + dx

$L'$ = lift per unit span .

One therefore recognizes that a knowledge of the induced velocity is sufficient to determine the induced drag and it becomes necessary to determine the induced downwash velocity.

B. Induced Flow Field For a Simple Vortex Filament

Consider a vortex filament as shown in Fig 4. The velocity induced at point P by the section of the filament denoted by dS is given by Biot-Savarts' law (Ref 2) as:

$$dV = \frac{\Gamma}{4\pi} \frac{\cos\beta}{r^2} dS = \frac{\Gamma}{4\pi} \frac{n\,ds}{r^3} \quad . \tag{43}$$

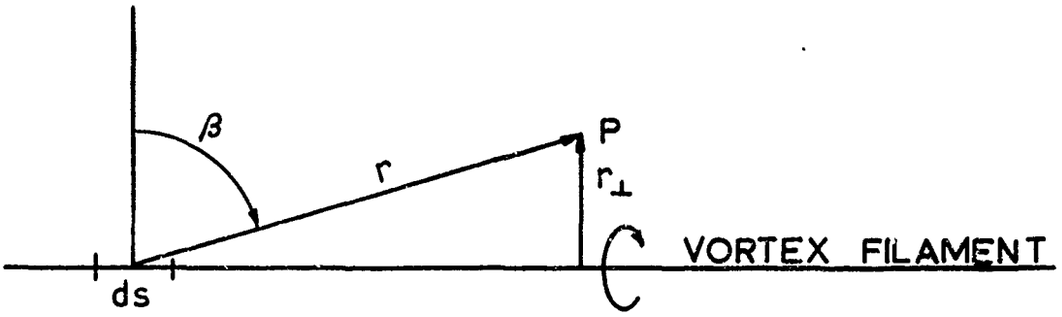


FIG 4. GEOMETRIC REPRESENTATION OF A SINGLE VORTEX FILAMENT OF STRENGTH $\Gamma$ PER UNIT LENGTH.

The induced velocity, for the given fluid rotational direction, is directed into the paper. This equation can be generalized for the case where we are concerned with a vortex sheet made up of infinitely many of the above described filaments. We shall now derive an expression giving the induced velocity at any point P (coordinates - $x_o, y_o, z_o$) as shown in Fig 5. The induced velocity at P due to the entire filament S-S' (where $S \rightarrow -\infty$) is given by Biot-Savarts law by integrating dy from 0 to $-\infty$ . From Fig 5 we see that

$$r_1 = \sqrt{(x-x_o)^2 + z_o^2} \quad .$$

Also we find:

$$r = \sqrt{(x-x_o)^2 + (y-y_o)^2 + z_o^2} \quad .$$

Substitution of these relations into Eqn (43) and letting $dS = dy$, we obtain:

$$dV = \frac{\Gamma}{4\pi} \frac{\sqrt{(x-x_o)^2 + z_o^2}\, dy}{\left[(x-x_o)^2 + (y-y_o)^2 + z_o^2\right]^{3/2}} \quad . \qquad (44)$$

To determine the entire contribution at P due to the filament S-S', we integrate over y and obtain:

$$V(x_o, y_o, z_o) = \int_{-\infty}^{0} \frac{\Gamma}{4\pi} \frac{\sqrt{(x-x_o)^2 + z_o^2}\, dy}{\left[(x-x_o)^2 + (y-y_o)^2 + z_o^2\right]^{3/2}} \quad . \qquad (45)$$

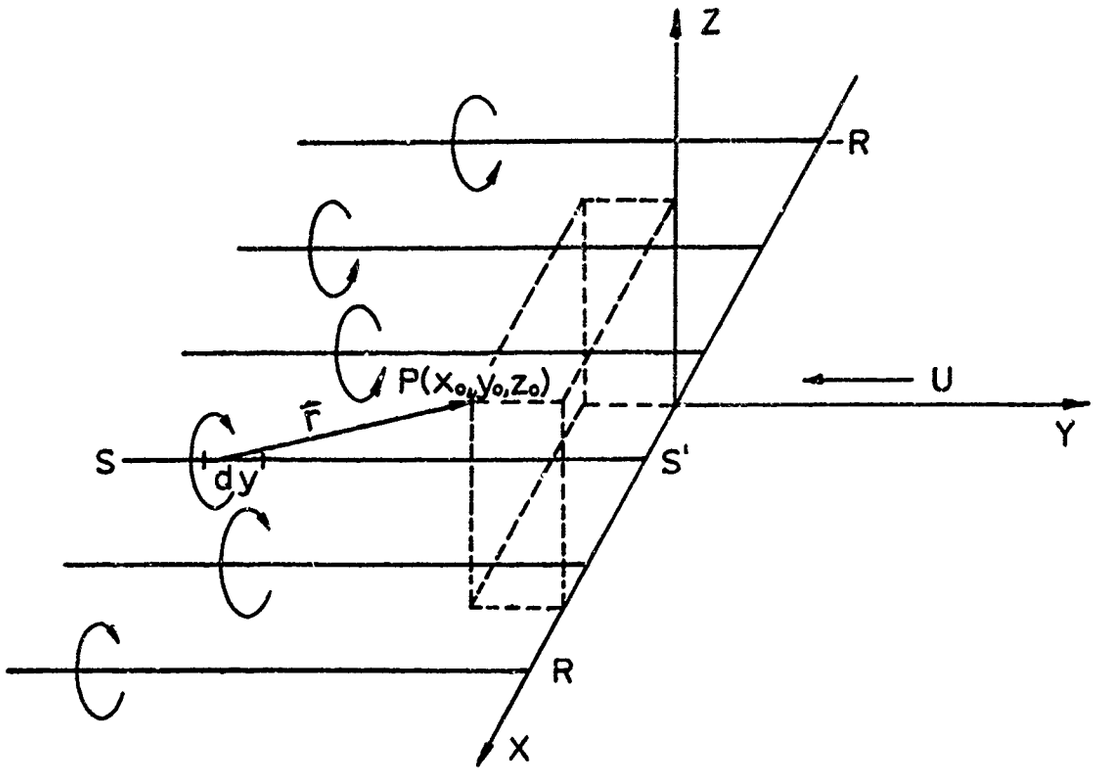


A. THREE-DIMENSIONAL VIEW OF A VORTEX SHEET

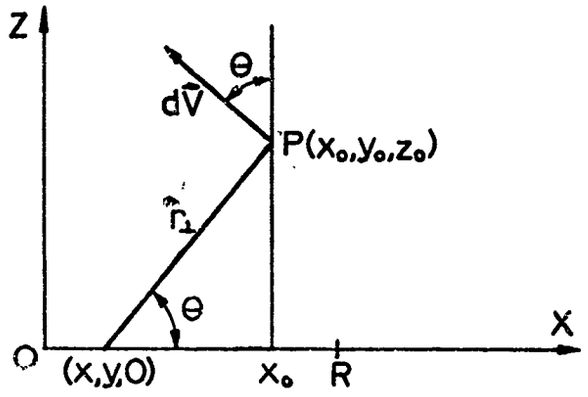


B. REAR VIEW OF A VORTEX SHEET AND A POINT P

FIG 5. GEOMETRIC REPRESENTATION OF A VORTEX FILAMENT AND AN ARBITRARY POINT P.

Remembering that the strength of a vortex filament is constant along its length, we may re-write Eqn (45) as:

$$V(X_o y_o Z_o) = \frac{\Gamma}{4\pi}\sqrt{(X-X_o)^2 + Z_o^2} \int_{-\infty}^{0} \frac{dy}{[(X-X_o)^2+(y-y_o)^2+Z_o^2]^{3/2}} \cdot$$

This standard integral can be found in tables and we obtain:

$$V(X_o y_o Z_o) = \frac{\Gamma}{4\pi}\frac{\sqrt{(X-X_o)^2+Z_o^2}}{[(X-X_o)^2+Z_o^2]} \frac{y-y_o}{\sqrt{(X-X_o)^2+(y-y_o)^2+Z_o^2}} \Bigg|_{y=-\infty}^{0}$$

$$= \frac{\Gamma}{4\pi}\frac{1}{\sqrt{(X-X_o)^2+Z_o^2}}\left[1 - \frac{y_o}{\sqrt{(X-X_o)^2+y_o^2+Z_o^2}}\right] ,$$

or:

$$V(X_o y_o Z_o) = \frac{\Gamma}{4\pi\sqrt{(X-X_o)^2+Z_o^2}}\left[1 - \frac{y_o}{\sqrt{(X-X_o)^2+y_o^2+Z_o^2}}\right] . \qquad (46)$$

We are only interested in the downward velocity W. From Fig 5-B, we find that this is connected with V by the relation:

$$w = V\cos\theta \quad . \qquad (47)$$

Also, from Fig 5-B, we find:

$$\cos\Theta = \frac{x_o - x}{\sqrt{(x_o - x)^2 + z_o^2}} \quad . \tag{48}$$

Combining relations (46) through (48) we find:

$$w = \frac{\Gamma}{4\pi} \frac{(x_o - x)}{\left[(x_o - x)^2 + z_o^2\right]} \left[1 - \frac{y_o}{\sqrt{(x - x_o)^2 + y_o^2 + z_o^2}}\right] \quad . \tag{49}$$

To obtain the total effect at P due to all of the filaments, we must now integrate relation (49) over x. Therefore, we obtain:

$$w = \frac{1}{4\pi} \int_{-R}^{R} \frac{(x_o - x)\frac{d\Gamma}{dx}}{\left[(x - x_o)^2 + z_o^2\right]} \left[1 - \frac{y_o}{\sqrt{(x - x_o)^2 + y_o^2 + z_o^2}}\right] dx \quad . \tag{50}$$

We have chosen the limits as shown since we consider the vortex sheet to originate along a diameter 2R of a sphere. If one knows the circulation distribution $\Gamma(x)$, Eqn (50) can be integrated to give the total downwash at $P(x_o, y_o, z_o)$.

C. Determination of the Circulation Distribution

From the Kutta-Joukowski theorem, the circulation and lift per unit span are related by

$$\Gamma = \frac{L'}{\rho U} \quad , \tag{51}$$

where: L' = lift per unit span.

Thus, it is seen that a knowledge of the lift distribution gives the circulation distribution.

To obtain the lift per unit span distribution, we refer to Fig 6. We shall use this coordinate system and transform all variables into x and $\gamma$. The force acting on the increment of projected area perpendicular to r is given by:

$$dL = -P\sin\gamma\, r\, d\gamma\, dx . \tag{52}$$

The lift per unit span is then given by:

$$\frac{dL}{dx} = d\left(\frac{L}{dx}\right) = dL' = -P\sin\gamma\, r\, d\gamma ,$$

or:

$$L' = \int_{\gamma=0}^{2\pi} P\sin\gamma\, r\, d\gamma . \tag{53}$$

Applying Bernoulli's Equation, we find:

$$L' = \int_{\gamma=0}^{2\pi} \left[\frac{1}{2}\rho(V^2-U^2) - P_\infty\right]\sin\gamma\, r\, d\gamma .$$

When integrating over $\gamma$, r remains constant.
Thus we obtain:

$$L' = \frac{\rho r}{2}\int_{\gamma=0}^{2\pi} V^2\sin\gamma\, d\gamma . \tag{54}$$

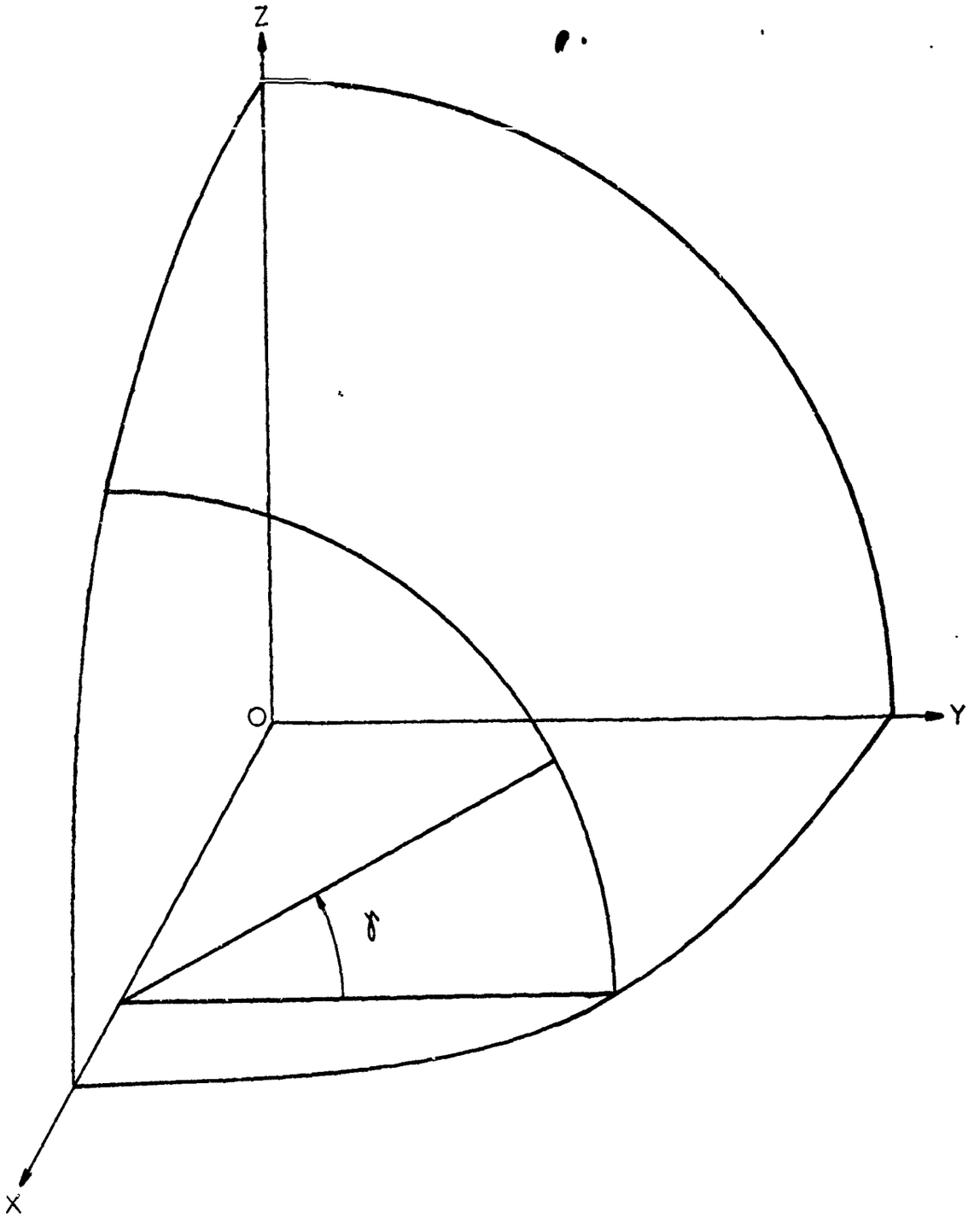


FIG 6. COORDINATE SYSTEM USED IN DETERMINING LIFT DISTRIBUTION.

We now must transform Eqn (25) into a function of $\gamma$ and x. Referring to Figs 1 and 6, we obtain the following relations:

$$\sin\Theta = \frac{\sqrt{R^2-y^2}}{R} \quad ; \quad \cos\Theta = \frac{y}{R}$$

$$\sin\phi = \frac{x}{\sqrt{R^2-y^2}} \quad ; \quad \cos\phi = \frac{z}{\sqrt{R^2-y^2}} \tag{55}$$

$$\sin\gamma = \frac{z}{\sqrt{R^2-x^2}} \quad ; \quad \cos\gamma = \frac{y}{\sqrt{R^2-x^2}} \tag{56}$$

$$r = \sqrt{R^2-x^2} \quad . \tag{57}$$

We wish to write $\Theta$ and $\phi$ in terms of $\gamma$ and x. Eliminating y and z between Eqns (55) and (56) yields:

$$\sin\Theta = \frac{\sqrt{R^2-(R^2-x^2)\cos^2\gamma}}{R}$$

$$\cos\Theta = \frac{\sqrt{R^2-x^2}\cos\gamma}{R} \tag{58}$$

$$\sin\phi = \frac{x}{\sqrt{R^2-(R^2-x^2)\cos^2\gamma}}$$

$$\cos\phi = \frac{\sqrt{R^2-x^2}\sin\gamma}{\sqrt{R^2-(R^2-x^2)\cos^2\gamma}} \quad .$$

Substituting relations (58) into (25), we find:

$$V^2 = \frac{9}{4}U^2\left[\sin^2\delta + \left(\frac{X}{R}\right)^2\cos^2\delta\right] + 3\omega RU\cos\alpha\sqrt{1-\left(\frac{X}{R}\right)^2}\sin\delta +$$

$$+\omega^2R^2\left\{1-\left(\frac{X}{R}\right)^2 + \sin^2\alpha\left[\left(\frac{X}{R}\right)^2\left(1+\cos^2\delta\right)-1\right] - \right. \qquad (59)$$

$$\left. - 2\sin\alpha\cos\alpha\sqrt{1-\left(\frac{X}{R}\right)^2}\ \frac{X}{R}\cos\delta\right\}.$$

Substituting relation (59) into (54) gives:

$$L' = \frac{\rho\sqrt{R^2-X^2}}{2}\int_{\delta=0}^{2\pi}\left\{\frac{9}{4}U^2\left[\sin^2\delta + \left(\frac{X}{R}\right)^2\cos^2\delta\right] + 3\omega RU\cos\alpha\sqrt{1-\left(\frac{X}{R}\right)^2}\sin\delta\right\}\sin\delta\,d\delta +$$

$$+\int_{\delta=0}^{2\pi}\omega^2R^2\left\{1-\left(\frac{X}{R}\right)^2 + \sin^2\alpha\left[\left(\frac{X}{R}\right)^2(1+\cos^2\delta)-1\right] - 2\sin\alpha\cos\alpha\sqrt{1-\left(\frac{X}{R}\right)^2}\cos\delta\right\}\sin\delta\,d\delta\,.$$

All integrals become zero except the one containing $3\omega RU\cos\alpha\sqrt{1-\left(\frac{X}{R}\right)^2}\sin\delta$ and thus:

$$L' = \frac{\rho\sqrt{R^2-X^2}}{2}\int_{\delta=0}^{2\pi}3\omega RU\cos\alpha\sqrt{1-\left(\frac{X}{R}\right)^2}\sin^2\delta\,d\delta$$

$$= \frac{3}{2}\rho\omega R^2U\cos\alpha\left[1-\left(\frac{X}{R}\right)^2\right]\pi\ ,$$

or:

$$L' = \frac{3}{2}\pi\,\omega R^2U\rho\cos\alpha\left[1-\left(\frac{X}{R}\right)^2\right]. \qquad (60)$$

Thus, utilizing relation (51), we find:

$$\Gamma = \frac{3}{2}\pi\omega R^2 \cos\alpha\left[1-\left(\frac{x}{R}\right)^2\right] , \tag{61}$$

and

$$\frac{d\Gamma}{dx} = -3\pi\omega x\cos\alpha \tag{62}$$

Substitution of Eqn (62) into (50) yields:

$$w(x_o y_o z_o) = -\frac{3}{4}\omega\cos\alpha\int_{-R}^{R}\frac{x(x-x_o)}{(x-x_o)^2+z_o^2}\left\{1-\frac{y_o}{\left[(x-x_o)^2+y_o^2+z_o^2\right]^{1/2}}\right\}dx . \tag{63}$$

In the original formulation, $d\Gamma$ was positive. Therefore, for a positive element dx, we want to obtain a positive $d\Gamma$ . Thus, we must introduce a negative sign in the relation for $\frac{d\Gamma}{dx}$ to make $d\Gamma$ positive when dx is positive. This explains the negative sign preceding the integral in Eqn (63).

To integrate this equation, we let:

$$\begin{aligned} \xi &= x-x_o \\ dx &= d\xi . \end{aligned} \tag{64}$$

The limits of integration become:

$$-R-x_o \leq \xi \leq R-x_o ,$$

and we obtain:

$$w(x_o y_o z_o) = -\frac{3}{4}\omega\cos\alpha \int_{-R-x_o}^{R-x_o} \frac{\xi(\xi + x_o)}{\xi^2 + z_o^2}\left[1 - \frac{y_o}{(\xi^2 + y_o^2 + z_o^2)^{1/2}}\right] d\xi \quad .$$

Thus we obtain:

$$w(x_o y_o z_o) = -\frac{3}{4}\omega\cos\alpha\,(I_1 + I_2 + I_3 + I_4)\,,$$

where

$$I_1 = \int_{-R-x_o}^{R-x_o} \frac{\xi^2 d\xi}{\xi^2 + z_o^2}$$

$$I_2 = x_o \int_{-R-x_o}^{R-x_o} \frac{\xi\, d\xi}{\xi^2 + z_o^2} \qquad (65)$$

$$I_3 = -y_o \int_{-R-x_o}^{R-x_o} \frac{\xi^2 d\xi}{(\xi^2 + z_o^2)(\xi^2 + z_o^2 + y_o^2)^{1/2}}$$

$$I_4 = -y_o x_o \int_{-R-x_o}^{R-x_o} \frac{\xi\, d\xi}{(\xi^2 + z_o^2)(\xi^2 + z_o^2 + y_o^2)^{1/2}} \quad .$$

The following standard integrals can be found in integral tables:

$$\int \frac{\xi^2 d\xi}{\xi^2 + z_o^2} = \xi - z_o \tan^{-1}\frac{\xi}{z_o}$$

$$\int \frac{\xi\, d\xi}{\xi^2 + z_o^2} = \frac{1}{2}\ln(\xi^2 + z_o^2) \quad ,$$

$$\int \frac{\xi^2 d\xi}{\left[\xi^2+z_o^2\right]\left[\xi^2+y_o^2+z_o^2\right]^{\frac{1}{2}}} = \ln\left[\xi+\sqrt{\xi^2+y_o^2+z_o^2}\right] - \frac{z_o}{y_o}\tan^{-1}\frac{y_o\,\xi}{z_o\sqrt{\xi^2+y_o^2+z_o^2}}$$

$$\int \frac{\xi d\xi}{\left[\xi^2+z_o^2\right]\left[\xi^2+y_o^2+z_o^2\right]^{\frac{1}{2}}} = \frac{1}{2y_o}\ln\left[\frac{\sqrt{\xi^2+y_o^2+z_o^2}-y_o}{\sqrt{\xi^2+y_o^2+z_o^2}+y_o}\right] .$$

Thus, we obtain:

$$W(x_o,y_o,z_o) = -\frac{3}{4}\omega\cos\alpha\left\{\xi - z_o\tan^{-1}\frac{\xi}{z_o} + \frac{x_o}{2}\ln(\xi^2+z^2) - \right.$$

$$- y_o\left[\ln(\xi+\sqrt{\xi^2+y_o^2+z_o^2}) - \frac{z_o}{y_o}\tan^{-1}\frac{y_o\,\xi}{z_o\sqrt{\xi^2+y_o^2+z_o^2}}\right] -$$

$$\left. - \frac{x_o}{2}\ln\left[\frac{\sqrt{\xi^2+y_o^2+z_o^2}-y_o}{\sqrt{\xi^2+y_o^2+z_o^2}+y_o}\right]\right\}\Bigg|_{-R-x_o}^{R-x_o} ,$$

or:

(See next page)

$$w(x_o y_o z_o) = -\frac{3}{4}\omega\cos\alpha\left[\xi + z_o\left(\tan^{-1}\frac{y_o\,\xi}{z_o\sqrt{\xi^2+y_o^2+z_o^2}} - \tan^{-1}\frac{\xi}{z_o}\right) + \frac{x_o}{2}\ln(\xi^2+z_o^2) - \right.$$

$$\left. - y_o \ln(\xi+\sqrt{\xi^2+y_o^2+z_o^2}) - \frac{x_o}{2}\ln\left(\frac{\sqrt{\xi^2+y_o^2+z_o^2}-y_o}{\sqrt{\xi^2+y_o^2+z_o^2}+y_o}\right)\right]\Bigg|_{-R-x_o}^{R-x_o} \quad (66)$$

Using the identity:

$$\tan^{-1}x - \tan^{-1}y = \tan^{-1}\left(\frac{x-y}{1+xy}\right),$$

we obtain:

$$w(x_o y_o z_o) = -\frac{3}{4}\omega\cos\alpha\left\{\xi + z_o\tan^{-1}\left[\frac{\frac{\xi}{z_o}\left(\frac{y_o}{\sqrt{\xi^2+y^2+z^2}}-1\right)}{1+\frac{y_o}{\sqrt{\xi^2+y_o^2+z_o^2}}\left(\frac{\xi}{z_o}\right)^2}\right] + \right. \quad (67)$$

$$\left. + \frac{x_o}{2}\ln\left[\frac{\sqrt{\xi^2+y_o^2+z_o^2}+y_o}{\sqrt{\xi^2+y_o^2+z_o^2}-y_o}(\xi^2+z_o^2)\right] - y_o\ln(\xi+\sqrt{\xi^2+y_o^2+z_o^2})\right\}\Bigg|_{-R-x_o}^{R-x_o}$$

After substituting the limits of integration, we find:

(See next page)

$$w(x_o y_o z_o) = -\frac{3}{4}\omega\cos\alpha\left\{2R + z_o\left[\tan^{-1}\left(\frac{z_o(R-x_o)\left|y_o - \sqrt{R^2+x_o^2+y_o^2+z_o^2-2Rx_o}\right|}{z_o^2\sqrt{R^2+x_o^2+y_o^2+z_o^2-2x_oR}+y_o(R-x_o)^2}\right)+\right.\right.$$

$$\left.+\tan^{-1}\left(\frac{z_o(R+x_o)\left|y_o - \sqrt{R^2+x_o^2+y_o^2+z_o^2+2x_oR}\right|}{z_o^2\sqrt{R^2+x_o^2+y_o^2+z_o^2+2x_oR}+y_o(R+x_o)^2}\right)\right] + \frac{x_o}{2}\ln\left[\frac{\sqrt{R^2+x_o^2+y_o^2+z_o^2-2x_oR}+y_o}{\sqrt{R^2+x_o^2+y_o^2+z_o^2+2x_oR}+y_o}\right]\cdot$$

$$\left.\cdot\left|\frac{\sqrt{R^2+x_o^2+y_o^2+z_o^2+2x_oR}-y_o}{\sqrt{R^2+x_o^2+y_o^2+z_o^2-2x_oR}-y_o}\right|\left|\frac{R^2+x_o^2+z_o^2-2x_oR}{R^2+x_o^2+z_o^2+2x_oR}\right|\right] + y_o\ln\left[\frac{R+x_o+\sqrt{R^2+x_o^2+y_o^2+z_o^2+2Rx_o}}{R-x_o+\sqrt{R^2+x_o^2+y_o^2+z_o^2-2Rx_o}}\right]\Bigg\}. \quad (68)$$

We will be mainly interested in the downwash distribution along the lifting line (i.e., along a diameter in the x direction). Along this lifting line ($y_o = 0$, $z_o = 0$) we have:

$$w(x_o,0,0) = -\frac{3}{4}\omega\cos\alpha\left[2R + \frac{x_o}{2}\ln\left|\frac{R^2+x_o^2-2Rx_o}{R^2+x_o^2+2Rx_o}\right|\right],$$

or, rewriting this in terms of x instead of $x_o$, we obtain:

$$w(x,0,0) = -\frac{3}{4}\omega\cos\alpha\left[2R + \frac{x}{2}\ln\left|\frac{R^2+x^2-2xR}{R^2+x^2+2xR}\right|\right], \quad (69)$$

or, in dimensionless form:

$$\frac{W(x,0,0)}{\omega R\cos\alpha} = -\frac{3}{4}\left[2 + \frac{1}{2}\left(\frac{x}{R}\right)\ln\left(\frac{1+\left(\frac{x}{R}\right)^2 - 2\left(\frac{x}{R}\right)}{1+\left(\frac{x}{R}\right)^2+2\left(\frac{x}{R}\right)}\right)\right] . \qquad (69a)$$

This downwash is presented in Fig 7 as a function of x/R. We now wish to calculate the entire induced drag due to this downwash distribution. Equation (42) presented the induced drag of a segment of the sphere of length dx as

$$dD_i = \frac{W}{U} L' dx . \qquad (42)$$

Utilizing Eqn (60) for L' and (69a) for w, we obtain:

$$dD_i = \frac{9}{8}\pi\omega^2 R^4 \rho\cos^2\alpha\left[1-\left(\frac{x}{R}\right)^2\right]\left[2 + \frac{1}{2}\left(\frac{x}{R}\right)\ln\left(\frac{1+\left(\frac{x}{R}\right)^2 - 2\left(\frac{x}{R}\right)}{1+\left(\frac{x}{R}\right)^2+2\left(\frac{x}{R}\right)}\right)\right] d\left(\frac{x}{R}\right) .$$

Letting $x/R = \xi$ and recognizing that $dD_i/d(x/R)$ is the induced drag distribution for the dimensionless distance $\xi$, we obtain:

$$D_i' = \frac{9}{8}\pi\omega^2 R^4 \rho\cos^2\alpha\left[1-\xi^2\right]\left[2 + \frac{\xi}{2}\ln\left(\frac{1+\xi^2-2\xi}{1+\xi^2+2\xi}\right)\right] , \qquad (70)$$

where: $D_i' = \dfrac{dD_i}{d(x/R)}$ = induced drag for dimensionless unit span.

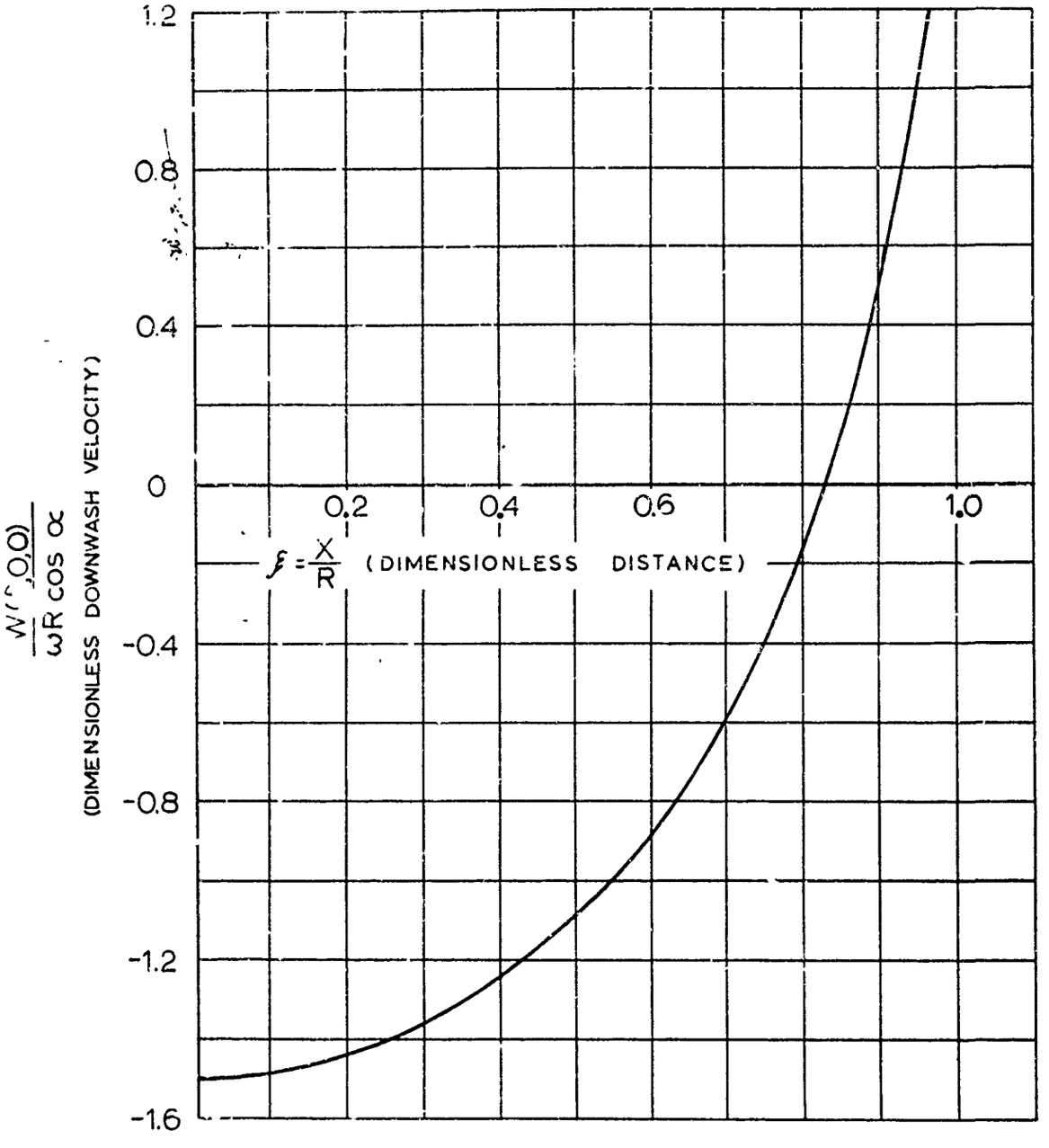


FIG 7. DIMENSIONLESS DOWNWASH DISTRIBUTION ALONG SPHERE DIAMETER PERPENDICULAR TO FREE STREAM VELOCITY.

It is obvious that $D_i'$ is an even function of $\xi$ since:

$$D_i'(-\xi) = \frac{9}{8}\pi\omega^2 R^4 \rho \cos^2\alpha \left[1-(-\xi)^2\right]\left[2 - \frac{\xi}{2}\ln\left(\frac{1+(-\xi)^2-2(-\xi)}{1+(-\xi)^2+2(-\xi)}\right)\right]$$

$$= \frac{9}{8}\pi\omega^2 R^4 \rho \cos^2\alpha \left[1-\xi^2\right]\left[2 + \frac{\xi}{2}\ln\left(\frac{1+\xi^2+2\xi}{1+\xi^2-2\xi}\right)^{-1}\right]$$

$$= \frac{9}{8}\pi\omega^2 R^4 \rho \cos^2\alpha \left[1-\xi^2\right]\left[2 + \frac{\xi}{2}\ln\left(\frac{1+\xi^2-2\xi}{1+\xi^2+2\xi}\right)\right]$$

$$= D_i'(\xi) .$$

Thus, $D_i'(-\xi) = D_i'(\xi)$ and therefore $D_i'(\xi)$ is an even function of $\xi$. The total induced drag on the sphere is given by:

$$D_i = \int_{-1}^{1} D_i'(\xi)\, d\xi .$$

Since $D_i'(\xi)$ is an even function, this can be written as:

$$D_i = 2\int_{0}^{1} D_i'(\xi)\, d\xi . \qquad (71)$$

We also recognize that

$$\xi^2 - 2\xi + 1 = (1-\xi)^2$$

$$\xi^2 + 2\xi + 1 = (1+\xi)^2 ,$$

and therefore:

$$D_i' = \frac{9}{8}\pi\omega^2 R^4 \rho \cos^2\alpha (1-\xi^2)\left[2 + \frac{\xi}{2}\ln\left(\frac{1-\xi}{1+\xi}\right)^2\right] ,$$

or:

$$D_i' = \frac{9}{8}\pi\omega^2 R^4 \rho \cos^2\alpha (1-\xi^2)\left[2 + \xi \ln\left|\frac{1-\xi}{1+\xi}\right|\right] . \qquad (72)$$

Substituting Eqn (72) into (71) yields:

$$D_i = \frac{9}{4}\pi\omega^2 R^4 \rho \cos^2\alpha \int_0^1 (1-\xi^2)\left[2 + \xi \ln\left|\frac{1-\xi}{1+\xi}\right|\right] d\xi . \qquad (73)$$

It only remains to evaluate the integral in relation (73) to obtain the total induced drag. Denoting this integral by I, we may write:

$$I = \int_0^1 (1-\xi^2)\left[2 + \xi \ln\left|\frac{1-\xi}{1+\xi}\right|\right] d\xi$$

$$= 2\int_0^1 (1-\xi^2)\, d\xi + \int_0^1 \xi(1-\xi^2) \ln\left|\frac{1-\xi}{1+\xi}\right| d\xi$$

$$= 2\left[\xi - \frac{\xi^3}{3}\right]_0^1 + \int_0^1 (\xi - \xi^3)\ln(1-\xi)\, d\xi - \int_0^1 (\xi - \xi^3)\ln(1+\xi)\, d\xi .$$

If we let $1-\xi = \eta$ in the first integral and $1+\xi = \eta$ in the second integral, we obtain:

$$I = \frac{4}{3} - \int_1^0 (\eta^3 - 3\eta^2 + 2\eta)\ln\eta\, d\eta + \int_1^2 (\eta^3 - 3\eta^2 + 2\eta)\ln\eta\, d\eta ,$$

or:

$$I = \frac{4}{3} + \int_0^1 (\eta^3 - 3\eta^2 + 2\eta) \ln \eta \, d\eta + \int_1^2 (\eta^3 - 3\eta^2 + 2\eta) \ln \eta \, d\eta \ ,$$

or, finally:

$$I = \frac{4}{3} + \int_0^2 (\eta^3 - 3\eta^2 + 2\eta) \ln \eta \, d\eta \ . \tag{74}$$

From standard integral tables we find:

$$\int \eta^3 \ln \eta \, d\eta = \eta^4 \left( \frac{\ln \eta}{4} - \frac{1}{16} \right)$$

$$\int \eta^2 \ln \eta \, d\eta = \eta^3 \left( \frac{\ln \eta}{3} - \frac{1}{9} \right)$$

$$\int \eta \ln \eta \, d\eta = \eta^2 \left( \frac{\ln \eta}{2} - \frac{1}{4} \right) .$$

Using the relations, we find:

$$I = \frac{4}{3} + \left[ \eta^4 \left( \frac{\ln \eta}{4} - \frac{1}{16} \right) - 3\eta^3 \left( \frac{\ln \eta}{3} - \frac{1}{9} \right) + 2\eta^2 \left( \frac{\ln \eta}{2} - \frac{1}{4} \right) \right]_0^2 \ ,$$

or:

$$I = \frac{4}{3} + \left[ -\frac{1}{3} - \lim_{\eta \to 0} \left( \eta^4 \frac{\ln \eta}{4} - \eta^3 \ln \eta + \eta^2 \ln \eta \right) \right] \ .$$

Utilizing L'Hopital's Rule, we find:

$$\lim_{\eta \to 0} \left[ \eta^4 \frac{\ln \eta}{4} - \eta^3 \ln \eta + \eta^2 \ln \eta \right] = 0 \ .$$

Therefore, we have:

$$I = \frac{4}{3} - \frac{1}{3} = 1 ,$$

or:

$$\int_0^1 (1-\xi^2)\left[2 + \xi \ln\left(\frac{1-\xi}{1+\xi}\right)\right] d\xi = 1 \quad . \tag{75}$$

Therefore, Eqn (73) becomes:

$$D_i = \frac{9}{4}\pi\omega^2 R^4 \rho \cos^2\alpha \quad . \tag{76}$$

With the definition of $C_{D_i} = \frac{D_i}{\frac{1}{2}\rho U^2 \pi R^2}$, we obtain

$$C_{D_i} = \frac{\frac{9}{4}\pi\omega^2 R^4 \rho \cos^2\alpha}{\frac{1}{2}\rho U^2 \pi R^2} = \frac{9}{2}\left(\frac{\omega R \cos\alpha}{U}\right)^2 \quad . \tag{77}$$

However, from Eqn (39), we have:

$$\frac{\omega R \cos\alpha}{U} = \frac{C_L}{4} \quad .$$

Therefore, we find:

$$C_{D_i} = \frac{9}{32} C_L^2 \quad . \tag{78}$$

It is interesting to compare this relation with that for a conventional airfoil which is:

$$C_{D_i} = \frac{C_L^2}{\pi AR\, e} \quad , \tag{79}$$

where: $AR = \frac{b^2}{S}$ = aspect ratio of airfoil.

$e$ = efficiency factor.

Using this form for Eqn (78) we have

$$\pi AR\, e = \frac{32}{9} \quad ,$$

or

$$e = \frac{32}{9\pi AR} \quad . \tag{80}$$

The aspect ratio for the sphere may be expressed as:

$$AR = \frac{b^2}{S} = \frac{(2R)^2}{\pi R^2} = \frac{4}{\pi} \quad .$$

and therefore:

$$e = \frac{32}{9\pi \frac{4}{\pi}} = \frac{8}{9} \quad .$$

Thus, the span efficiency factor for the sphere is 0.89. This factor is extremely close to the efficiency factor of a tapered wing which has a tip chord equal to zero. From Ref 3, Fig 5:4 and Eqn 5:16, we find for this case $e = 0.912$.

## IV. SUMMARY AND DISCUSSION

The study shows that the lift and induced drag acting on a rotating sphere, for relatively small angular velocities ($\omega$) are given by:

$$L = C_L \tfrac{1}{2} \rho U^2 \pi R^2$$

$$D_i = C_{D_i} \tfrac{1}{2} \rho U^2 \pi R^2 \quad ,$$

where:

$$C_L = 4 \left( \frac{\omega R \cos\alpha}{U} \right)$$

$$C_{D_i} = \frac{9}{32} C_L^2 \quad .$$

The direction of the lift force is given by the direction in which a right hand thread would move if the free stream velocity vector were rotated into the angular velocity vector $\vec{\omega}$ . This is illustrated in Fig 8.

In particular, we see that when the axis of rotation coincides with the free stream velocity ( $\alpha = \pi$ or $\alpha = -\pi$), the lift and induced drag become zero.

We recall that the lift and induced drag distribution are given by:

$$L' = \frac{3}{2} \pi \omega R^2 U \rho \cos\alpha \left[ 1 - \left( \frac{x}{R} \right)^2 \right]$$

$$D_i' = \frac{9}{8} \pi \omega^2 R^4 \rho \cos^2\alpha \left[ 1 - \left( \frac{x}{R} \right)^2 \right] \left[ 2 + \frac{x}{R} \ln \left( \frac{1 - \frac{x}{R}}{1 + \frac{x}{R}} \right) \right] \quad .$$

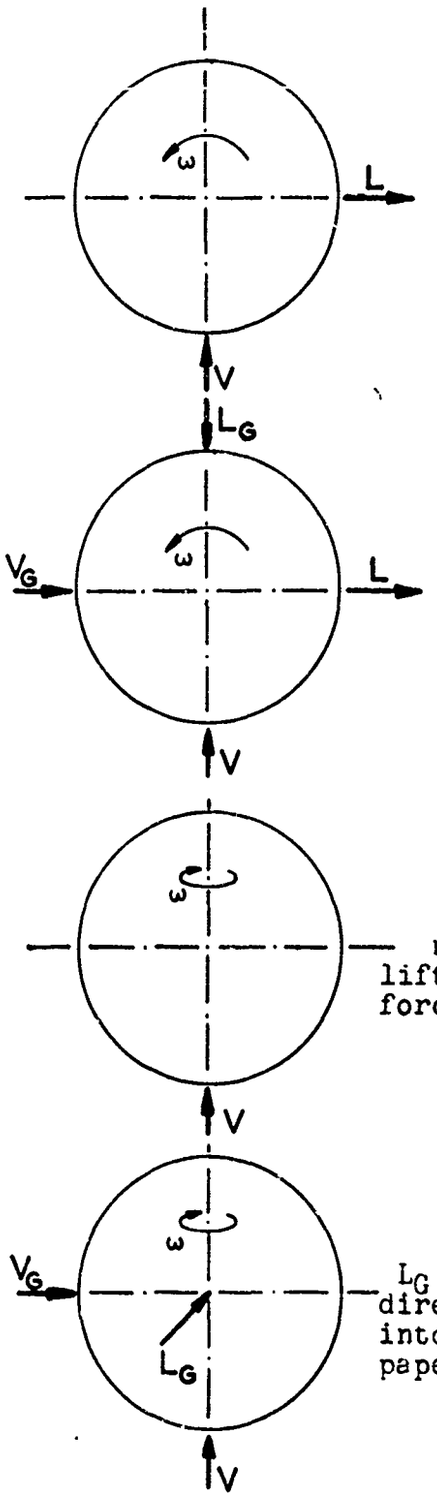


Axis of rotation perpendicular to the free stream velocity gives a net lift force perpendicular to the free stream velocity.

Axis of rotation perpendicular to the free stream velocity and gust gives a net lift force in the direction of the free stream velocity and gust velocity.

Axis of rotation parallel to the free stream velocity gives no lift force.

Axis of rotation parallel to the free stream velocity with a gust perpendicular to the axis of rotation gives a net lift force perpendicular to the gust and free stream velocity.

FIG 8. SCHEMATIC REPRESENTATION OF THE EFFECT OF ROTATION ON SPHERES EXPERIENCING STEADY FALL OR GUSTS.

To find the maximum of $L'$ and $D'$, we differentiate with respect to $x/R$, set the results equal to zero, and find that $L'$ and $D_i'$ attain a maximum at $x/R = 0$. Thus, we may write:

$$L'_{max} = \frac{3}{2} \pi \omega R^2 U \rho \cos \alpha$$

$$D'_{i\,max} = \frac{9}{4} \pi \omega^2 R^4 \rho \cos^2 \alpha \quad ,$$

and, consequently we may write

$$\frac{L'}{L'_{max}} = 1 - \xi^2$$

$$\frac{D'_i}{D'_{i\,max}} = \frac{1}{2} \left[1 - \xi^2\right] \left[2 + \xi \ln \left(\frac{1-\xi}{1+\xi}\right)\right] \quad ,$$

where:

$$\xi = \frac{x}{R} \cdot$$

These relations are presented in Fig 9.

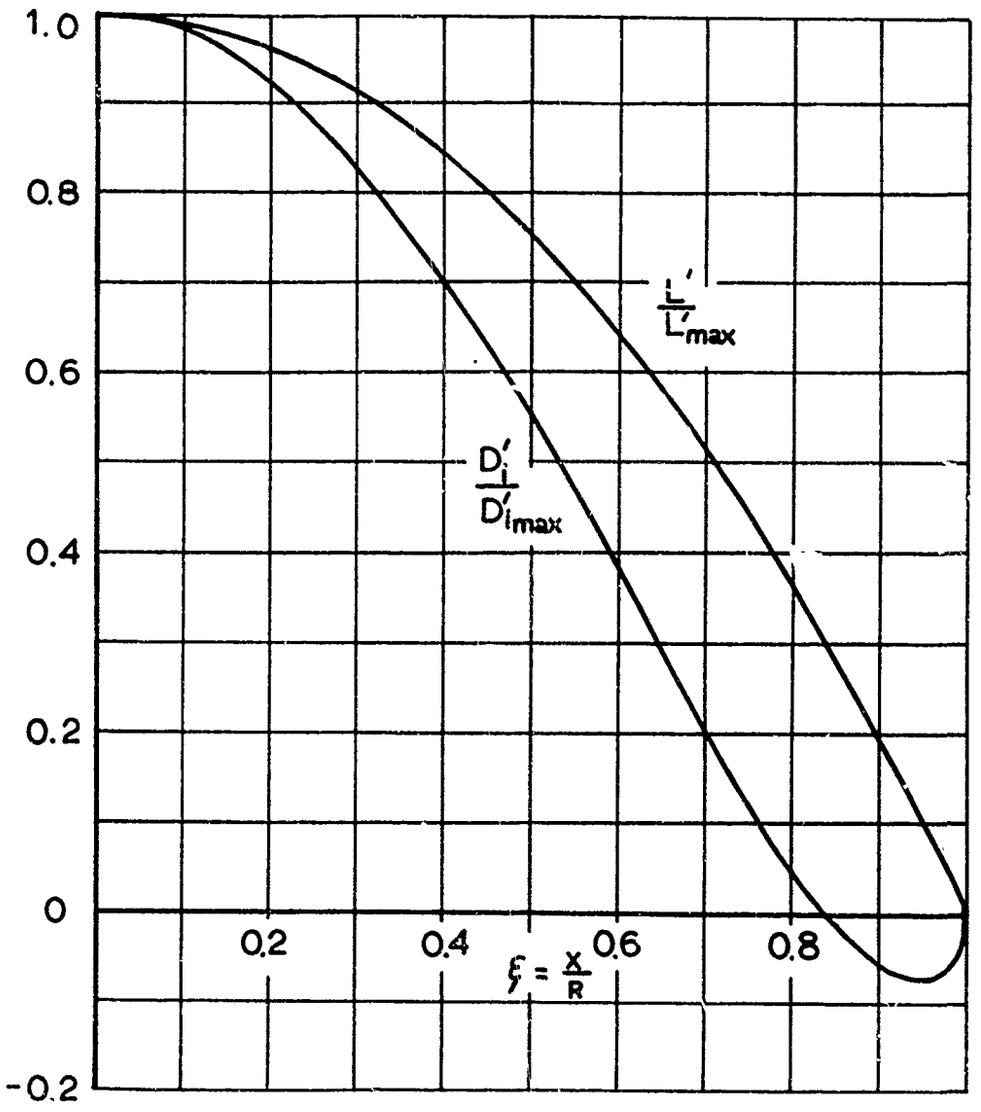


FIG 9. LIFT AND INDUCED DRAG DISTRIBUTION FOR ROTATING SPHERE.

## REFERENCES


1. Streeter, V.L.: Fluid Dynamics, 1st Edition, McGraw-Hill Book Company, Inc., 1948, New York.

2. Kuethe, A.M. and Schetzer, J.D.: Foundation of Aerodynamics, 2nd Edition, John Wiley and Sons, Inc., 1959, New York.

3. Dommasch, D.O., Sherby, S.S., and Connolly, T.F.: Airplane Aerodynamics, 2nd Edition, Pitman Publishing Corporation, 1957, New York.

# THE DRAG OF SPHEROIDS RELATED TO THE DRAG OF A SPHERE WITH AN IDENTICAL SURFACE AREA

Helmut G. Heinrich
Eugene L. Haak
Ronald J. Niccum

University of Minnesota
Minneapolis, Minnesota

The
Project was sponsored by
G. T. Schjeldahl Company, Northfield, Minnesota

ABSTRACT

This investigation is concerned with drag changes associated with the deformation of an originally spherical balloon descending in the atmosphere. Under the assumption that the original sphere deformed into a spheroidal shape of the same surface area, wind tunnel drag measurements were made on two spheroids and compared with the drag of a true sphere over a range of Mach and Reynolds numbers. The results show an appreciable change in drag coefficient due to a relatively small deviation from a spherical shape. Furthermore, in the region under investigation the spheroid drag changes with Mach and Reynolds numbers in about the same manner as the drag of the sphere.

TABLE OF CONTENTS

LIST OF FIGURES

## LIST OF SYMBOLS

| | | |
|---|---|---|
| $A$ | = | Projected area |
| $C_{D_o}$ | = | Drag coefficient of an oblate spheroid |
| $C_{D_p}$ | = | Drag coefficient of a prolate spheroid |
| $C_{D_s}$ | = | Drag coefficient of a sphere |
| $d$ | = | Diameter of the spheroid's largest circular cross section |
| $L$ | = | Length along the spheroid axis of revolution; axis orientated in the flow direction |
| $S$ | = | Total surface area |

# I. INTRODUCTION

In order to determine by means of a descending spherical balloon the air densities at high altitudes, the drag coefficients for a sphere under the related Mach and Reynolds numbers have been determined in Ref 1. A summary of the results of these studies are presented in Fig 1.

If the balloon deviates from the spherical form, its drag coefficients may differ considerably from those determined for the perfect sphere. If this deviation is not properly considered, it leads to faulty information concerning the atmospheric density derived in these experiments. In order to determine the magnitude of this possible discrepancy, the drag coefficients of two spheroids have been measured and compared with those of a perfect sphere under the same aerodynamic conditions.

In reference to this investigation, the authors wish to express their appreciation to Mr. Richard Strom, Mr. Robert Noreen, and Mr. Keith Goar who have contributed greatly to its success.

## II. TEST ARRANGEMENT AND PROCEDURE

As a basis for this investigation, it was assumed that the deformed balloon takes on the shape of a spheroid which has the same surface area as the original sphere.

Three models, an oblate spheroid, a prolate spheroid, and a related true sphere, were tested at Mach numbers of 0.39, 0.685, and 0.90 throughout the range of Reynolds numbers corresponding to the ROBIN sphere tests, illustrated in Fig 1.

The oblate spheroid has a length over diameter (L/d) ratio of 0.9 while the prolate spheroid is characterized by an L/d = 1.11. Both models and their orientation to the flow are shown in Fig 2. The surface area of the three models is $S = 1.767\ in^2$. For the spheroids the axis of revolution was orientated parallel to the flow direction so that the spheroid models would have their circular cross section normal to the flow direction. Figure 3 (a & b) shows how models were mounted in the wind tunnel.

In the ROBIN sphere studies (Ref 1) the drag was derived from the deflection of a simple pendulum under the effect of the aerodynamic force. But in the case of spheroids, where the model axes must be oriented to the flow, the following balance system was used.

The model was sting mounted and supported by a balance strut. This strut transmits the drag force to a cantilever upon which strain gages were attached (Fig 4)

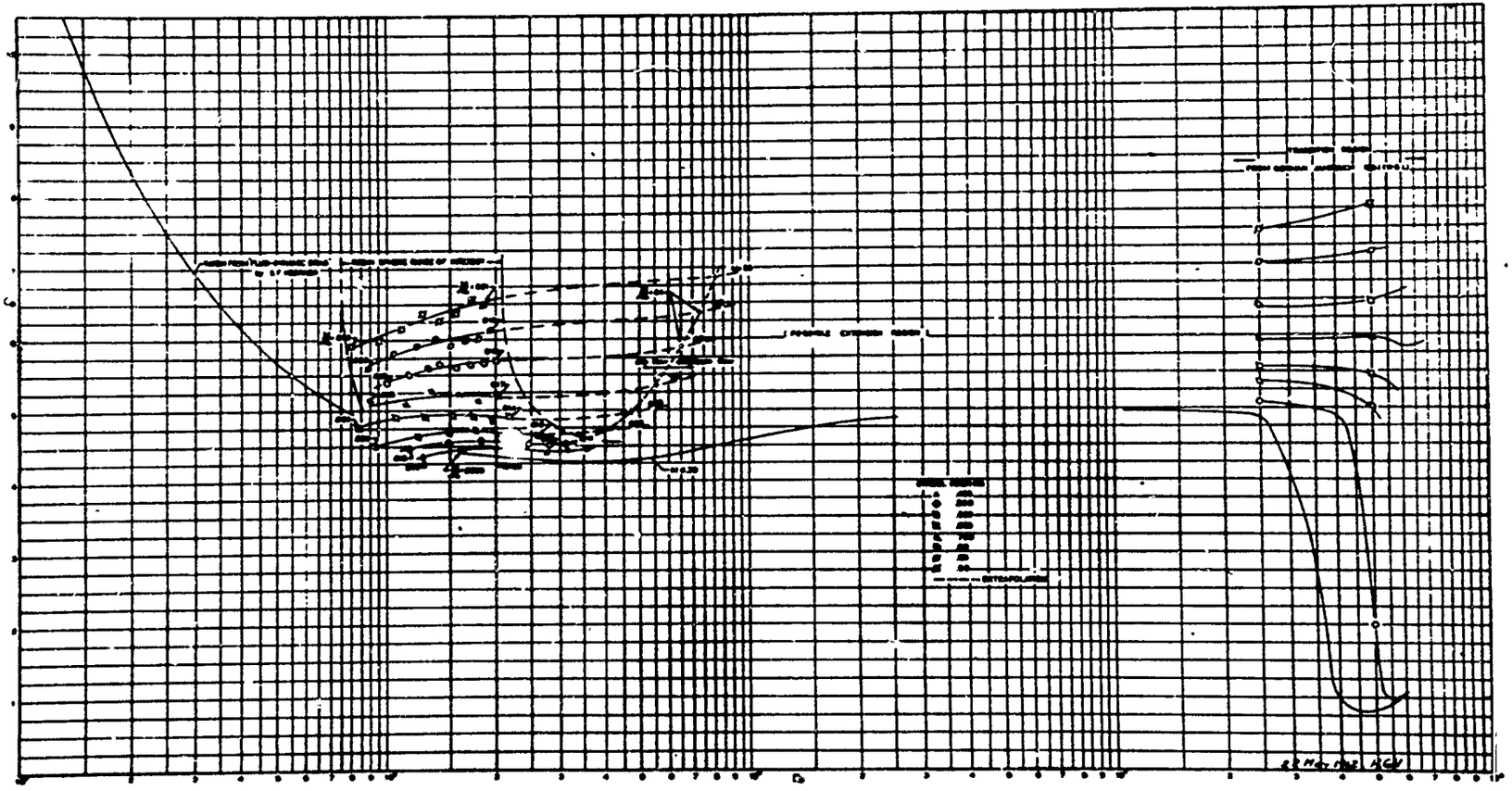

FIG 1. DRAG COEFFICIENT OF A SPHERE AT VARIOUS REYNOLDS NUMBERS

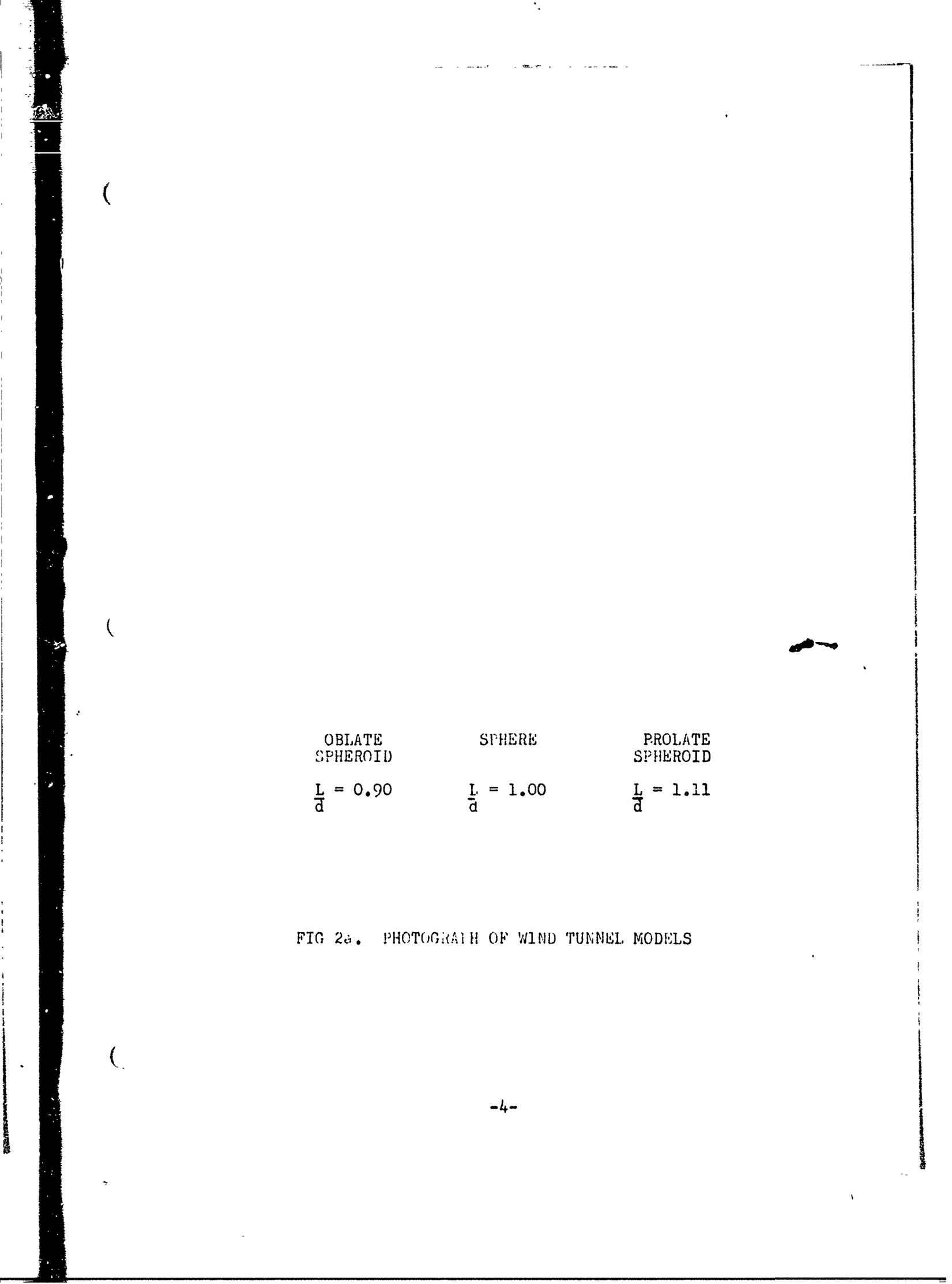


FIG 2a. PHOTOGRAPH OF WIND TUNNEL MODELS

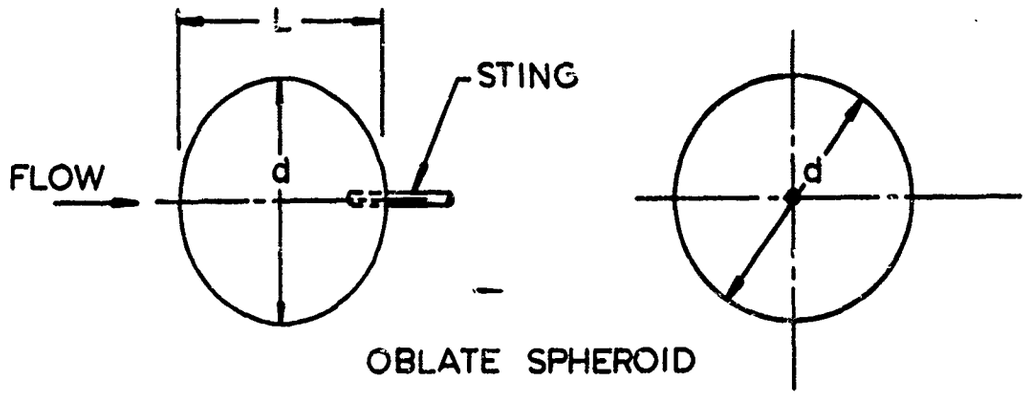


OBLATE SPHEROID

L/d = 0.90 S=1.767 in² A=0 473 in²

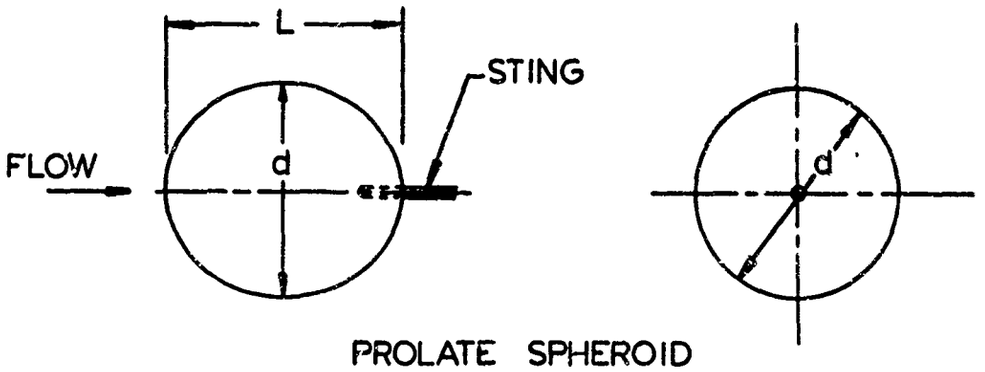


PROLATE SPHEROID

L/d = 1.11 S= 1.767 in² A= 0.411 in²

FIG 2b. SCHEMATIC DIAGRAM OF SPHEROID MODELS

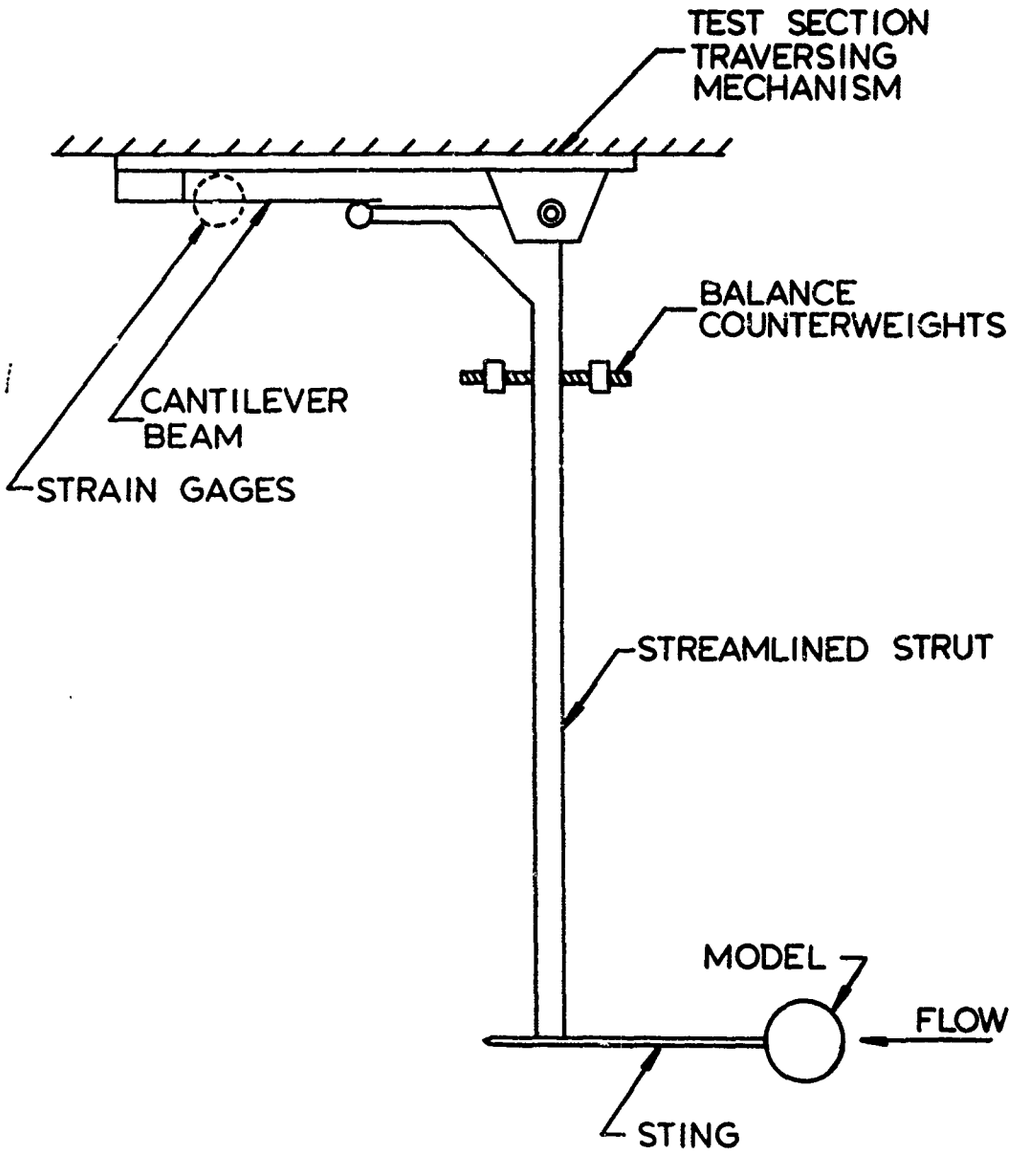


FIG 4. SCHEMATIC DIAGRAM OF DRAG BALANCE

The output from these strain gages was electrically amplified and fed to a recording oscillograph.

To account for the drag and interference of the model support, a spherical model used in the previous experiments was placed on the balance, and the drag of the entire system was measured. The difference between this drag, including the effect of the sting and the strut, and the drag of the sphere alone, obtained from Ref 1, is the interference drag and the drag of the support.

As validation for this method of drag determination, the following experiment was made. The sphere was placed in the flow at its proper location, but not connected to the balance. Then the balance system was moved to its proper position, but the sting did not touch the model. Under these conditions the drag of the balance system was measured.

The sum of the known drag of the sphere (Ref 1) and the drag of the balance system measured as described above amounts to a total drag practically identical to the one which was measured in total by the balance with the rigidly connected sphere (Figs 3 and 4). Therefore, this check can be considered as proof of the validity of the results presented in the following chapter.

## III. RESULTS

The results of the experiments indicate an appreciable difference between the drag of a sphere and that of the particular spheroids under study.

In Fig 5 the ratio of the drag coefficients of the spheroids to the drag coefficient of a sphere is shown as a function of Reynolds number for the three Mach numbers used. Both coefficients are based on surface area. From the results the following general conclusions can be drawn:

1) The oblate spheroid has approximately 20% more drag than the sphere. This can be understood in view of the fact that under similar aerodynamic conditions the oblate spheroid presents a larger frontal area to the flow than does a sphere with the same total surface area.

2) The prolate spheroid has approximately 8% less drag than the sphere. Again this may be considered to be primarily a consequence of a difference in frontal area.

3) In general, the drag coefficients of the spheroids vary with the Mach and Reynolds numbers in approximately the same manner as the drag coefficient of the sphere. Therefore, one may state that for small deviations, the drag of the spheroids related to that of the sphere is almost independent of Reynolds and Mach number. For more accurate consideration, one may use the particular values shown in Figs 5 and 6a to 6c.

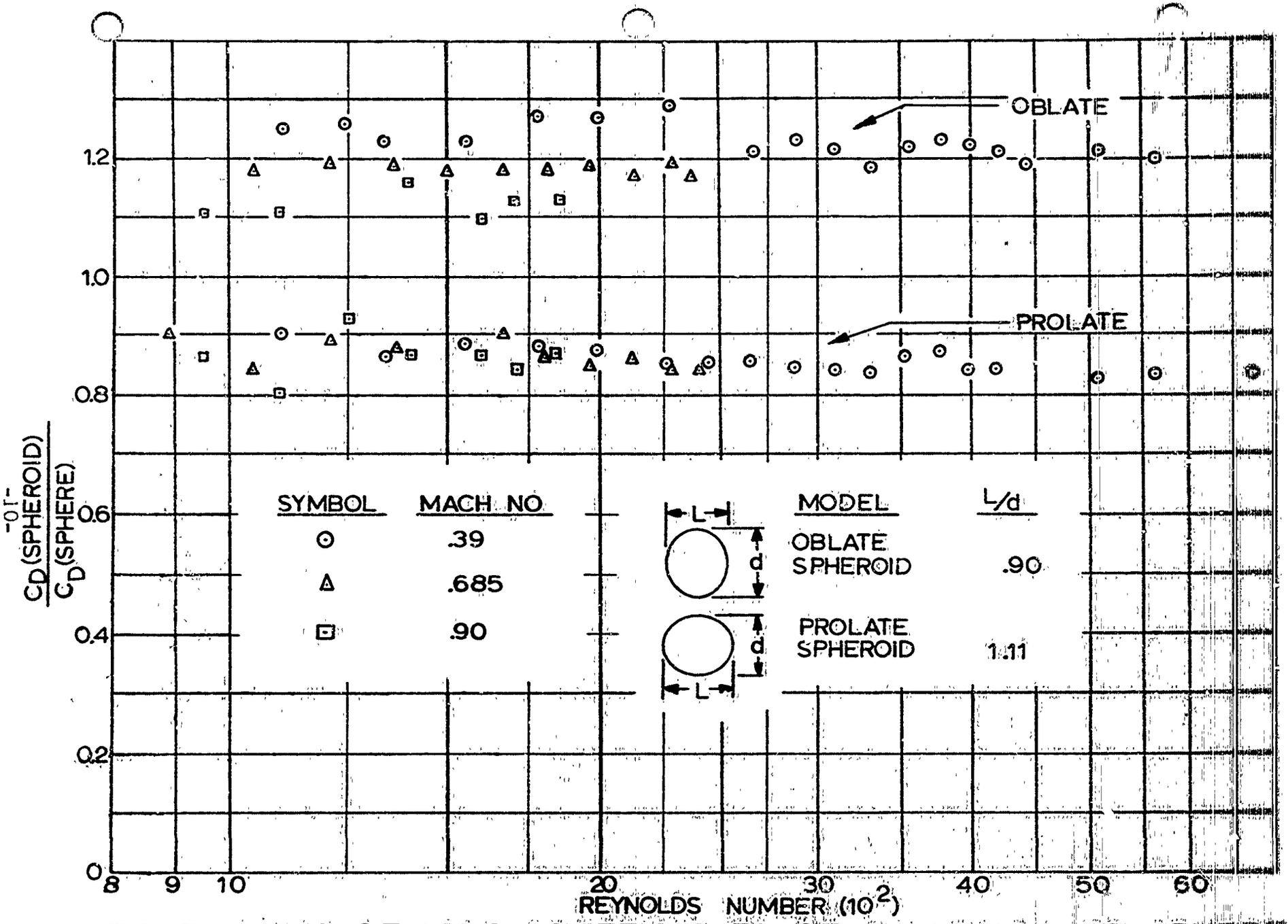


FIG 5. RATIO OF DRAG COEFFICIENTS OF SPHEROIDS TO SPHERE VERSUS REYNOLDS NUMBER.

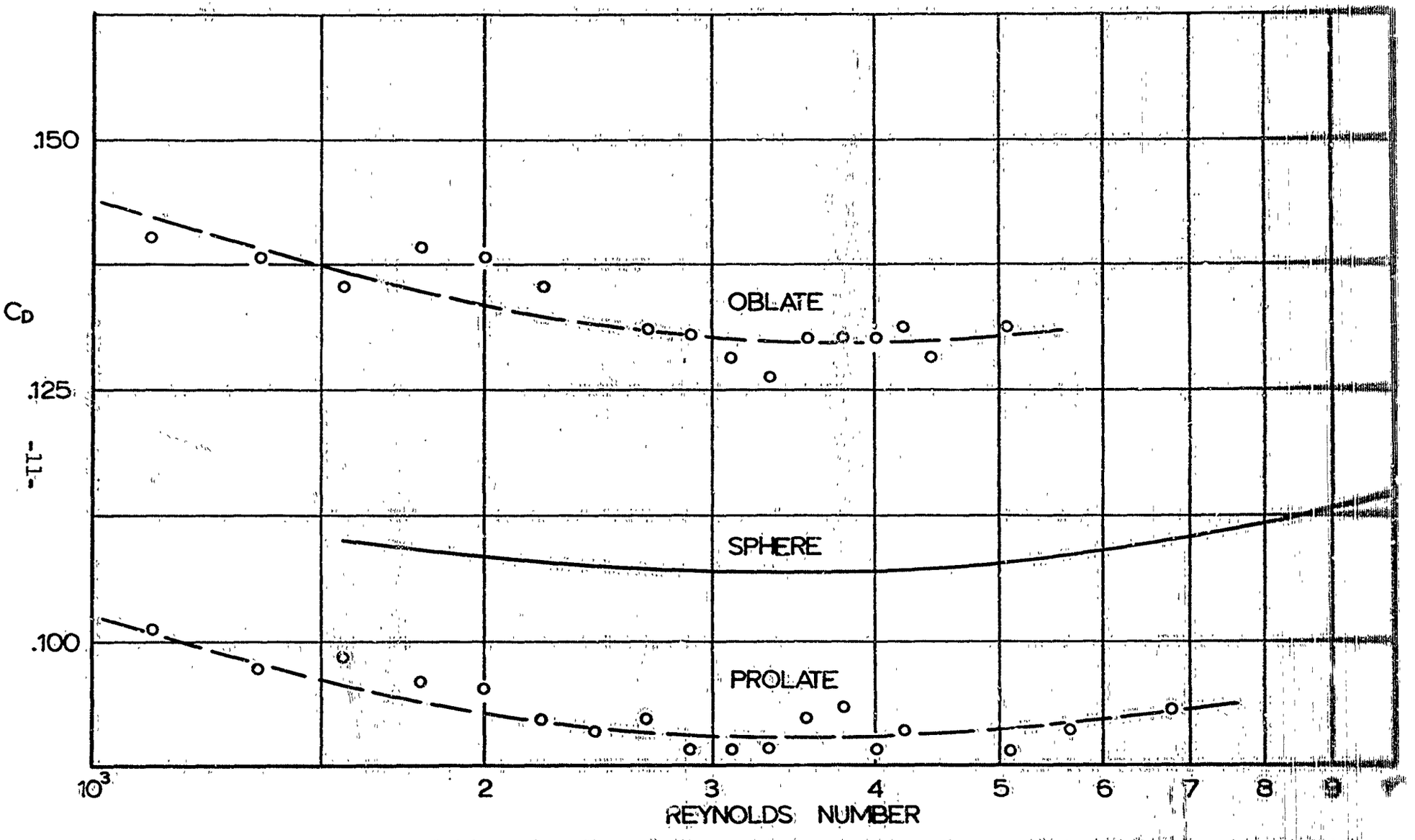


FIG 6a. DRAG COEFFICIENTS OF A SPHERE AND SPHEROIDS VERSUS REYNOLDS NUMBER AT M = 0.39

(BASED ON TOTAL SURFACE AREA)

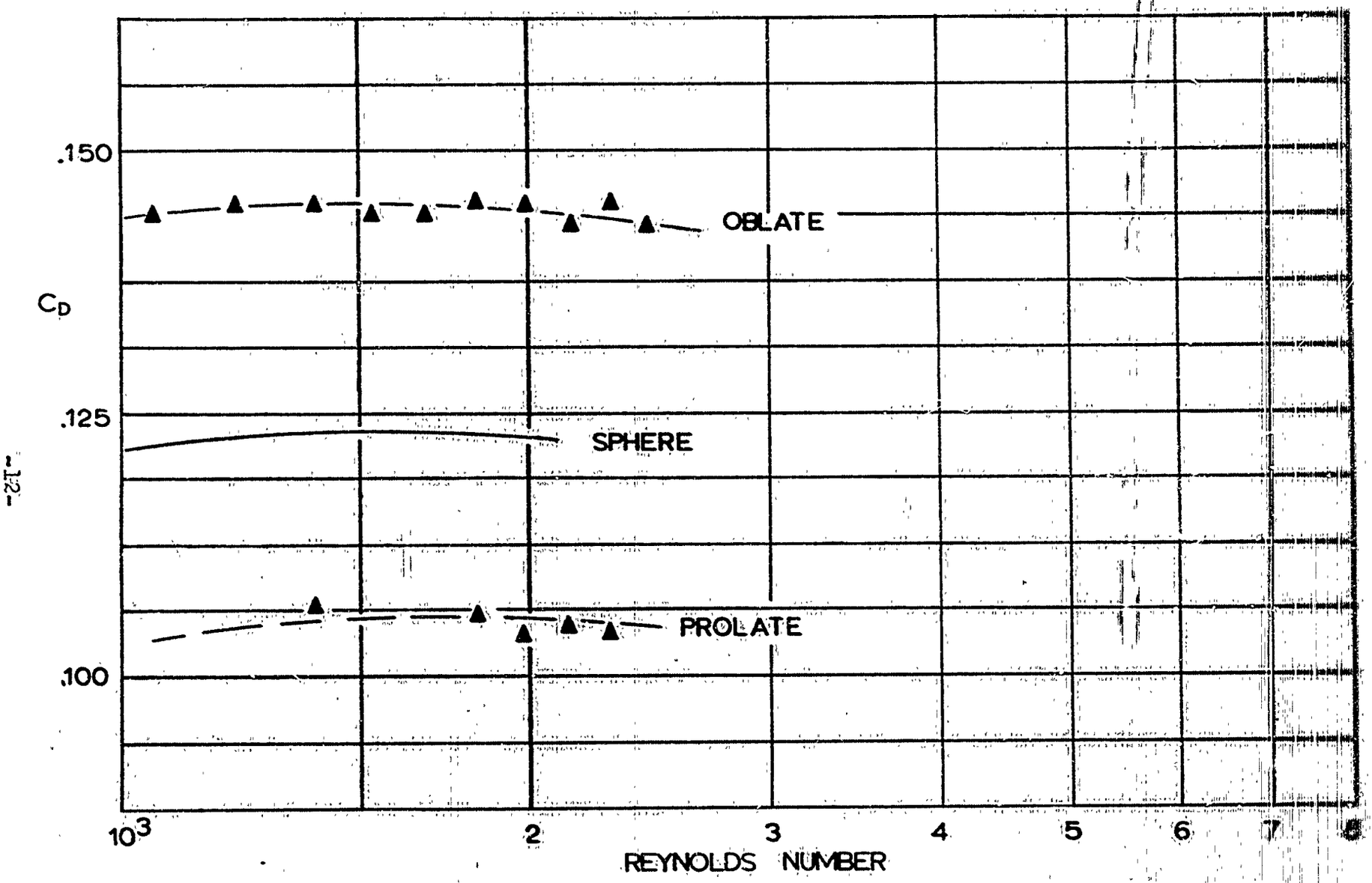


FIG 6b. DRAG COEFFICIENTS OF A SPHERE AND SPHEROIDS VERSUS REYNOLDS NUMBER AT M=0.685
(BASED ON TOTAL SURFACE AREA)

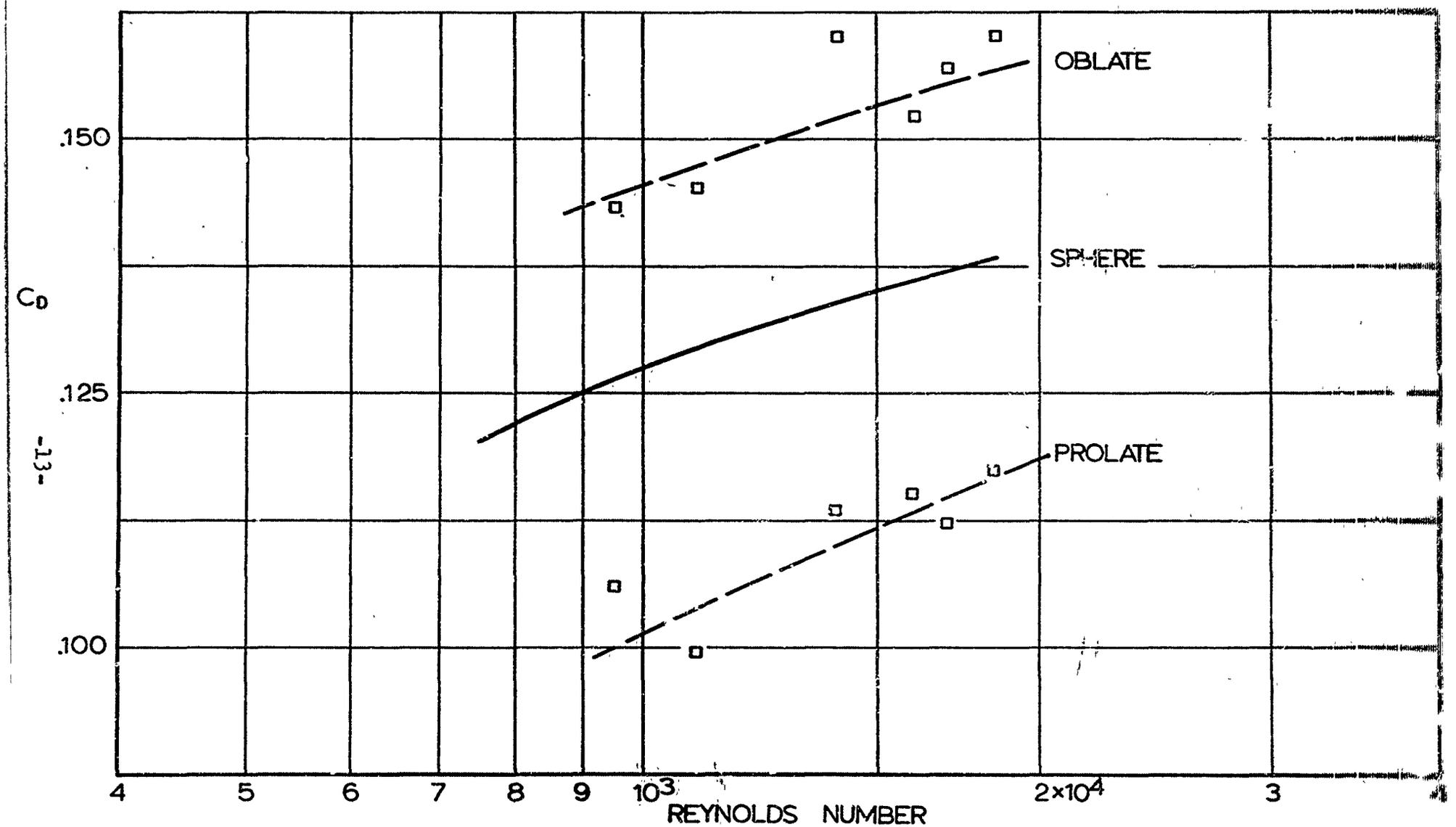




FIG 6c. DRAG COEFFICIENTS OF A SPHERE AND SPHEROIDS VERSUS REYNOLDS NUMBER AT M = 0.90

(BASED ON TOTAL SURFACE AREA)

## IV. SUMMARY

The drag of two spheroids having small deviations from a spherical shape was measured with a sensitive strain gage balance at three subsonic Mach numbers over the Reynolds number range between Re = 900 to Re = 7000. The drag coefficient subsequently obtained was compared with that of a sphere measured at the same aerodynamic conditions. The results showed that the drag coefficient changes significantly with the deformation. The Mach and Reynolds number effects upon the spheroids in the range under investigation seem to be the same as upon the sphere.

## REFERENCES


1. Heinrich, H. G., Niccum, R. J., Haak, E. L.: The Drag Coefficient of a Sphere Corresponding to a "One Meter ROBIN Sphere" Descending from 260,000 Ft Altitude (Reynolds Nos 789 to 23,448, Mach Nos 0.056 to 0.90), G. T. Schjeldahl Company, Northfield, Minnesota, 1963.

2. Minzner, R. A., Champion, K. S. W., and Pond, H. L.: The ARDC Model Atmosphere, August, 1959.

3. Goldstein, S.: Modern Developments in Fluid Dynamics, Vol. I, Oxford, 1938.

4. Kane, E. D.: Sphere Drag at Supersonic Speeds and Low Reynolds Numbers, Journal of the Aeronautical Sciences, Vol. 18, No. 4, pp. 259-270, April, 1951.

5. Sphere Drag in Rarefied Supersonic Gas Flows, Research Summary No. 36-5, Vol. II, pp. 10-11, Jet Propulsion Laboratory, Pasadena, California, November 1, 1960.

6. Ashkenas, H. I.: Sphere Drag at Low Reynolds Numbers and Supersonic Speeds, Research Summary No. 36-12, Vol. I, pp. 93-96, Jet Propulsion Laboratory, Pasadena, California, January 2, 1962.

7. Naumann, Alexander: Aerodynamische Gesichtspunkte Der Windkanalentwicklung, Jahrbuch, 1954, Der Wissenschaftlichen Gesellschaft fuer Luftfahrt, E. V. (WGL).

8. Hoerner, S. F.: Fluid Dynamic Drag, published by author, Midland Park, New Jersey, 1958.

9. Taylor, Angus E.: Advanced Calculus, Ginn and Company, Boston, Massachusetts, 1955.

# (NEW) MILITARY SPECIFICATION

## BALLOON, RADAR TARGET, METEOROLOGICAL ML-568/AM (ALT.)

1. SCOPE

1.1 Scope. - This specification covers one type of Balloon, Radar Target, Meteorological ML-568/AM (alternate design) suitable for ejection from a rocket nose cone at heights above 200,000 feet mean sea level. The balloon is inflated after ejection. While in descent, it is tracked by radar to determine wind velocity and air density.

2. APPLICABLE DOCUMENTS

2.1 The following documents form a part of this specification to the extent specified herein. Unless otherwise indicated, the issue in effect on the date of invitation for bids shall apply.

SPECIFICATION

Military

| | |
|---|---|
| MIL-T-9107 | Test Reports, Preparation of |
| MIL-F-14072 | Finishes for Ground Signal Equipment |
| MIL-D-70327 | Drawings, Engineering and Associated Lists |
| MIL-STD. 105C | Sampling Procedures and Tables for Inspection by Attributes |

Other

| | |
|---|---|
| ASTM D882-56T | Tests for Tensile Properties of Thin Plastic Sheets |

DRAWINGS

G. T. Schjeldahl Company

| | |
|---|---|
| D 1001501 B | ARCAS ROBIN packing |
| C 1001513 B | 1 Meter Diameter Sphere Assembly |
| C 1000009 | Sphere Gore Calculations |
| A 1000291 | Butt Joint |
| B 1001549 | Adhesive Ring |
| B 1001514 | North Polar Cap |
| B 1001515 A | South Polar Cap |
| B 1001516 B | Tape Ring |
| B 1001511 A | Seal |
| B 1001510 P | Tab South Polar Cap |
| C 1001375 A | Cylindrical Inflation Capsule Assembly |
| B 1001374 A | Cap Inflation Capsule |
| B 1001377 B | Rear Inflation Capsule |
| B 1001378 A | Forward Inflation Capsule |
| B 1001379 B | Stopper Inflation Capsule |
| B 1001376 C | Pillow Inflation Capsule |
| B 1001500 A | Pillow |
| A 1001502 A | Poly Wrap |

(Copies of documents required by contractors in connection with specific procurement functions should be obtained from the procuring activity or as directed by the contracting officer.)

3. REQUIREMENTS

3.1 Parts. - Balloon, Radar Target, Meteorological ML-568/AM (alternate design) shall consist of the following parts:

| Item No. | Quantity | Description | See Requirement |
|---|---|---|---|
| 1 | 1 each | Balloon | (3.3.1) |
| 2 | 1 each | Inflation Capsule | (3.3.3) |

3.2 Materials

3.2.1 Fungus-proof materials. - Materials that are nutrients for fungi shall not be used where it is practical to avoid them. Where used and not hermetically sealed, they shall be treated with a fungicidal agent acceptable to the procuring activi . However, if they will be used in a hermetically sealed enclosur fungicidal treatment will not be necessary.

3.2.2 Metals. - Metals shall be of the corrosion-resistant type, or suitably treated to resist corrosion due to fuels, salt spray, or atmospheric conditions likely to be met in storage or normal service.

3.2.2.1 Dissimilar Metals. - Unless suitably protected against electrolytic corrosion, dissimilar metals shall not be used in intimate contact with each other. Dissimilar metals are defined in MIL-F-14072.

3.3 Design and construction

3.3.1 Balloon

3.3.1.1 Material. - The balloon shall be fabricated of E. I. duPont de Nemours Company Type A Mylar, or equal. This material shall in addition be metalized (aluminum vacuum deposited) on one side to a maximum resistivity of 5 ohms per square.

3.3.1 2 Shape. - The balloon shall be a one meter (plus or minus 0.5 cm) diameter sphere at superpressures between 2 and 10 millibars.

3.3 1.3 Gores. - The balloon shall consist of 20 identical gores. The gores shall be cut such that the balloon conforms to the shape specified in 3.3.1.2 (Drawing number C 1[illegible]).

3.3.1.4 Seams - The seams shall be constructed per drawing number A 10000291. Seams shall be continuous with no visible air enclosures, neither drawn nor puckered. Tensile strength of the seams shall be at least equal to the tensile strength of the gore material over the operational temperature range.

3.3.1.5 End caps. - The balloon shall be terminated at both poles in end caps. Fabrication and installation of the end caps shall be in accordance with drawing number C 1001513 B.

3.3.2 Inflation capsule

3.3.2.1 Capsule. - The inflation capsule parts shall be constructed in accordance with drawing numbers B 1001374 A, B 1001377 B, and B 1001378 A.

3.3.2.2 Pillow. - A pillow shall be provided in accordance with drawing number B 1001376 C.

3.3.2.3 Rubber hole stopper. - A stopper shall be provided in accordance with drawing number B 1001379 B.

3.3.2.4 Isopentane. - The inflation media provided shall be isopentane of 99 molecular percent minimum purity.

3.3.2.5 Assembly of inflation capsule. - The inflation capsule shall be filled and assembled in accordance with drawing number C 1001375 A.

3.3.3 System Assembly. - The inflation capsule (drawing number C 1001375 A) is inserted in balloon assembly (drawing number C 1001513 B) through slit in gore seal near polar cap. Slit is then resealed with tape specified for gore seal (drawing number A 1000291).

3.3.3.1 System Weight. - The assembly (Balloon, Radar Target, Meteorological ML-568/AM (Alternate Design) shall weigh not more than 100 grams.

3.4 Packing in nose cone. - The finished balloon shall be packed in the nose section (3.5) in accordance with drawing number D 1001501 B.

3.5 Government-Furnished property. - When the contract or purchase order so provides, the Government will furnish the following to the contractor for use in packing the Balloon, Radar Target, Meteorological ML-568/AM (Alternate Design).

| Item No. | Quantity | Description |
|---|---|---|
| 1 | 1 | Nose Section, Rocket EX4-MOD 0. |

3.6 Workmanship. - The balloon, including all parts and accessories, shall be fabricated and finished in a thoroughly workmanlike manner. Particular attention shall be given to assure the quality of seals, accuracy of dimensions, and weight.

4. QUALITY ASSURANCE PROVISIONS

4.1 Unless otherwise specified herein, the supplier is responsible for the performance of all inspection requirements prior to submission for Government inspection and acceptance. Except as otherwise specified, the supplier may utilize his own facilities or any commercial laboratory

acceptable to the Government. Inspection records of the examinations and tests shall be kept complete and available to the Government as specified in the contract or order.

4.2 Classification of tests. - Tests shall be classified as preproduction (first article) tests and production tests.

4.2.1 Preproduction Tests. - To be considered as an optional requirement. Will not be included in standard procurements unless specifically requested by the procuring agency.

4.2.1.1 Seal Test. - Seals to be inspected for compliance with 3.3.1.4 Representative seals to be tested in accordance with ASTM Test Standard D882-56T to demonstrate contractor's ability to produce seals with strength equal to parent material. The number of samples and environmental conditions of testing to be specified by the procuring agency.

4.2.2 Production Tests. - No Balloon, Radar Target, Meteorological ML-568/Am (Alternate Design) shall be accepted until all appropriate test requirements have been satisfied.

4.2.2.1 Test Facilities. - The tests shall be performed at the contractor's plant or a commercial testing laboratory approved by the procuring agency.

4.2.2.2 Production sampling plan shall be established per MIL-STD-105 as specified by procuring agency.

4.2.2.3 Balloon

4.2.2.3.1 Material. - All balloon materials shall conform to 3.3.1.1.

4.2.2.3.2 Seals. - Shall be inspected per Item 3.3.1.4.

4.2.2.3.3 End caps - Shall be inspected to conformance with Item 3.3.1.5.

4.2.2.4 Balloon. - Every balloon procured under this military specification shall be subjected to the following tests and results thereof submitted with the completed assembly per Item 5.2.

4.2.2.4.1 Balloon is inflated and diameter measured through three approximately mutually perpendicular axes per Item 3.3.1.2.

4.2.2.4.2 Pressure Test. - Balloon shall be inflated to 10 millibars of superpressure. After 30 minutes, inspection shall ascertain that no more than 0.5 mb of pressure loss has occured.

4.2.5.4.3 During pressure test, assembly will be visually inspected to insure compliance with Item 3.6.

4.2.2.5 Inflation Capsule

4.2.2.5.1 Materials . = All materials shall conform with requirements called out on pertinent drawings.

4.2.2.5.2 All capsules shall be completely assembled per drawing number C 1001375 A without isopentane. Place each capsule in a vacuum chamber and reduce pressure to 300 millibars. Those capsules from which the cover has been ejected at greater pressures are rejected. Chamber pressure is further reduced to 50 millibars. Those capsules which have not opened before reaching this pressure are also rejected.

4.2.2.5.3 All capsules accepted per item 4.2.2.6.2 are reassembled per drawing number C 1001375 A. The filled capsule shall be weighed to the nearest thousandth of a gram. The capsule shall then be stored at a temperature of not more than -40° C for a period of not less than two hours. Remove capsule from low temperature environment and store at room temperature for not less than one hour. Then expose capsule to a temperature of not less than +50° C for not less than two hours. Thereafter store capsule for not less than 24 hours at room temperature. The maximum allowable weight loss at the end of this period shall be 0.005 gram.

4.2.2.6 System Assembly. - Shall be inspected for conformance with Item 3.3.3.

5.2.2.6.1 Each system assembly shall be weighed per Item 3.3.3.1 and the weight recorded on data sheet included with each assembly per Item 5.2.

4.2.2.7 Nosecone packing. - Inspection shall assure that packing conforms to drawing number D 1001501 B.

5. PREPARATION FOR DELIVERY

5.1 Preservation, packaging, packing and marking. - Preservation, packaging, packing and marking for delivery shall be as specified by the procuring activity.

5.2 Data sheet. - A data sheet shall be packed in each nose section shipping container. The data sheet shall have at least the following information:

a. Contract number
b. Serial number of balloon
c. Weight of balloon (grams)
d. Date of packing (3.4)

5.2.1 Data sheet shall be duplication of Exhibit "A" attached.

6. NOTES

6.1 Intended use. - The Balloon, Radar Target, Meteorological [illegible]-568/AM (Alternate Design) is intended for use in obtaining wind and [illegible]sity data above those altitudes which can be reached by buoyant balloons.

6.2 Ordering data. - Procurement documents should specify the following:

a. Title, number, and data of this specification
b. Desirability to perform preproduction tests (4.2.1)
c. Government-furnished property (3.5)
d. Levels of preservation, packaging, packing and marking for delivery
e. Availability of inspection records (4.1)



Preparing Activity

Air Force - ARDC

SUGGESTED REVISION TO

# MILITARY SPECIFICATION

## BALLOON, RADAR TARGET, METEOROLOGICAL ML-568/AM

### 1. SCOPE

1.1 Scope. - This specification covers one type of Balloon, Radar Target, Meteorological ML-568/AM suitable for ejection from a rocket nose cone at heights above 200,000 feet mean sea level. The balloon is inflated after ejection. While in descent, it is tracked by radar to determine wind velocity and air density.

### 2. APPLICABLE DOCUMENTS

2.1 The following documents form a part of this specification to the extent specified herein. Unless otherwise indicated, the issue in effect on the date of invitation for bids shall apply.

SPECIFICATION

Military

| | |
|---|---|
| MIL-T-9107 | Test Reports, Preparation of |
| MIL-F-14072 | Finishes for Ground Signal Equipment |
| MIL-D-70327 | Drawings, Engineering and Associated Lists |
| MIL-STD-105C | Sampling Procedures and Tables for Inspection by Attributes |

Other

| | |
|---|---|
| ASTM D882-56T | Tests for Tensile Properties of Thin Plastic Sheets |

DRAWINGS

G. T. Schjeldahl Company

| | |
|---|---|
| D 1001501 B | ARCAS ROBIN Packing |
| C 1001532 B | Balloon Reflector Assembly |
| B 1001547 A | Reflector Sub Assembly |
| B 1001545 B | Six Point Reflector |
| A 1001548 B | Corner Reflection Spring |
| B 1001533 | Reinforcement Patch |
| B 1001546 | Hold Tab |
| C 1001530 E | 1 Meter Diameter Sphere Assembly |
| C 1000009 | Sphere Gore Calculations |
| A 1000291 | Butt Joint |
| B 1001549 | Adhesive Ring |
| B 1001779 A | North Polar Cap |
| B 1001780 A | South Polar Cap |

| | | |
|---|---|---|
| B | 1001516 B | Tape Ring |
| B | 1001511 A | Seal |
| B | 1001510 B | Tab South Polar Cap |
| C | 1001375 A | Cylindrical Inflation Capsule Assembly |
| B | 1001374 A | Cap Inflation Capsule |
| B | 1001377 B | Rear Inflation Capsule |
| B | 1001378 A | Forward Inflation Capsule |
| B | 1001379 B | Stopper Inflation Capsule |
| B | 1001376 C | Pillow Inflation Capsule |
| B | 1001500 A | Pillow |
| A | 1001502 A | Poly Wrap |
| A | 1001503 A | Cover Sheet |
| A | 1001504 A | Balloon Ejection Sheet |

(Copies of documents required by contractors in connection with specific procurement functions should be obtained from the producing activity or as directed by the contracting officer.)

3. REQUIREMENTS

3.1 Parts. - Balloon, Radar Target, Meteorological ML-568/AM shall consist of the following parts:

| Item No. | Quantity | Description | See Requirement |
|---|---|---|---|
| 1 | 1 each | Balloon | (3.3.1) |
| 2 | 1 each | Corner Reflector | (3.3.2) |
| 3 | 1 each | Inflation Capsule | (3.3.3) |

3.2 Materials

3.2.1 Fungus-proof materials. - Materials that are nutrients for fungi shall not be used where it is practical to avoid them. Where used and not hermetically sealed, they shall be treated with a fungicidal agent acceptable to the procuring activity. However, if they will be used in a hermetically sealed enclosure, fungicidal treatment will not be necessary.

3.2.2 Metals. - Metals shall be of the corrosion-resistant type, or suitably treated to resist corrosion due to fuels, salt spray, or atmospheric conditions likely to be met in storage or normal service.

3.2.2.1 Dissimilar metals. - Unless suitably protected against electrolytic corrosion, dissimilar metals shall not be used in intimate contact with each other. Dissimilar metals are defined in MIL-F-14072.

3.3 Design and construction

3.3.1 Balloon

3.3.1.1 Material. - The balloon shall be fabricated of E. I. duPont de Nemours Company Type A Mylar, or equal.

3.3.1.2 Shape. - The balloon shall be a one meter (plus or

minus 0.5 cm) diameter sphere at superpressures between 2 and 10 millibars. (It is acknowledged that some local deformation occurs at corner reflector attachment points under 1G conditions at lower superpressures.)

3.3.1.3 Gores. - The balloon shall consist of 20 identical gores. The gores shall be cut such that the balloon conforms to the shape specified in 3.3.1.2. (Drawing number C 1000009).

3.3.1.4 Seams. - The seams shall be constructed per drawing number A 1000291. Seals shall be continuous with no visible air enclosures, neither drawn nor puckered. Tensile strength of the seams shall be at least equal to the tensile strength of the gore material over the operational temperature range.

3.3.1.5 End caps. - The balloon shall be terminated at both poles in end caps. Fabrication and installation of the end caps shall be in accordance with drawing number C 1001530 E.

3.3.1.6 Spring attachment. - Shall be made according to drawing number C 1001532 B

3.3.2 Corner Reflector

3.3.2.1 Material. - The corner reflector shall be fabricated of 0.00025-inch thick type C Mylar, aluminized both sides, maximum resistivity 1.0 ohm per square per side.

3.3.2.2 Fabrication. - The corner reflector shall be fabricated in accordance with drawing number B 1001547 A.

3.3.2.3 Suspension springs shall be in accordance with drawing number A 1001548 B.

3.3.2.4 Spring Attachment. - The springs (3.3.2.3) shall be attached to the reflector in accordance with drawing number B 1001547 A.

3.3.2.5 Reflector-balloon assembly. - The corner reflector (3.3.2) shall be attached to the inside surface of the balloon (3.3.1) in accordance with drawing number C 1001532 B.

3.3.3 Inflation capsule

3.3.3.1 Capsule. - The inflation capsule parts shall be constructed in accordance with drawing numbers B 1001374 A, B 1001377 B, and B 1001378 A.

3.3.3.2 Pillow. - A pillow shall be provided in accordance with drawing number B 1001376 C.

3.3.3.3 Rubber hole stopper. - A stopper shall be provided in accordance with drawing number B 1001379 B.

3.3.3.4 Isopentane. - The inflation media provided shall be isopentane of 99 molecular percent minimum purity.

3.3.3.5 Assembly of inflation capsule. - The inflation capsule shall be filled and assembled in accordance with drawing number C 1001375 A.

3.3.4 System Assembly. - The inflation capsule (drawing number C 1001375 A) is inserted in balloon assembly (drawing number C 1001532 B) through slit in gore seal near polar cap. Slit is then resealed with tape specified for gore seal(drawing number A 1000291).

3.3.4.1 System Weight. - The assembly (Balloon, Radar Target, Meteorological ML-568/AM) shall weigh not more than 125 grams.

3.4 Packing in nose cone. - The finished balloon shall be packed in the nose section (3.5) in accordance with drawing number D 1001501 B.

3.5 Government-furnished property. - When the contract or purchase order so provides, the Government will furnish the following to the contractor for use in packing the Balloon, Radar Target, Meteorological ML-568/AM:

| Item No. | Quantity | Description |
|---|---|---|
| 1 | 1 each | Nose Section, Rocket EX4 - MOD 0 |

3.6 Workmanship. - The balloon, including all parts and accessories, shall be fabricated and furnished in a thoroughly workmanlike manner. Particular attention shall be given to assure the quality of seals, accuracy of dimensions, and weight.

4. QUALITY ASSURANCE PROVISIONS

4.1 Unless otherwise specified herein, the supplier is responsible for the performance of all inspection requirements prior to submission for Government inspection and acceptance. Except as otherwise specified, the supplier may utilize his own facilities or any commercial laboratory acceptable to the Government. Inspection records of the examinations and tests shall be kept complete and available to the Government as specified in the contract or order.

4.2 Classification of tests. - Tests shall be classified as preproduction (first article) tests and production tests.

4.2.1 Preproduction Tests. - To be considered as an optional requirement. Will not be included in standard procurements unless specifically requested by the procuring agency.

4.2.1.1 Seal Test. - Seals to be inspected for compliance with 3.3.1.4. Representative seals to be tested in accordance with ASTM Test Standard D 882-56T to demonstrate contractor's ability to produce seals with strength equal to parent material between +130°F and -70° F. The number of samples and environmental conditions of testing to be specified by the procuring agency.

4.2.2 Production Tests. - No Balloon, Radar Target, Meteorological ML-568/AM shall be accepted until all appropriate test requirements have been satisfied.

4.2.2.1 Test Facilities. - The tests shall be performed at the contractor's plant or a commercial testing laboratory approved by the procuring agency.

4.2.2.2 Production sampling plan shall be established per MIL-STD-105 as specified by procuring agency.

4.2.2.3 Balloon

4.2.2.3.1 Material. - All balloon materials will be certified per 3.3.1.1

4.2.2.3.2 Seals. - Shall be inspected per Item 3.3.1.4

4.2.2.3.3 End caps. - Shall be inspected to conformance with Item 3.3.1.5

4.2.2.4 Corner Reflector

4.2.2.4.1 Material. - All corner reflector film shall be as required by Item 3.3.2.1.

4.2.2.4.2 Fabrication. - Corner reflector pattern shall be inspected for conformance with drawing number B 1001545 B. Panels cut using pattern must conform to the tolerances shown on this drawing.

4.2.2.4.3 Suspension springs. - Shall be inspected for conformance to drawing number A 1001548 B. Spring attachment to the corner reflector assembly shall conform with drawing number B 1001547 A.

4.2.2.4.4 Corner Reflector assembly will be mounted in a test fixture and visually inspected to assure quality of workmanship. Supported panels shall be inspected to insure that minimum sagging or wrinkling is found in separate panels and panel junctions.

4.2.2.5 Balloon and Corner Reflector Assembly. - Every balloon procured under this specification shall be subjected to the following tests and results thereof submitted with the completed assembly per Item 5.2.

4.2.2.5.1 Balloon is inflated and diameter measured through three approximately mutually perpendicular axes per Item 3.3.1.2.

4.2.2.5.2 Pressure Test. - Balloon shall be inflated to 10 millibars of superpressure. After 30 minutes, inspection shall ascertain that less than 0.5 mb pressure loss has occurred.

4.2.2.5.3 During pressure test, assembly will be visually inspected to insure that the corner reflector is properly installed.

4.2.2.6 Inflation Capsule

4.2.2.6.1 Materials. - All materials conform with requirements call out on pertinent drawings.

4.2.2.6.2 All capsules shall be completely assembled per drawing number C 1001375 A without isopentane. Place each capulse in a vacuum chamber and reduce pressure to 300 millibars. Those capsules from which the cover has been ejected at greater pressures are ejected. Chamber pressure is further reduced to 50 millibars. Those capsules which have not opened before reaching this pressure are also rejected.

4.2.2.6.3 All capsules accepted per Item 4.2.2.6.2 are reassembled per drawing number C 1001375 A. The filled capsule shall be weighed to the nearest thousandth of a gram. The capsule shall then be stored at a temperature of not more than -40° C for a period of not less than two hours. Remove capsule from low temperature environment and store at room temperature for not less than one hour. Then expose capsule to a temperature of not less than +50°C for not less than two hours. Thereafter store capsule for not less than 24 hours at room temperature. The maximum allowable weight loss at the end of this period shall be 0.005 grams.

4.2.2.7 System Assembly. - Shall be inspected for conformance with Item 3.3.4.

4.2.2.7.1 Each system assembly shall be weighed per Item 3.3.4.1 and the weight recorded on data sheet included with each assembly per Item 5.2.

4.2.2.8 Nosecone packing. - Inspection shall assure that packing conforms to drawing number D 1001501 B.

5. PREPARATION FOR DELIVERY

5.1 Preservation, packaging, packing and marking. - Preservation, packaging, packing and marking for delivery shall be as specified by the procuring activity.

5.2 Data Sheet. - A data sheet shall be packed in each nose section shipping container. The data sheet shall have at least the following information:

a. Contract number
b. Serial number of balloon
c. Weight of balloon (grams)
d. Date of packing (3.4)

5.2.1 Data sheet shall be duplication of Exhibit "A" attached.

6. NOTES

6.1 Intended Use. - The Balloon, Radar Target, Meteorological ML-568/AM is intended for use in obtaining wind and density data above those altitudes which can be reached by buoyant balloons.

6.2 Ordering data. - Procurement documents should specify the following:

a. Title, number, and date of this specification
b. Desirability to perform preproduction tests (4.2.1).
c. Government furnished property (3.5)
d. Levels of preservation, packaging, packing and marking for delivery.
e. Availability of inspection records (4.1).



Preparing Activity

Air Force - ARDC

G. T. SCHJELDAHL COMPANY
NORTHFIELD, MINNESOTA

ROBIN BALLOON SYSTEM

Contract No. _____ Nosecone No. _____
Shipped To _____
Date Shipped _____
Waybill No. _____

I. Fabrication

A. Sphere (Balloon No. _____)

1. Date Fabricated _____ by _____

2. Diameter Calibration

a. Measured at 10 mb superpressure

b.

| | X | Y | Z |
|---|---|---|---|
| 1. | IM( ) .00 _____ | IM( ) .00 _____ | IM( ) .00 _____ |
| 2. | IM( ) .00 _____ | IM( ) .00 _____ | By _____ |
| 3. | IM( ) .00 _____ | IM( ) .00 _____ | |

B. Corner Reflector Fabricated By _____

1. Fabrication Checked

a. Corner seals complete _____ Checked By _____

b. Panels smooth _____

2. Springs attached on center of seal _____

C. Balloon Corner Assembly Date _____ By _____ Checked By _____

D. Pressure Test

1. Inflate to 10 mb superpressure and hold for 30 minutes.
Pressure reading at end of test period _____ mb (Not less than 9.5 mb)

2. Final Assembly Check (Concurrent with pressure test)

a. Proper corner alignment _____ By _____
b. Gore seals checked _____
c. End cap seals checked _____
d. Spring alignment checked _____

II. Nosecone Packing

A. Capsule Model-Unit No. _____

1. Empty capsule weight _____ grams
2. Capsule filled with _____cc of liquid _____ on _____(Date) By_____
3. Capsule weight on date filled _____ grams
4. Capsule weight on date packed _____ grams

B. Packing

1. Date Packed _____
2. Balloon Assembly (with capsule) weight _____ By _____

Quality Control Verification: _____

Comments:

GTS Form 51.105 Rev.

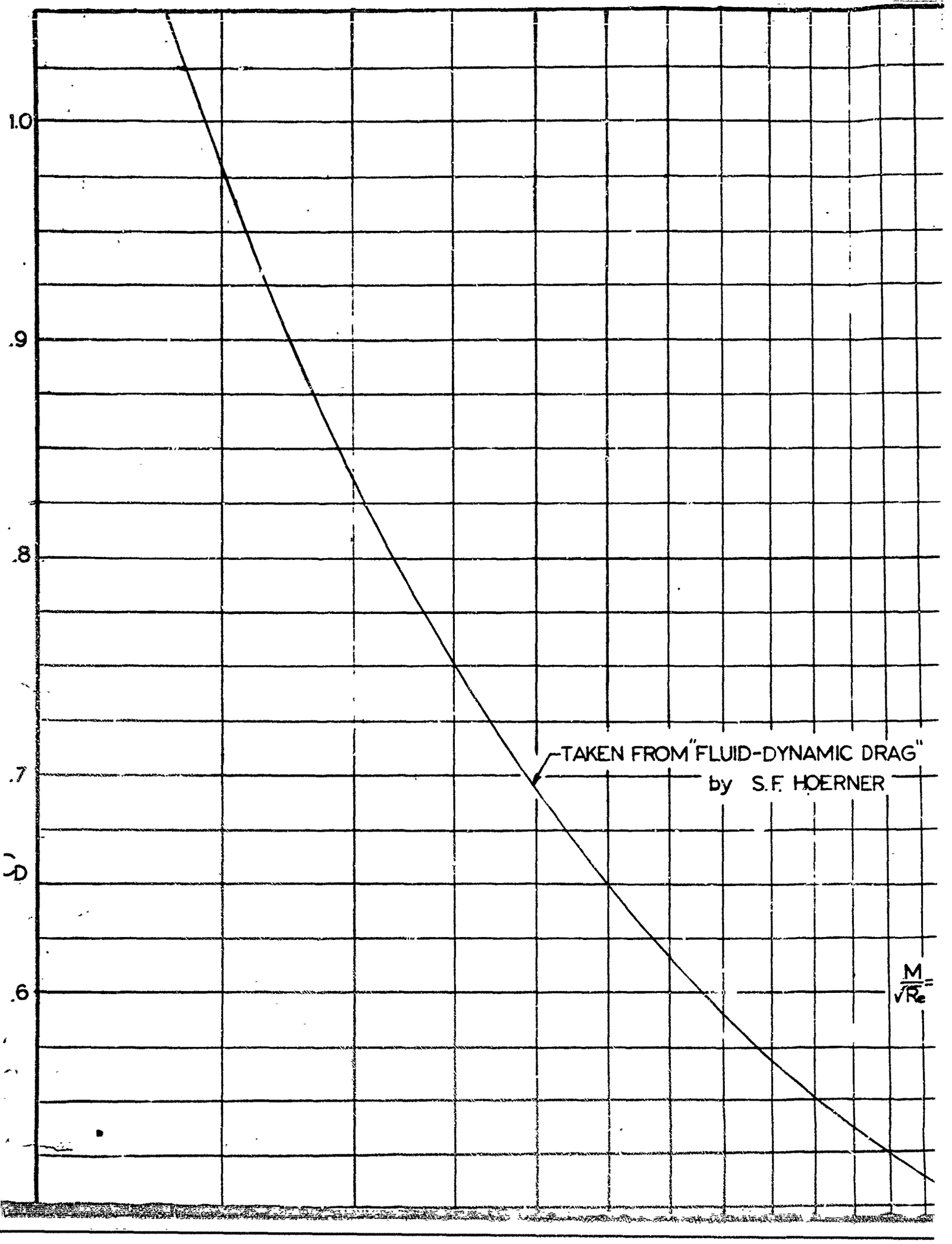
1.0
.9
.8
.7
.6
$C_D$
TAKEN FROM "FLUID-DYNAMIC DRAG"
by S.F. HOERNER
$\frac{M}{\sqrt{R_e}}$ =

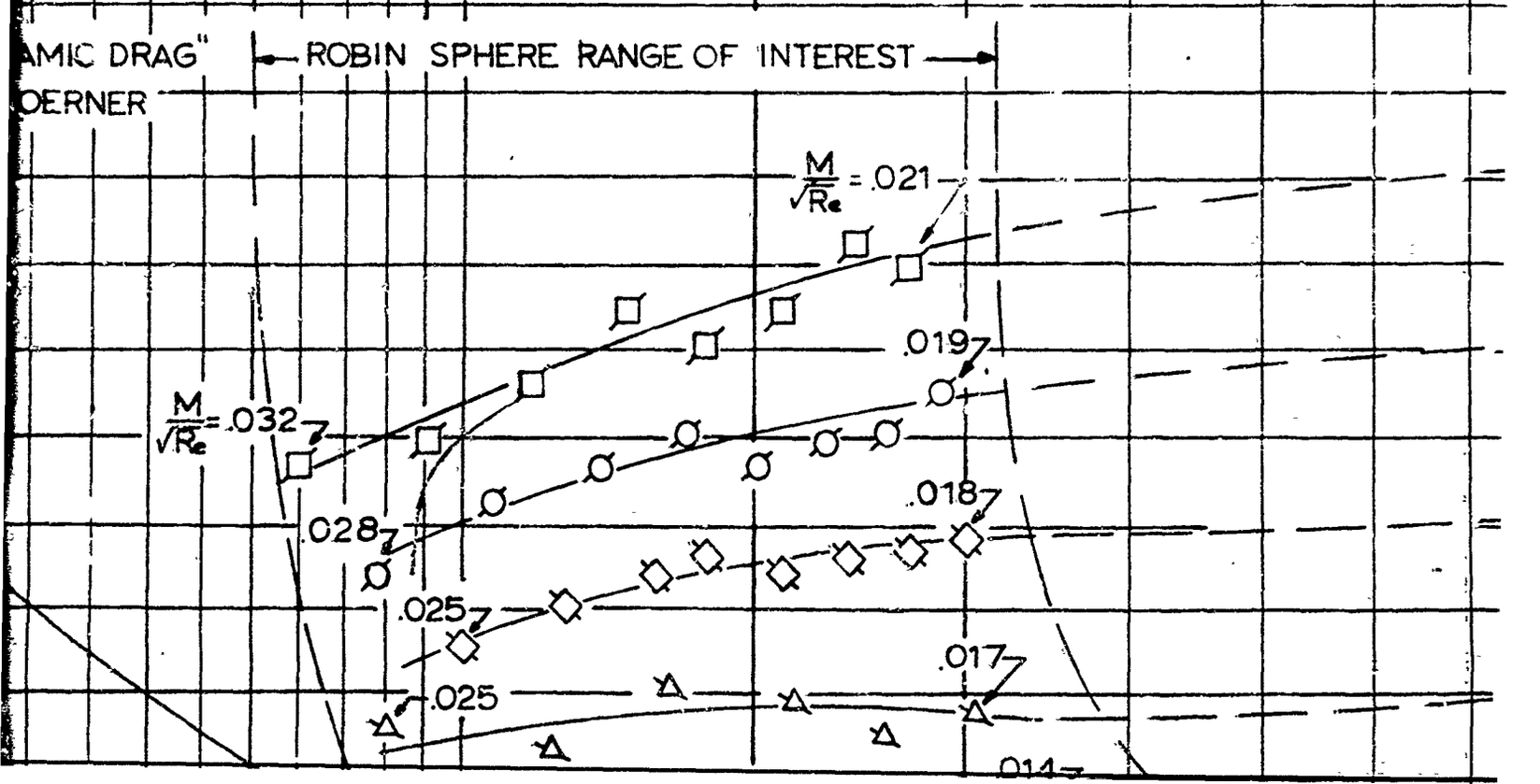
AMIC DRAG"
ROBIN SPHERE RANGE OF INTEREST
OERNER
M/√Re = .021
.019
M/√Re = .032
.028
.018
.025
.017
.025
.014

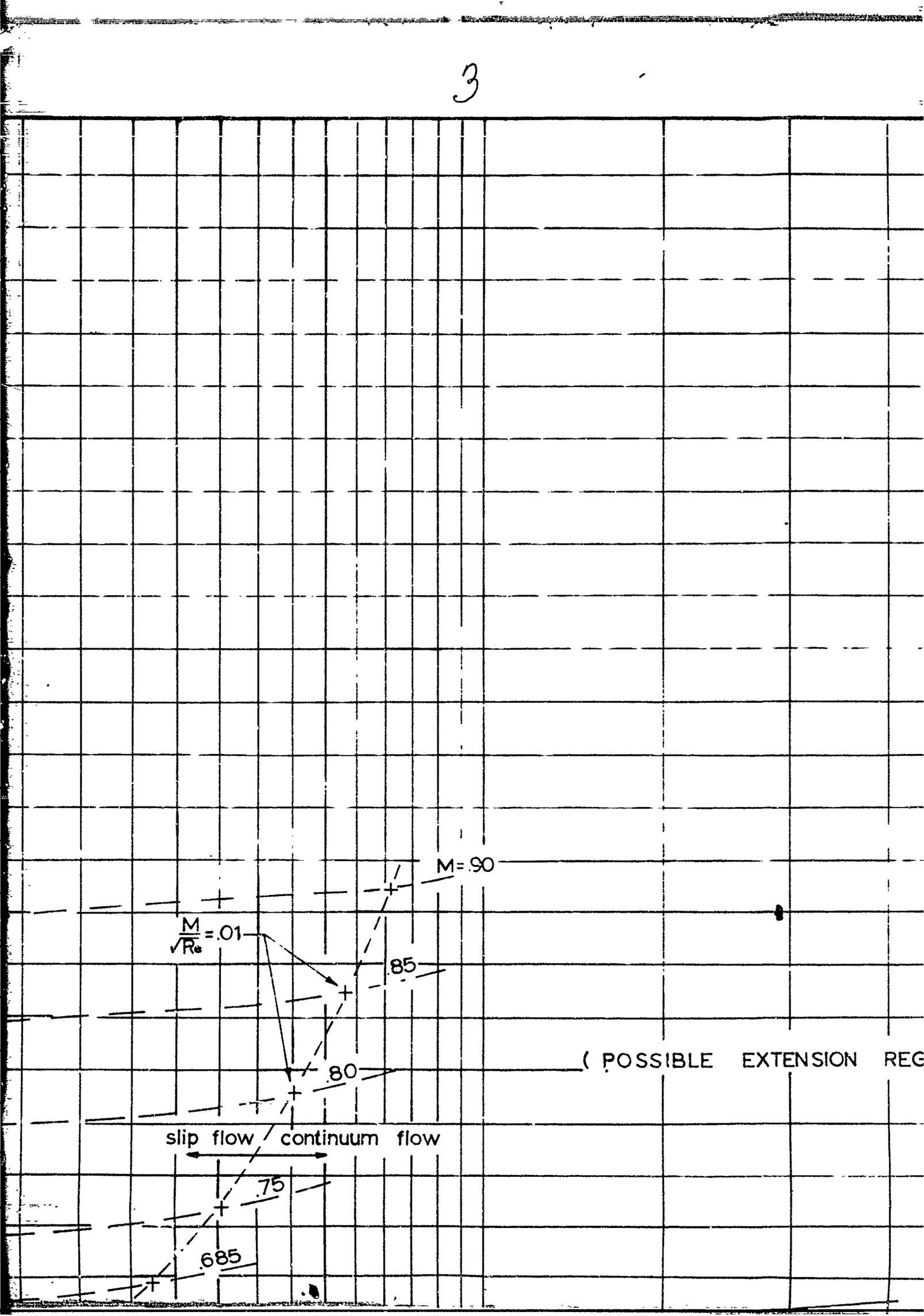
M = .90
$\frac{M}{\sqrt{Re}}$ = .01
.85
.80
( POSSIBLE EXTENSION REG
slip flow / continuum flow
.75
.685

XTENSION REGION )

TRANSITION REGION

FROM GERMAN JAHRBUCH 1954 (WGL)

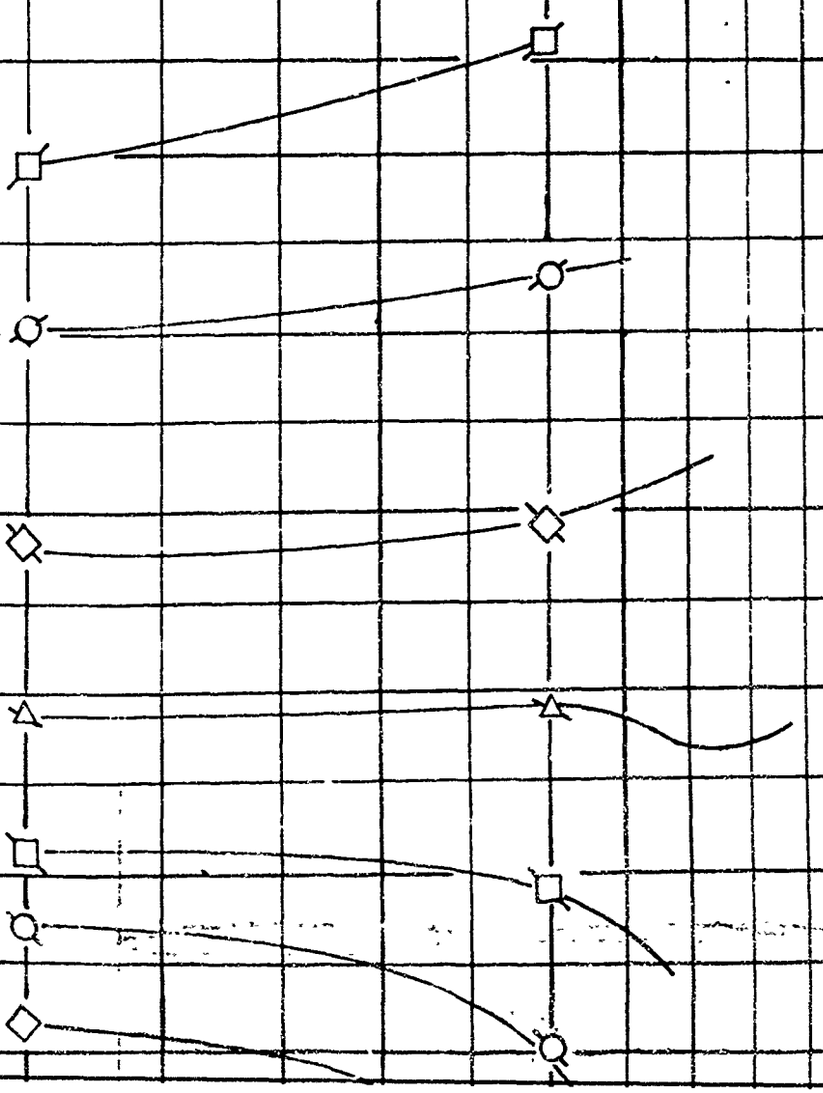

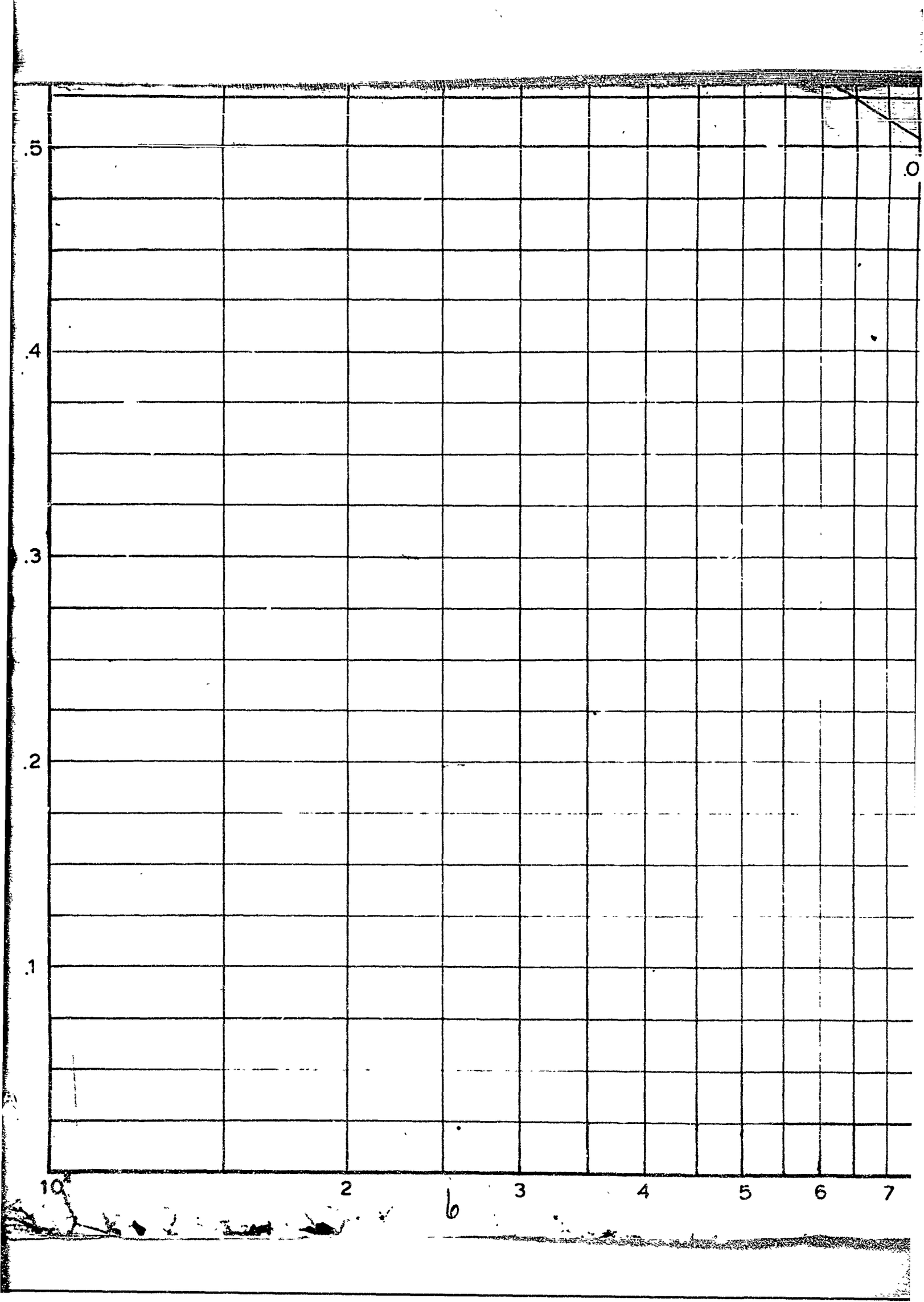
.5
.4
.3
.2
.1
0
10
2
3
4
5
6
7

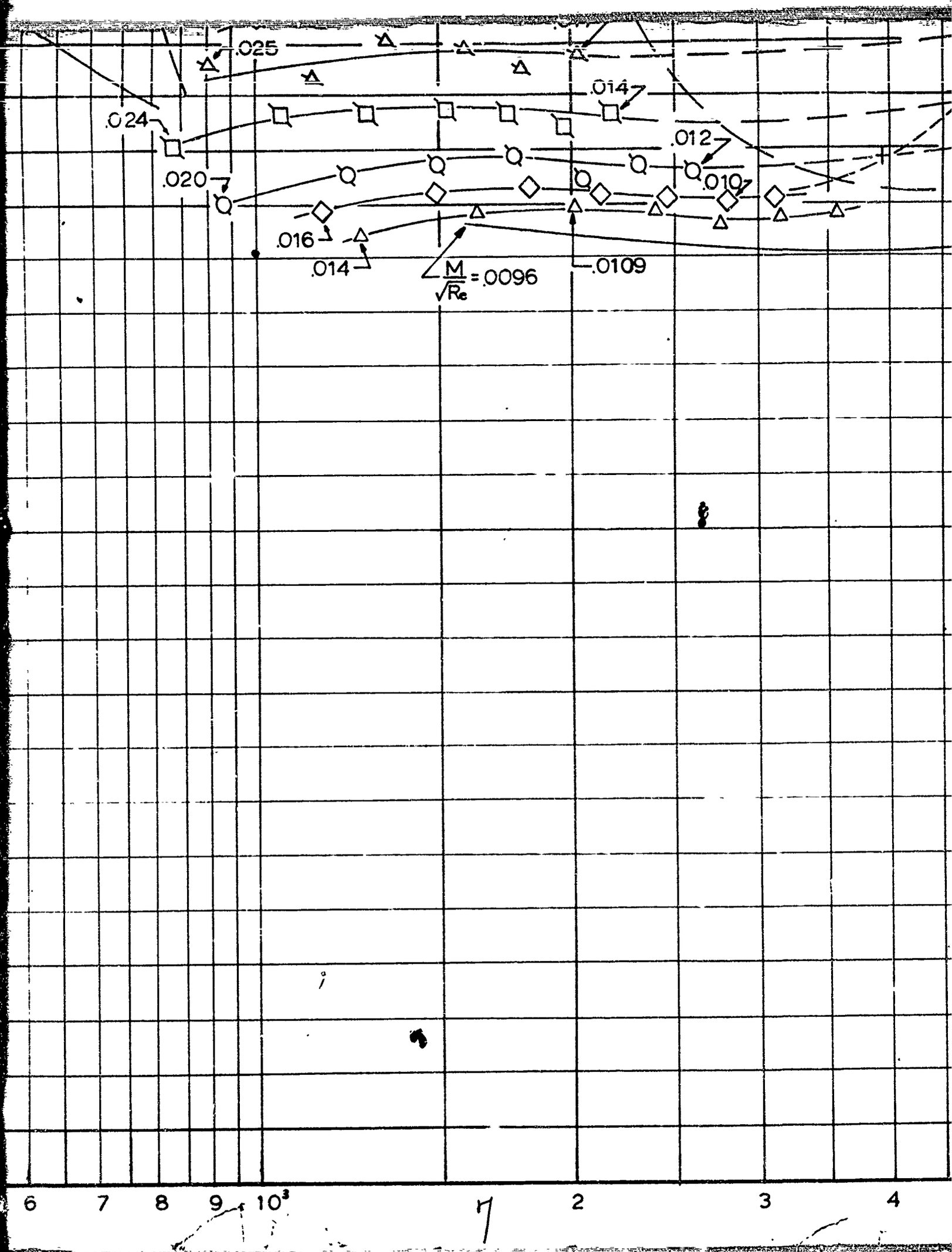
.025
.024
.020
.014
.012
.010
.016
.014
$\frac{M}{\sqrt{Re}}$ = .0096
.0109
6
7
8
9
$10^3$
2
3
4

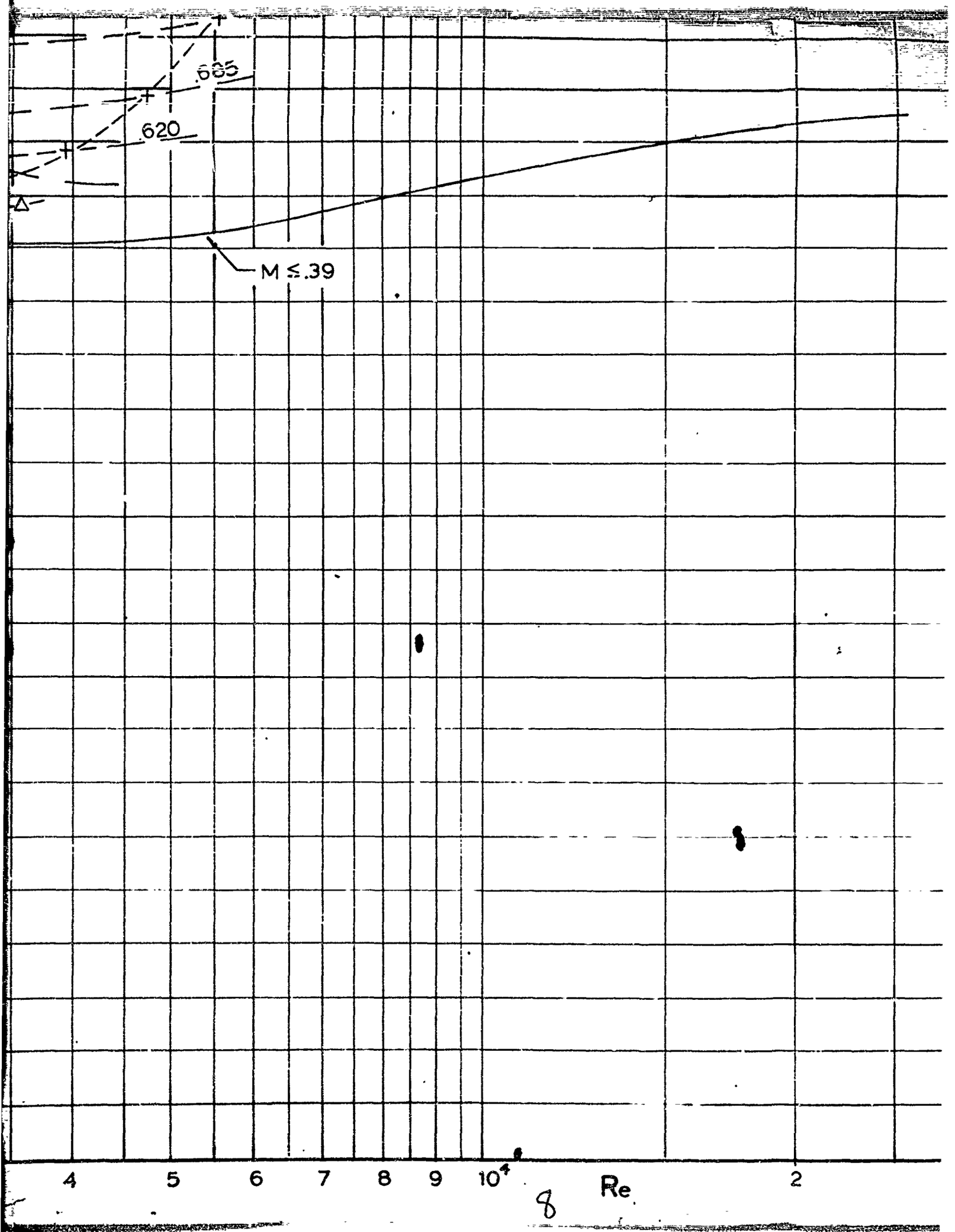
.665
.620
M ≤ .39
4
5
6
7
8
9
10⁴
Re
2

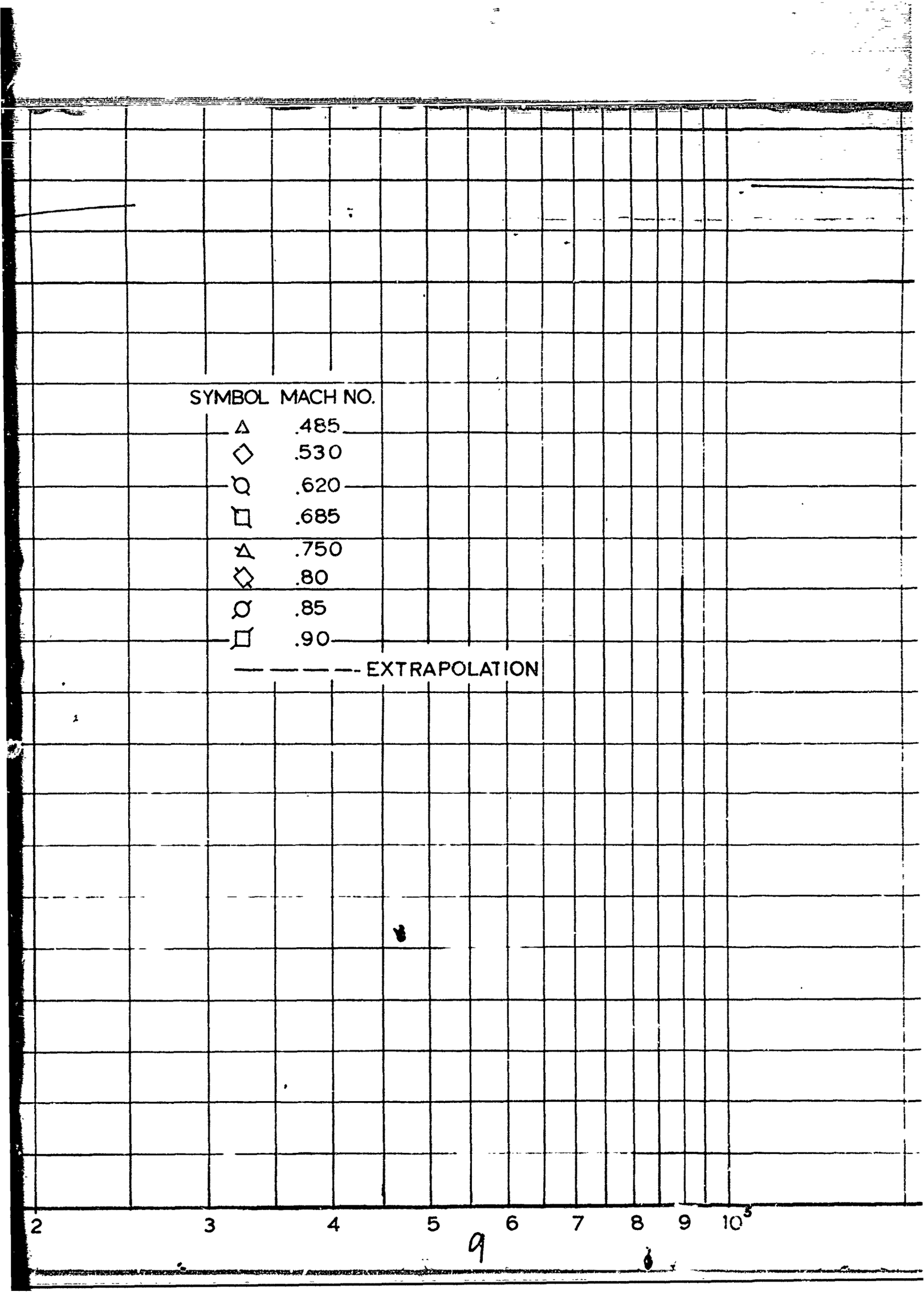
SYMBOL MACH NO.
.485
.530
.620
.685
.750
.80
.85
.90
EXTRAPOLATION
2
3
4
5
6
7
8
9
10³

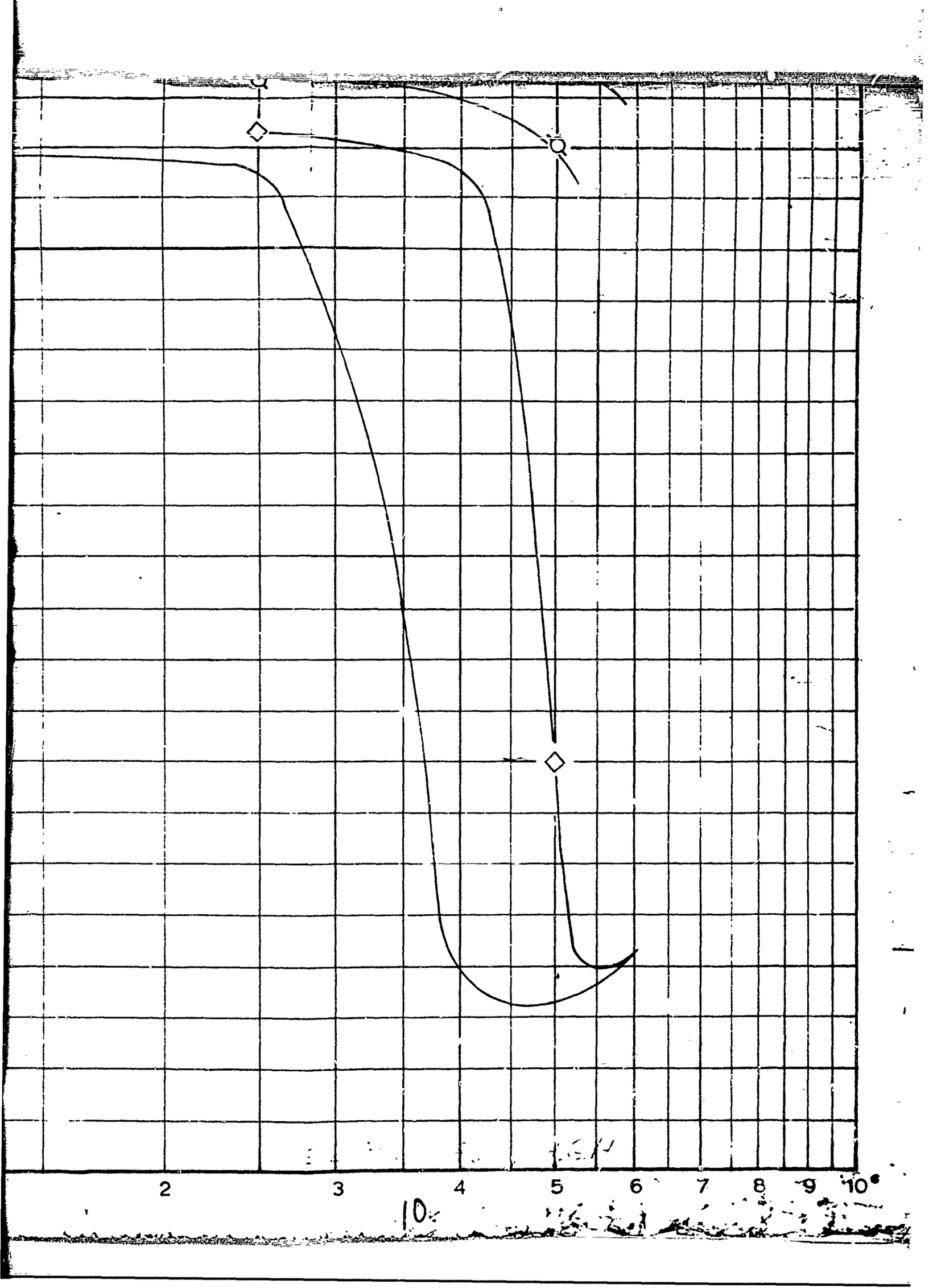
2
3
4
5
6
7
8
9
10